UNIVERSITÀ DEGLI STUDI DI CATANIA

International PhD in Chemical Science

XXIX ciclo

Cunsolo Alessandra

PORPHYRIN DERIVATIVES AS VERSATILE PROTEASOME MODULATORS

PhD Thesis

Tutor : Prof. R. Purrello

Co-Tutor : Dr. A.M. Santoro

PhD Coordinator : Prof. S. Sortino

2013 - 2016

"Learn from yesterday, live for today, hope for tomorrow. The important thing is not to stop questioning"

Albert Einstein, *Relativity: The Special and the General Theory*

Preface

The focus of this research has been the proteasome, with a particular emphasis on its interaction with porphyrins.

It is known that cationic porphyrins behave as proteasome inhibitors and their potency depends on the number of positive charges. During this PhD study, carried out in close collaboration with other Italian and foreign research groups, we have worked towards a deeper understanding of the molecular mechanisms responsible for the interactions between proteasome and the tetra cationic porphyrin H2T4. Moreover, other porphyrin, porphyrinoid derivatives and bio-inspired molecules have been studied for their potential roles in modulating proteasome function. Surprisingly, the tetra anionic porphyrin H2TPPS has an unexpected activator quality on 20S proteasome in both cell based assays and purified 20S CP.

From these studies emerge a new scenario where these macrocyclic molecules, thanks to their inhibitory action on the proteasome, are becoming increasingly rich multi-target molecules for oncological applications.

This research has also uncovered novel porphyrin molecules capable of activating the proteasome suggesting that they are capable of not just inhibition but "proteasomal modulation" and, if correctly designed, they are able to interact with the electrostatic access code of proteasome's core particle allowing for biological activities.

Table of Contents

Chapter 1 - Introduction

The ubiquitin–proteasome system (UPS) is the primary degradation system in eukaryotic cells, with high selectivity for a myriad of soluble proteins, and perturbations in the UPS are associated with numerous human disorders. For this reason the proteasome has become a pharmacological target for cancer and neurodegenerative diseases[1] where opposite effects are desirable, inhibition and activation respectively.

Interestingly, accumulation of the ubiquitin-conjugated proteins, which have been tagged for degradation, but not efficiently degraded have been observed at advanced age in many tissues. Similar phenomena have been observed in many diseases such as Alzheimer, Parkinson, and other neurodegenerative disorders[2]. In-line with these data the efficiency of the UPS and the proteasome in particular decrease with age, which suggests a link between neurodegenerative diseases and UPS dysfunction. Ubiquitinylated protein accrual has also been observed in senescent cells (which accumulate with age) and maybe caused by dysfunction of the proteasome or the ubiquitinating/deubiquitinating machinery[3]. It has been suggested that activation of the proteasome core might be a potential strategy to minimize protein homeostasis deficiencies underlying aggregation-related diseases, such as Alzheimer's and Huntington's disease[4]. Therefore, stimulating proteasome activity seems to be very promising as a therapeutic strategy for this type of pathology.

It is also known that multiple hallmarks of cancer such as replicative immortality, apoptosis resistance, and increased proliferation, are clearly dependent on the proteasome and UPS. For this reason proteasome inhibition is a very promising anti-cancer therapy yet there are very few drugs available for this use.

Also, despite the initial success of these treatments competitive proteasome inhibitors have severe side effects and specific cancers show resistance to these drugs.[5]

For this reason scientists are trying to develop new inhibitors, which can act as proteasome allosteric modulators, because this class of compounds could offer several advantages. Allosteric modulators have the potential for greater specificity and reduced side effect profiles.

Another promising anti-cancer therapy could emerge from promiscuous proteasome inhibitors, which target both the proteasome, as well as other known cancer viability pathways such as pro-growth, anti-apoptotic, and cell cycle pathways (*multi-target molecule*).

Porphyrins are excellent candidates for multi-target molecules because:

1. Cationic porphyrins are proteasome inhibitors.

2. Porphyrins inhibit the activity of telomerase, an enzyme responsible of the telomeric elongation. Porphyrin's can stabilize the telomeric G-quadruplex structure by capping it, which subsequently decreases cancer cell growth[6].

3. These molecules are already in use as an anticancer treatment for PDT[7] and BNCT[8].

4. They are natural products present in our bodies (heme in hemoglobin) and therefore do not cause problems in terms of biocompatibility.

5. They have a very versatile chemistry. In fact, porphyrins are unique molecules; their extended π system leads to a remarkably high extinction coefficient making them highly hydrophobic. Moreover, fictionalization (mainly at the meso-positions) with charged substituents makes them water-soluble; the number and reciprocal dispositions of charged peripheral groups allows, in turn, to modulate their tendency to (self-) aggregate.[9,10]

Porphyrins can be regarded as polytopic complexing agents because, in addition to the chemistry related to the periphery (which is tunable in terms of number, nature, and reciprocal disposition of substituents), the central core also has a manifold role in determining their physicochemical behavior.[11,12]

In fact, besides protonation, insertion of different metal ions in the four-nitrogen core, gives additional control of the spectroscopic features (especially concerning the emission properties) and permits us to tune the interactions of these macrocycles with templates, as well as their self-assembly processes.

Moreover, there is increasing interest for natural compounds with medicinal properties termed nutraceuticals within the scientific community. Natural products have been the source of most active ingredients in medicine; for this reason, more than 80% of drug substances were natural products or inspired by a natural compound. In particular, molecules such as quercetin[13], resveratrol[14], epigallocatechin-3-gallate (EGCG)[15]. It has been shown that consumption of fruits and vegetables containing these compounds reduces the risk of cancer by inhibiting proteasomal activities. Derivatives of cinnamic acids are ubiquitous in plants and foods (i.e., fruits, vegetables, coffee) and have been identified as interesting compounds with antioxidant, anti-inflammatory and cytotoxic properties[16].

This research project is centered around the proteasome, with a particular emphasis on the interaction between porphyrins/porphyrinoids and this multi-proteolytic system.

Finally, we have begun to investigate the anti-proteasomal activity of a new class of bio-inspired natural compound derivatives.

These studies have been carried out using different approaches and techniques: spectroscopic, computational, imaging-microscopy (AFM), molecular/cell biology.

Chapter 2 - State of the art

2.1 Proteasome

The ubiquitin–proteasome system (UPS) is the major cytosolic proteolytic system in prokaryotes and eukaryotes[17] with critical functions in cell cycle control, apoptosis, inflammation, transcription, signal transduction, protein quality control, then it also responsible to eliminate defective proteins and it determine the half-life of every protein in cell.[18]

The end point of the UPS is the 26S proteasome, an endoprotease of about 2.5 megadaltons that functions primarily to degrade proteins that have been modified by the attachment of ubiquitin.[19] (**Figure 1**)
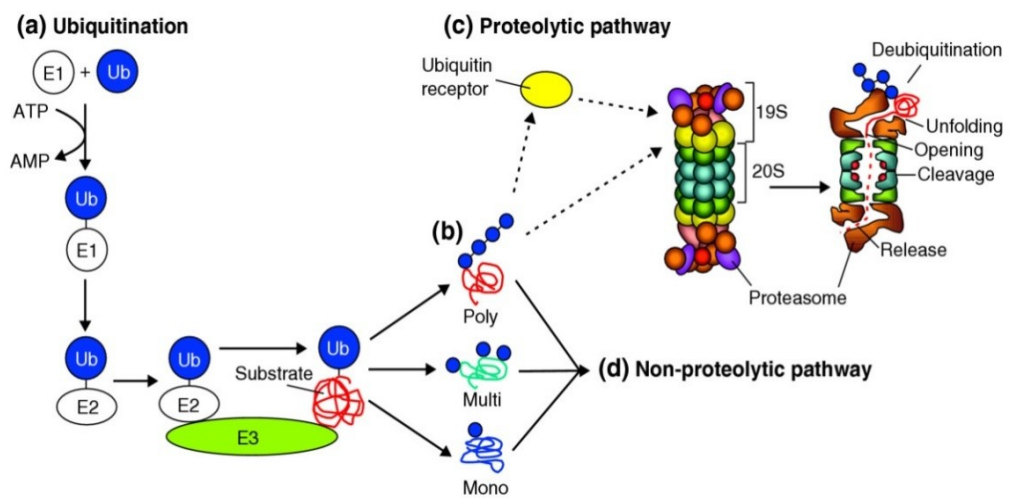
Figure 1: UPS behavior.

Proteasome 26S consist of a barrel-shaped 20S core particle (CP) capped by one or two 19S Regulatory Particles (RP).[20]

The core particle (CP), 20S proteasome, is a tube-shaped complex of 28 subunits arranged in four hetero heptameric rings. According to the crystal

structure models of yeast and mammalian 20S proteasomes, the diameter of the cylinder is nearly 12 nm, and the length approaches 16 nm[21] . It is made of four rings with seven members each: two external α-subunits rings (antechambers) and two central β-subunits rings (catalytic chamber).[22,23]

In the catalytic chamber there are two duplicates of three different proteolytically active β-subunits: β1, β2 and β5, exhibiting caspase- (CP-L), trypsin- (T-L) and chymotripsin-like (ChT-L) activity, respectively.[24,25,26]

In the α face there is a swinging gate which is responsible of the substrate entrance which in this way is able to arrive to the catalytic chamber (**Figure 2).**
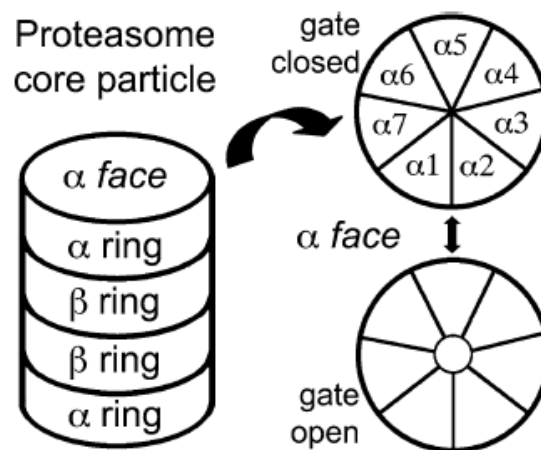
Figure 2: Diagram of eukaryotic core proteasome particle (20S proteasome) and the α face in which there is the swinging gate[27] .

The gate is built from short N-terminal sequences of α subunits[28].

The conformation of the gate: closed or open (**Figure 3**), determines if the core proteasome is in the "latent" or "activated" state, prohibitive or receptive to the uptake of substrates[29].
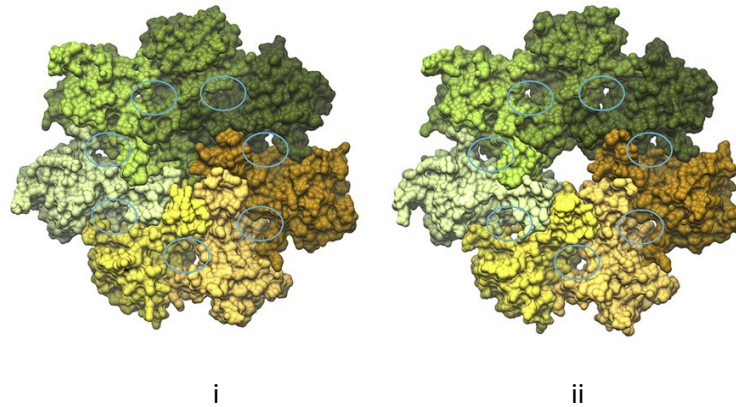
Figure 3: Top view of the α rings for closed (i) and open (ii) CP configurations. The intersubunit clefts where C termini of many proteasome regulators dock, including the regulatory particle (RP), are circled [30].

The diameter of the gate, which is about 2 nm, defines the nature of substrate polypeptides: they need to be unfolded or at least have a poorly organized structure to fit into the narrow opening[31].

The gate movements are regulated by two processes: "from the inside" and "from the outside"[32].The first one doesn't require additional protein cofactors and it's an example of allostery[33].

In fact, the active sites send an allosteric signal to the gate and a gate opening is obtained thus making the proteasome ready to accept the substrate molecule.[33]

The signal for gate opening in the latent proteasome may still originate in the active center, perhaps as a result of the reorganization of water molecules and hydrogen bonds around the catalytic threonine[33].

Polypeptide are able to enter in the native latent core particle because the 20S constantly switches between the closed-gate and open-gate states[32,33]. The more stable closed-gate conformation prevails and is more abundant than the open-gate conformation. However, even less abundant, the amount of 20S with open gate is sufficient to accept a substrate and to activate the allosteric feedback loop[34].

The "from the outside" or extra molecular path of gate opening provides an excellent example of protein-protein interaction. The ring is not only a receptor

of allosteric signals from the catalytic chamber; in fact it's used as platforms for the attachment of protein complexes which are able to modulate the core particle activity, forming "proteasomal assemblies" (**Figure 4**)[35]. A closer inspection of α-face reveals the presence of shallow grooves between the subunits[36] (**Figure 3**) which serve as anchor pits for all the known regulatory modules.

The best-known and most physiologically relevant module is a 900 kDa heteromultimeric protein complex called regulatory particle (RP) or 19S cap[37]. The architecture of RP was revealed using cryo-electron microscopy imaging, X-ray diffraction modeling and affinity mapping[38] .

How previously said, the core can be capped by two 19S complexes; however a single 19S assembly is sufficient for bestowing the ability to process polyubiquitinated substrates to the proteasome, and for general increase of the enzyme's activity.

The 26S proteasome is the most structurally and functionally advanced form of the proteasome.

Thus, the assembly of the mature 26S proteasome is a tightly regulated and reversible process which leads to conformational changes displacing α subunit tails and opening the gate[39]; however, it's not still well known the mechanistic features of the process.
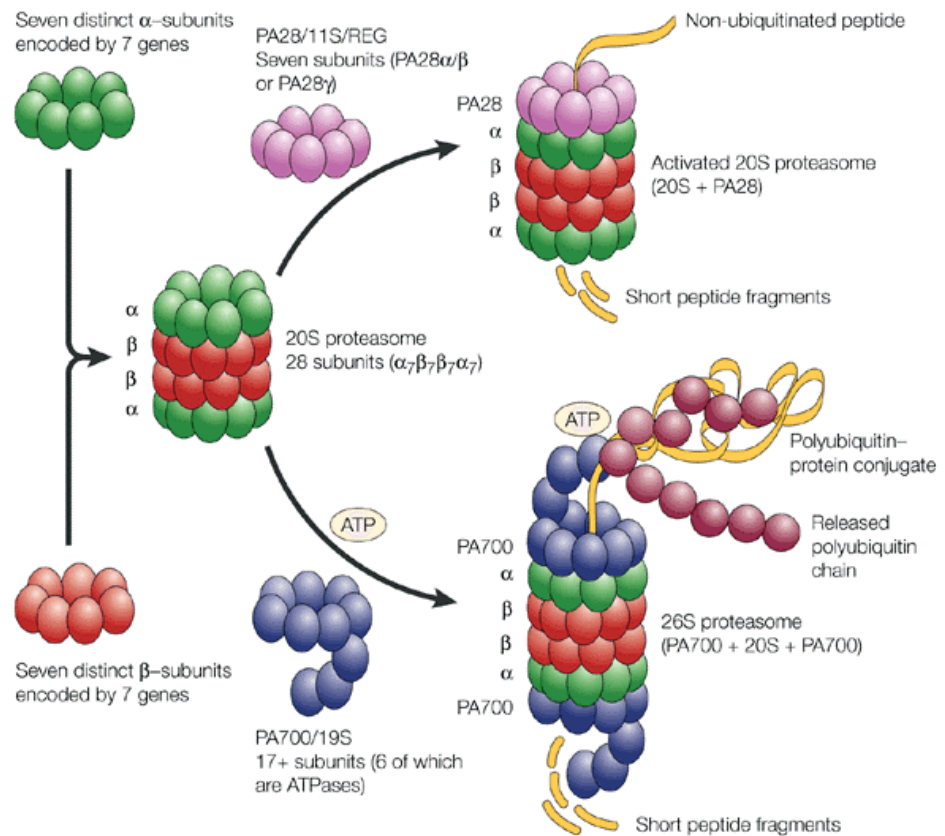
Figure 4: Proteasome assembly - *Left :* 20S CP composed by seven β-subunits (with two duplicates of three different proteolytically active β-subunits) and seven different α-subunits which anchor different regulatory complexes: 19S (PA700)(*right, below*) or PA28 (11S/REG) (*right, upward*) [40]

Instead, it's know that the peptidase activity of eukaryotic CP can be activated by a variety of treatments;[41] for example, exposure to low levels of sodium dodecylsulfate (SDS).

Moreover, It was shown that the nine residual tails (GSRRYDSRT) from the N-terminus of the α3-subunit are important for the function of the CP. The importance of the tails in the function of CP is indicated by the remarkable evolutionary conservation of these sequences across eukaryotes. Of the seven tails the one in α3 subunit is unusual and its rearrangement is fundamental for opening of an axial channel and its deletion cause a structural perturbation. Actually, the deletion of the α3 tail (artificial modification which allow to obtain a "mutant" α3ΔN 20S proteasome) has little effect on peptide hydrolysis by

the 26S proteasome; instead the principal in vitro effect is to activate the free CP from the repressed state that it exhibits in its free form.[42]

(a)   (b)
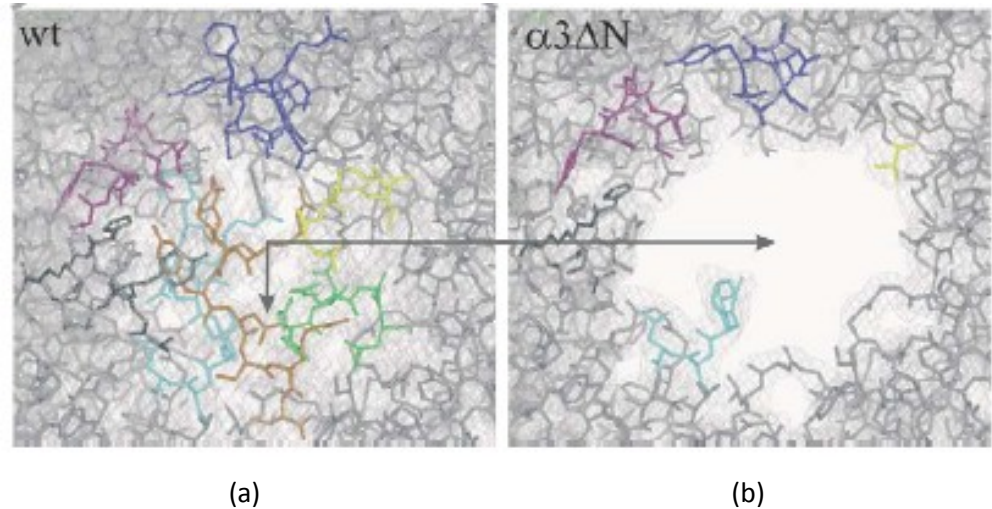
Figure 5 : Electron density maps (colored in gray) of the yeast core particle (gray sticks) from (a) wild type and (b) α3ΔN. The maps are contoured at 1σ, with $2F_O–F_C$ coefficients after two-fold averaging. Each N-terminal tail of the α-subunits is drawn in a specific color. Asp9 of subunit α3 plays a key role in the stabilization of the closed state of the channel and is marked with a black arrow. Mutagenesis within this residue generates an axial channel (b) whose dimensions are comparable to the archaeal CP channels[43].

Therefore, the properties of the mutant proteasome α3ΔN reflect the general properties of core particles in an open / semi-open channel state.

2.2 Proteasome activation

How previously described, excessive accumulation of the Ub-conjugates is observed in many pathological conditions such as Alzheimer, Parkinson and other neurodegenerative disorders. Accumulation of ubiquitinylated proteins in senescent cells may be caused by dysfunction of the proteasome or the ubiquitinating/ deubiquitinating machinery, or both[44]. For example, in the

human fibroblast model peptidase activities and levels of proteasome subunits decreased during replicative senescence[45]. Consequently, a partial proteasomes inhibition resulted in accelerated senescence in fibroblasts[46]; instead, an over expression of proteasome catalytic subunits helped the fibroblasts to overcome effects of cellular stressors[47].

It has been shown that the involvement of the UPS in neurodegeneration is indisputable, but the exact role of this system in neurodegenerative diseases it's not known yet[48].

For example, in Alzheimer's disease a reduced proteasome activity is detected in the brain regions affected by Alzheimer and it was reported that oligomers of $A\beta(1-40)$ and $A\beta(1-42)$ significantly decreased all three proteolytic activities of the 20S proteasome in a dose-dependent manner[49]. Moreover, both $A\beta$ peptides are degraded by the proteasome *in vitro*. Therefore, the proteasome activity block causes an increase in the intracellular $A\beta$ level[50].

It has been shown that also the paired, helical filaments of *tau* protein can impair the proteasome function, mostly in the areas crucial for long term memory formation[50]. Moreover, *in vitro* and *in vivo* studies confirmed that proteasome inhibition results in *tau* accumulation[51].

Amyotrophic lateral sclerosis (ALS) is characterized by motor neurons degeneration resulting in a progressive paralysis, atrophy of devastated muscles and severe disability. In 5-10% of patients, the disease occurs in the familial form, in which mutated copper-zinc superoxide dismutase 1 (SOD1) forms aggregates[52].

It was shown that with a pharmacological inhibition of the proteasome (with MG-132) the number of aggregates significantly increases[53]. In turn, the misfolded SOD1 mutant is able to arrest the proteasome activity, expecially in motoneuronal cells[54]. Recently it have been found that small pyrazolone molecules have the effect of activating the proteasome. The results presented provide strong evidence that the mode of action by which pyrazolone-containing compounds is through direct binding to constituent proteins of the 26S proteasome[55].

Moreover, the literature reveals another one small molecule compound which have the effect of activating the proteasome. This compound acts by inhibiting USP14, a proteasome-associated deubiquitinating enzyme that can inhibit the processing of ubiquitin−protein complexes destined for degradation by the proteasome. Inhibition of USP14, in turn, results in proteasome activation[56]. Such activation may be of significance in the protection against cellular dysfunction typical for aging and neurodegeneration.

2.3 Proteasome inhibition

A large number of studies have demonstrated that proteasome inhibition may represent a promising therapeutic strategy in the treatment of malignancies[57]. Proteasome inhibition causes the accumulation of misfolded proteins and reactive oxygen species[58,59,60,61] and, ultimately, the intensification of proapoptotic signals leading to cell-cycle interruption.[62]

Indeed, tumor cells divide and grow rapidly and this accelerated cell cycle needs to be managed by an increased capacity of the proteasome to degrade accumulating misfolded proteins. Therefore, proteasome inhibitors (PIs) mainly induce apoptosis in malignant cells, whereas healthy cells may better overcome this stress.[63]

Several compounds, both natural and synthetic, have been found to affect UPS functionality,[64] and some proteasome inhibitors are already efficient anticancer drugs.

Bortezomib is the first proteasome inhibitor that it was approved for clinical use in human cancers.[65] (**Figure 6**)

Figure 6: Bortezomib structure.

However, there are still many problems to be faced: i) relapse, as often cancer patients develop drug resistance, and ii) severe side effects. Accumulating evidence suggests that the challenge of developing new anti-cancer agents is to design molecules able to allow a finer regulation of proteasome and thereby potentially develop improved efficacy and safety profiles compared with Bortezomib.

In accordance with the hypothesis, the search of new molecules that may affect proteasome activity by binding outside of the active site may be regarded as a promising strategy; allosteric inhibition of proteasome may overcome resistance to competitive inhibitors, by a noncompetitive mechanism. There are already some promising molecules, such as chloroquine,[66] 5-amino-8-hydroxyquinoline (5AHQ), [67] and PR-39, an antimicrobial peptide found in pig intestine.[68,69]

In particular, experimental data suggest that PR-39 is a noncompetitive and reversible proteasome inhibitor.

Atomic force microscopy (AFM) studies demonstrate that 20S and 26S proteasome striated with PR39 or its derivatives exhibit serious perturbations in their structure and their normal allosteric movements[69]. This peptide binds to top of the antechamber and interferes with the CP-RP assembly preventing the formation of the mature 26S proteasome.

In fact, in AFM experiments, 26S complexes were typically found with one or two dragonhead-shaped 19S caps attached to the 20S core. After the treatment with PR39, they noticed a dramatic transition in the shape of the

molecules; an immediately lost features typical of the 26S complexes have been observed, giving the impression that two 19S caps almost touched each other with hardly recognizable 20S core[69]. Their hypothesis was that either the 19S caps partially dissociated or they vibrated too fast for recognition of 20S core and these findings fully correlate with the inhibition of 26S proteasome by PR39.

Despite the biochemical data collected so far for allosteric inhibitors are convincing, any advance of these results to the clinic treatment remains challenging and there is still an urgent need of novel compounds targeting the CP at regions distant from the active sites.

2.3.1 Enzymatic Inhibition Mechanisms.

Enzymes are attractive targets for drug therapy because of their essential roles in life processes. The function of enzymes is to accelerate the rates of reaction for specific chemical species. Substrate is a compound that became, thanks the enzyme action, a reaction products[70]. Chemical reaction, like enzymatic reaction, can be analyze by kinetic way for obtain information about reaction mechanism. The discussion above of enzyme reactions treated the formation of the initial *ES* complex as an isolated equilibrium that is followed by slower chemical steps of catalysis. This "rapid equilibrium"[70] model was first proposed by Henri (1903) and independently by Michaelis and Menten (1913). However, in most laboratory studies of enzyme reactions the rapid equilibrium model does not hold; instead, enzyme reactions are studied under steady state conditions. The term steady state refers to a situation where the concentration of *ES* complex is held constant by a balance between the rate of *ES* formation[70] (by association of the free enzyme and free substrate) and the rate of *ES* complex disappearance (through dissociation back to the free reactants and by forward progress to form products)[70]. The rate, or velocity, of an enzymatic reaction, measured either as the disappearance of substrate or the formation of product, is proportional to the concentration of *ES* complex as:

$$E + S \xrightleftharpoons[K_S]{} ES \xrightarrow{k_{cat}} E + P \qquad v = \frac{-d[S]}{dt} = \frac{d[P]}{dt} = k_{cat}[ES]$$

The condition of constant ES is experimentally achieved by having a large molar excess of substrate over enzyme concentration, so that there is a relatively constant pool of substrate available to bind of the free enzyme[70].

The fundamental enzymatic equation is "*Michaelis-Menten equation*":

$$V = \frac{V_{max}[S]}{K_M + [S]}$$

V_{max} and K_M can be obtained using plots where reaction velocity is in function of substrate concentration (**Figure 7**).
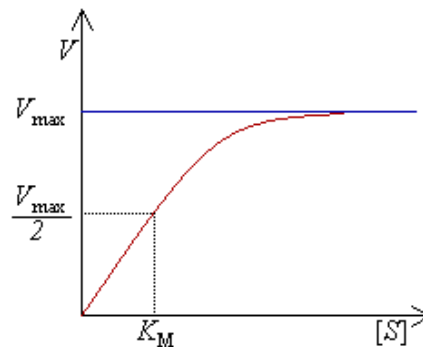
Figure 7: Graph of reaction velocity in function of substrate concentration.

The term V_{max} refers to the maximum velocity obtained at infinite substrate concentration. K_M is the substrate concentration that yields a velocity equal to half of the maximum velocity.[70]

Stated another way, the K_M is that concentration of substrate leading to half saturation of the enzyme active sites under steady state conditions. This constant is specific for each emzyme-substrate complex and depends on temperature or pH[70].

The term K_M relates mainly to the dissociation reaction of the encounter complex *ES* returning to *E* + *S*. Conversely, the reciprocal of K_M (1/K_M) relates to the association step of *E* and *S* to form *ES*[70].

It's possible show Michelis-Menten equation in other way:

$$\frac{1}{V} = \frac{K_M}{V_{max}[S]} + \frac{1}{V_{max}}$$

It is possible obtain a double-reciprocal graph, where 1/V is in function of 1/[S] (**Figure 8**).
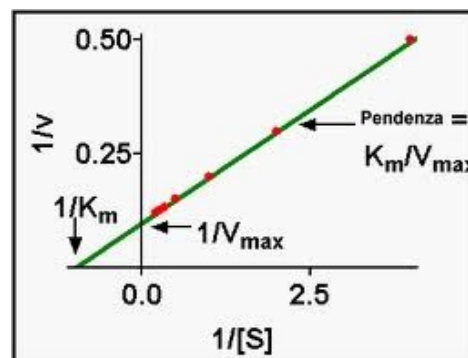
Figure 8: Double Reciprocal Graph.

This type of graph is useful for understand the inhibition mechanisms. Hence, like other protein ligand equilibrium, we can quantify such enzyme–inhibitor binary complexes such as an equilibrium dissociation constant (given the special symbol K_i for enzyme inhibition)[70] **(Figure 9a).**

There are three types of inhibition mechanism: Competitive (A), Noncompetitive (B) and Uncompetitive (C)[70] **(Figure 9b)**.
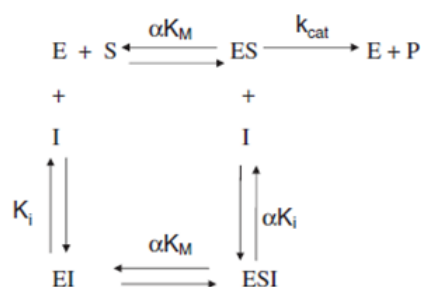
(a)
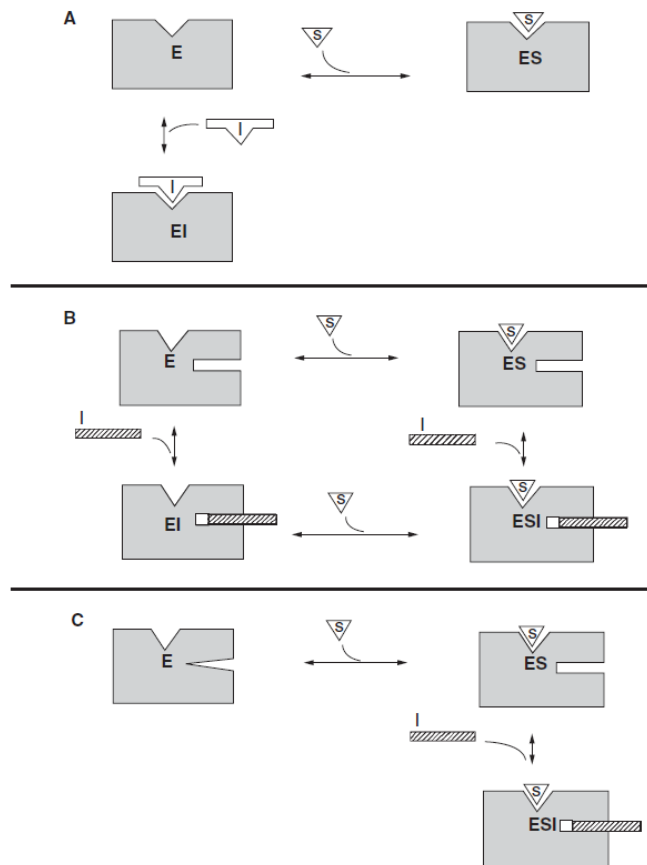
(b)

Figure 9: a) Equilibrium scheme for enzyme turnover in the presence and absence of reversible inhibitors. **b)** (A) Competitive Inhibition; (B) Noncompetitive Inhibition; (C) Uncompetitive Inhibition[70].

Competitive Inhibition

An inhibitor that binds exclusively to the free enzyme (i.e., for which $\alpha=\infty$) is said to be competitive because the binding of the inhibitor and the substrate to the enzyme are mutually exclusive; hence these inhibitors compete with the substrate for the pool of free enzyme molecules[70].

The presence of a competitive inhibitor thus influences the steady state velocity equation as described by following equation:

$$v = \frac{V_{max}[S]}{[S] + K_M\left(1 + \dfrac{[I]}{K_i}\right)}$$

If we were to plot the velocity as a function of substrate at varying concentrations of a competitive inhibitor (**Figure 10a**), we would obtain graphs such as those shown in Figure The value of V_{max} is constant at all inhibitor concentrations, but the apparent value of K_M (defined as $K_M(1 + [I]/K_i)$) increases with increasing inhibitor concentration.

The effects are perhaps most apparent in the double reciprocal plot (**Figure 10b**) where the intercept value (i.e., $1/V_{max}$) is constant but the slope (K_M/V_{max}) and x-intercept ($-1/K_M$) values of the line change with inhibitor concentration[70].

(a)   (b)
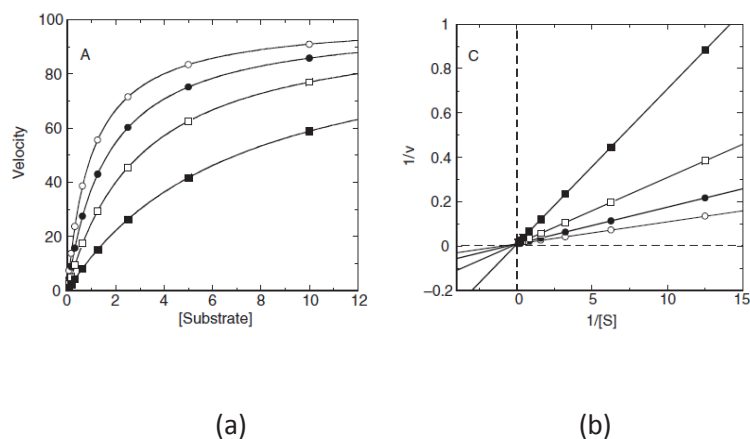
Figure 10: Substrate titration of steady state velocity for an enzyme in the presence of a competitive inhibitor at varying concentrations. (**a**) Untransformed data;(b) plotted in double reciprocal form[70].

Because competitive inhibitors bind to the free enzyme to the exclusion of substrate binding, it is easy to assume that this results from a direct competition of the two ligands (substrate and inhibitor) for a common binding pocket (i.e., the active site) on the enzyme molecule. While this is very often the case, it is not a mechanistic necessity. Inhibitor and substrate could bind to separate sites on the enzyme molecule that somehow exert a negative regulation on one another (i.e., through negative allosteric interactions, driven

by ligand-induced conformational changes)[70]. This type of negative regulation via allosteric communication between separate binding sites on a protein is well represented in biology, especially in metabolic pathways, in the form of feedback regulation. Thus, one cannot assume that because an inhibitor displays the kinetic signature of a competitive inhibitor that it necessarily binds to the enzyme active site.

Non Competitive Inhibition

A noncompetitive inhibitor is one that displays binding affinity for both the free enzyme and the enzyme– substrate complex or subsequent species. In this situation the binding affinity cannot be defined by a single equilibrium dissociation constant; instead, we must define two dissociation constants, one for the binary enzyme–inhibitor complex (Ki) and one for the ternary *ESI* complex (αKi)[70]. When the constant is unity, the inhibitor displays equal affinity for both the free enzyme and the *ES* complex. When α>1, the inhibitor preferentially binds to the free enzyme, and when α<1, the inhibitor binds with greater affinity to the *ES* complex or subsequent species[70].

Because noncompetitive inhibitors bind to both the free enzyme and the *ES*-complex, or subsequent species in the reaction pathway, we would expect these molecules to exert a kinetic effect on the $E+S \longrightarrow ES^{\ddagger}$ process, thus effecting the apparent values of both V_{max}/K_M (influenced by both the Ki and αKi terms) and V_{max} (influenced by the αKi term)[70]. This is reflected in the velocity equation for noncompetitive inhibition:

$$v = \frac{V_{max}[S]}{[S]\left(1+\dfrac{[I]}{\alpha K_i}\right) + K_M\left(1+\dfrac{[I]}{K_i}\right)}$$

The equation can be simplified further in the specific case where the inhibitor displays equal affinity for both enzyme forms (i.e., where α = 1, therefore Ki = αKi):

$$v = \frac{V_{max}[S]}{([S] + K_M)\left(1 + \dfrac{[I]}{K_i}\right)}$$

The double reciprocal plot (for noncompetitive inhibitors) display a nest of lines that intersect at a point other than the *y*-axis. This is a diagnostic signature of noncompetitive inhibition[70].

(a)   (b)
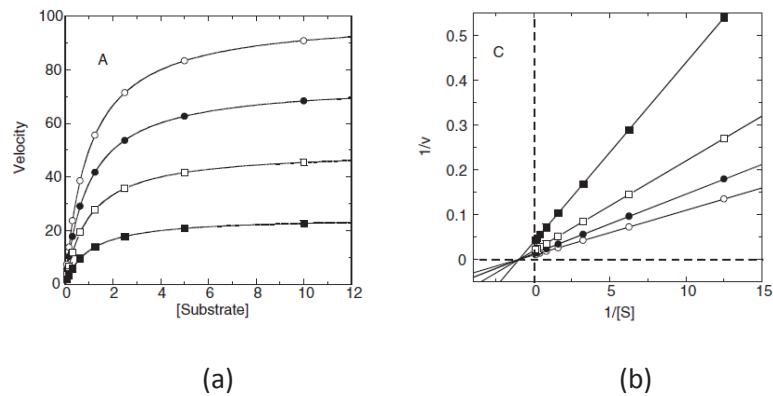
Figure 11: Substrate titration of steady state velocity for an enzyme in the presence of a noncompetitive inhibitor ($\alpha = 1$) at varying concentrations. (a) Untransformed data; (b) plotted in double reciprocal form[70].

The plot in **Figure 11b** was generated for an inhibitor with $\alpha = 1$, for which the nest of line converge at the *x*-axis. When $\alpha > 1$, the lines intersect above the *x*-axis of a double reciprocal plot, and when $\alpha < 1$, the lines intersect below the *x*-axis[70].

Uncompetitive Inhibition

An inhibitor that binds exclusively to the ES complex, or a subsequent species, with little or no affinity for the free enzyme is referred to as uncompetitive. Inhibitors of this modality require the prior formation of the ES complex for binding and inhibition[70].

One might then expect that these inhibitors would exclusively affect the apparent value of V_{max} and not influence the value of K_M[70]. This, however, is incorrect.

The velocity equation for uncompetitive inhibition is as follows:

$$v = \frac{V_{max}[S]}{[S]\left(1+\frac{[I]}{\alpha K_i}\right)+K_M}$$

Both V_{max} and K_M decrease with increasing concentration of an uncompetitive inhibitor, and these effects are clearly seen in Figure 11a. In the double reciprocal plot for uncompetitive inhibition (**Figure 12b**) the diminution of the apparent V_{max} is reflected in different y-intercept values for the different concentrations of uncompetitive inhibitor[70].


(a) (b)
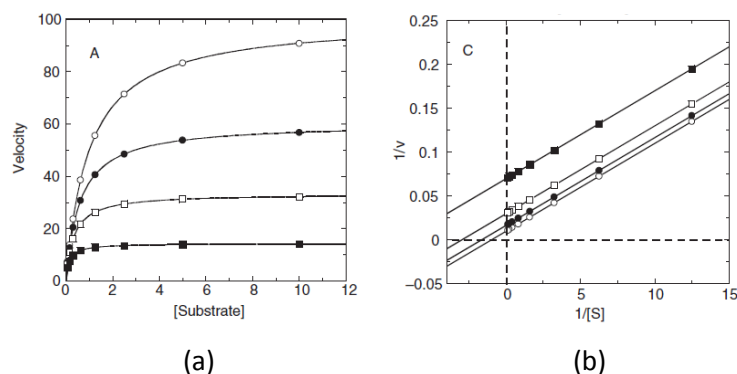
Figure 12: Substrate titration of steady state velocity for an enzyme in the presence of an uncompetitive inhibitor at varying concentrations. (a) Untransformed data; (b) plotted in double reciprocal form[70].

Therefore, the diagnostic signature of uncompetitive inhibition is a double reciprocal plot composed of parallel lines.

2.4 AFM study on Proteasome 20S.

Many proteins exist in more than one conformational state and exist an intrinsic dynamics which regulate allosterically many enzymes[71]. Allosteric transitions are known for many enzymes and these transitions induce nanometer-scale movements. Atomic force microscopy (AFM) imaging performed in a tapping mode (in liquid environment) is a very effective technique for real-time analysis of single protein molecules without disturbing their natural dynamics in order to get information about conformational diversity, allosteric transitions, and their coupling. For this reason, single 20S proteasome molecule can be detected and studied by AFM[27].

Here, a method that probes the conformational diversity and dynamics of 20S core particle using the AFM in liquid will be presented. Concerning the sample immobilization, the simplest and least invasive, is to let the particles electrostatically attach to the mica surface. Two different alignments of CP are possible. In the first case, the cylinder-shaped molecule is "standing" upright on its α ring (top view), allowing for direct observation of the gate status. In the second orientation, the particle is lying on its side (side view) and observation of the gate is not possible. To distinguish between these two orientations, it is necessary to measure the length (l) to width (w) ratio (l/w)[72] (**Figure 13**). In all experiments with yeast and human proteasomes, it has been found that the top-view particles are prevalent (>90%)[73].
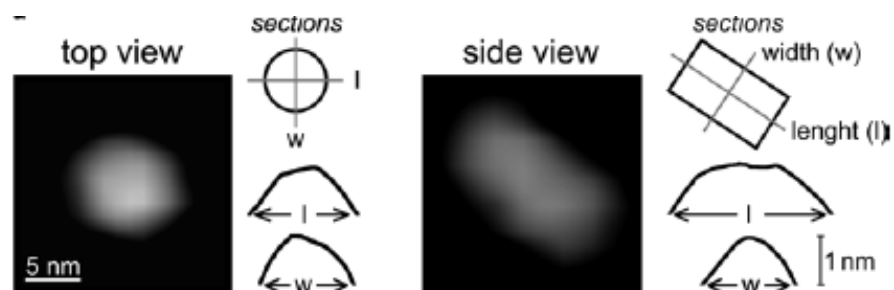
Figure 13: Two different 20S proteasome orientations: "standing" or in "lying". AFM topographs of typical particles in top-view ("standing"; *left*) and side-view ("lying"; *right*) orientations. Sections of the topmost parts of the particles accompany the topographs[27].

The particles (standing orientation) showed a cylinder diameter of about 8–12 nm and a cylinder length of 13–17 nm, which agreed well with crystallographic[74] and electron microscopic data[75].

Usually, the top-view particles with a "smooth" alpha ring surface are considered to have a closed gate. Instead, if the alpha ring surface has the "crater-like" appearance, the gate is presumed open; more in detail: if sections of a molecule performed in four different directions were all cone shaped, the particle should be considered closed. If all four sections are crater shaped (with a dip or hole surrounded by a higher-positioned rim), the particle is classified as open (**Figure 14**)[27].
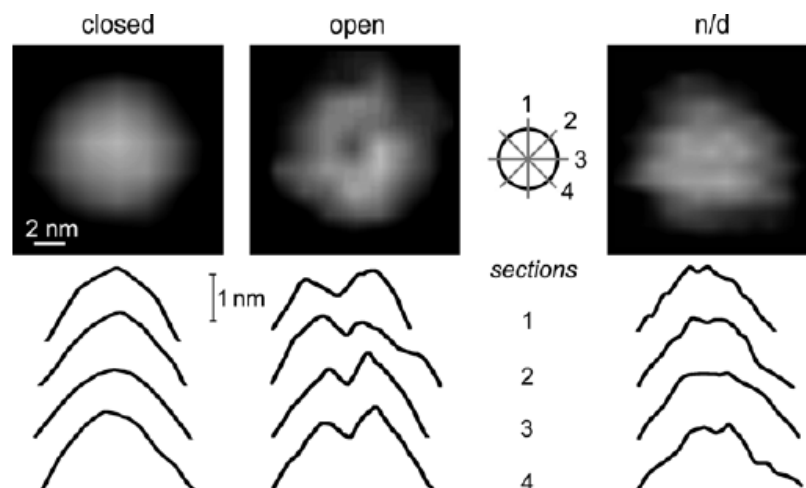
Figure 14: The AFM images of yeast core proteasomes show two stable conformations distinguishable by the shapes of sections through the topmost parts of their topographs. *Left* : the particle with a smooth and concave α face is classified as closed. *Middle* : the particle with a deep central opening in α face, prominent in all four sections, is labeled as open. *Right*: indistinguishable conformation - intermediate.[27]

It's possible to observe individual proteasomes to alternate between the open and closed states on the mica surface. Moreover, it was confirmed that approximately 25% of wild-type *S. cerevisiae* proteasomes imaged without addition of a ligand were in open state, instead, the 75% are in closed state (1:3 ratio)[76]. On the contrary, a ratio 3:1 of open-to-closed conformers has

been observed when a substrate is added for any of the three active centers. This allow to hypothesize that the catalytic act promoted channel opening [77].

It was shown that inactivation of each active site specifically disrupts the shift toward the open channel conformation normally induced by a peptide substrate specific to that site[33].

Moreover, certain proteasome inhibitors are able to generate a conformational switch.

In fact, the binding of bortezomib to the proteasome active center is able to generate an increase of open conformers in a dose-dependent manner (**Figure 15**).
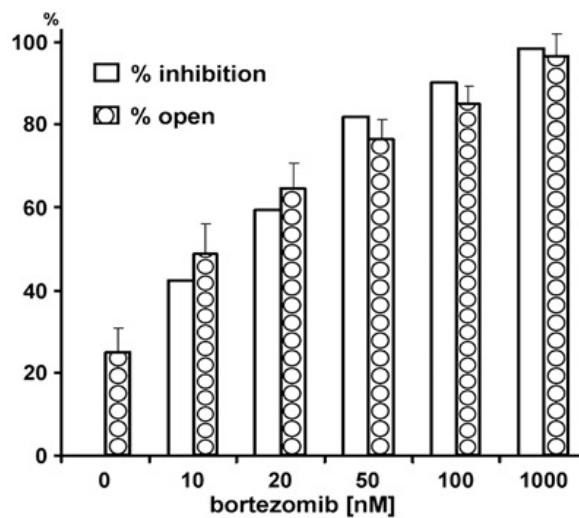
Figure 15: Proteasomes trited with bortezomib, which is able to induce the opening of the proteasome gate. The percentage of open particles (bars with white circles) increased with the increasing concentration of the inhibitor, while the ChT-L activity (white bars) decreased. Black bars represent means ± SD (n = 9 to 17 fields with 300 to 600 top-view particles). [33]

Boronic acid derivatives occupying the binding pocket, block directly the hydroxyl group and increasing the basicity of the catalytic amine in serine or threonine proteases (**Figure 16**).
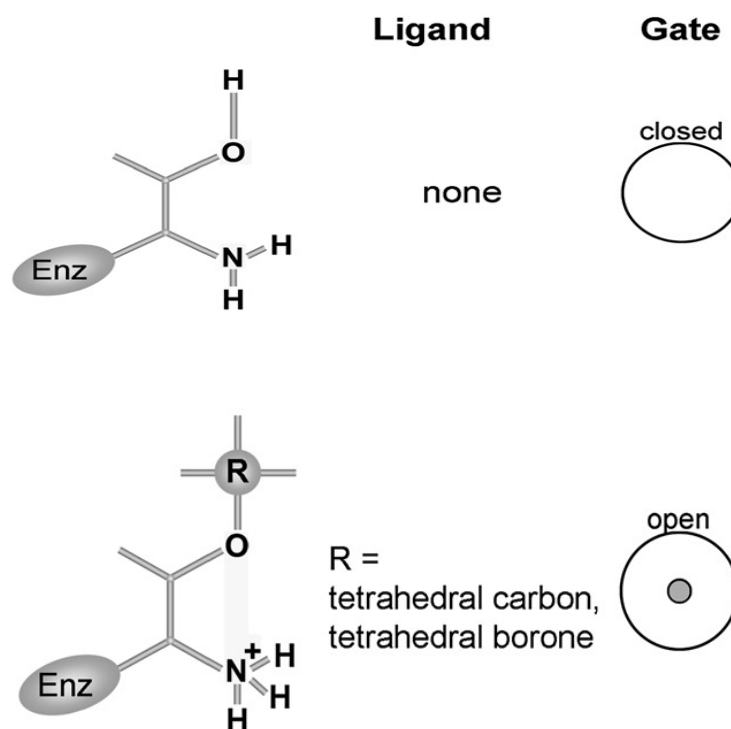
Figure 16: The shift toward open gate is noted when the α amine is blocked. *Left column*: Schematic representation of catalytic Thr1 without ligand an in presence of a ligand. *Middle column*: The ligand used. *Right column:* The prevailing conformation of the gate computed from AFM images[33].

The stable, anionic covalent adduct formed by boronic acids closely mimics the transition-state tetrahedral complex created during peptide bond hydrolysis[33]. These results suggest that formation of a tetrahedral transition state during peptide bond cleavage, which is mimicked by the boronic acid adduct, is linked to the conformational shift from closed to open proteasomes[33].

2.5 Porphyrins as proteasome's inhibitors.

In oncology, porphyrins find extended application such as photosensitizers in photodynamic therapy (PDT) for their light-absorbing properties, and some of them were approved for the treatment of certain cancers, especially in the area of dermatology.

Szokalska et al. observations[78] that demonstrated the cytotoxic effects caused by a porphyrinic photosensitizer, in PDT, could be potentiated through inhibition of proteasome, encouraged to scan the ability of porphyrins to inhibit the proteasome activity. Then in 2012 was published the first paper on the inhibition ability of cationic porphyrins on the proteasome 20S[79]. It was shown that micromolar amounts of porphyrins inhibiting, reversibly, all three main protease activities of the proteasome. In this first study was reported a screening including the tetra-cationic porphyrin (H2T4 - *meso*-tetrakis (4-N-methylpyridyl) porphyrin), the tetra-anionic porphyrin (H2TPPS - meso-tetrakis (4-sulphonatophenyl)-porphyrin) and tri and bi cationic substituents. (**Figure 17**)

	R₁	R₂	R₃	R₄	M
H2T4	A	A	A	A	2H
TrisT4	A	A	A	C	2H
cis-T4	A	A	C	C	2H
CuT4	A	A	A	A	Cu
ZnT4	A	A	A	A	Zn
MnT4	A	A	A	A	Mn
TPPS	B	B	B	B	2H
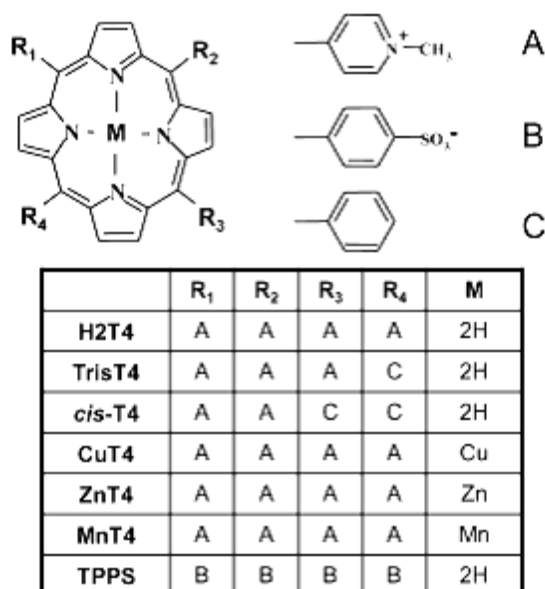
**Figure 17**: Chemical structure of all the porphyrin derivatives used in a preliminary study[79].

From the preliminary screening emerged the key rule that electrostatic effect is a driving force in the porphyin–proteasome interactions. In fact, any inhibition was observed in presence of the tetra anionic porphyrin (**Figure 18a**) and the inhibitory efficiency of the cationic macrocycles increase with the number of positive substituents (**Figure 18b**).

a   b
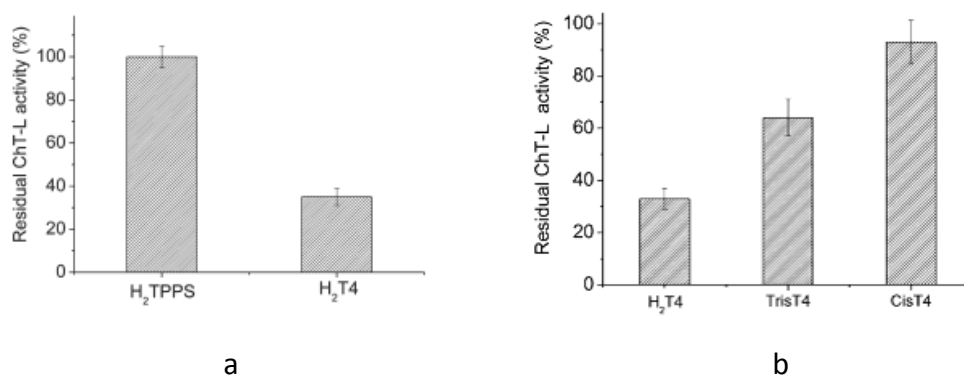
Figure 18: a) Residual chymotryptic-like activity of 20S proteasome in *cell lysates* in presence of H2TPPS and H2T4 at 1µM. Data are referred to control sample normalized to 100%. b) Residual chymotryptic-like activity of 20S proteasome in cell lysates with di-, tri- and tetra-cationic porphyrins at 1 µM. Data are related to control sample normalized to 100%[79].

Furthermore investigating various metallo-derivatives (**Figure 17**), which differ to the different propension of the central metal ion toward axial coordination, results that the naked cationic porphyrins are the most active and the molecule should be flat in order to interact effectively with proteasome.

In particular, a regular increase of inhibition of proteasome activity is observed going from hexa-(MnT4) to penta-coordinated (ZnT4) to planar (CuT4) porphyrins suggesting that axially coordinated water molecules get in the way of porphyrin–proteasome interactions (**Figure 19**).
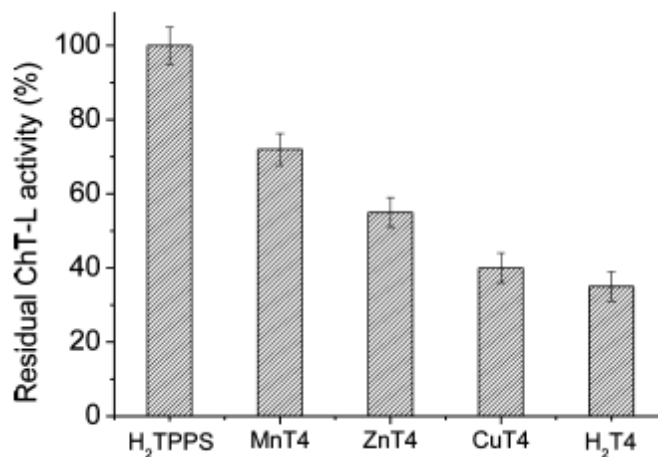
Figure 19: Residual chymotryptic-like activity of 20S proteasome in cell lysates with different metalated porphyrins (MnT4, ZnT4, and CuT4) at 1 µM. Data are referred to control sample normalized to 100[79].

These experiments, as the previous, underline the major activity of H2T4 with respect to all the other porphyrins.

A spectroscopic characterization of porphyrin–proteasome interactions by UV–vis spectra opened another prospective, identifying in porphyrins the new molecular "probes" .
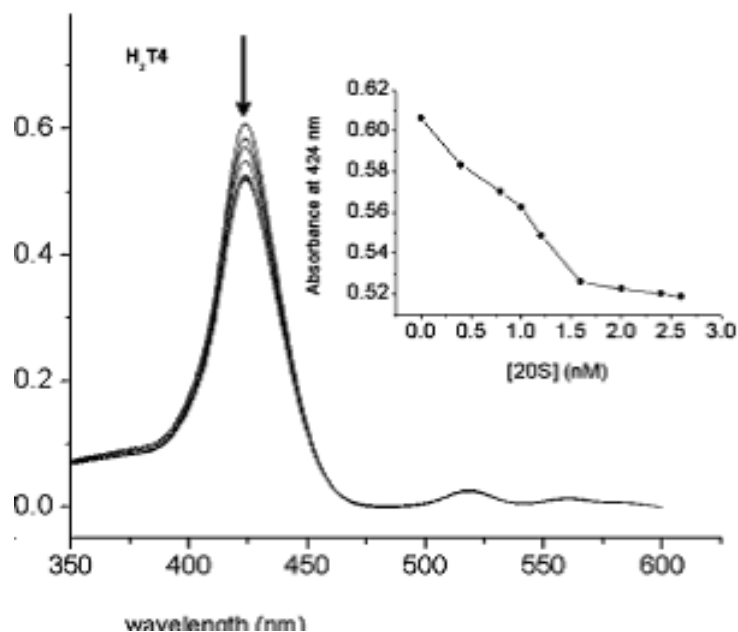
Figure 20: UV–vis titration of 4 µM H2T4 with increasing amounts of 20S proteasome. The insert reports a plot of the hypochromic effect vs proteasome concentration[79].

The ChT-L activity of the proteasome is mostly probed to evaluate proteasomal activity; in fact, previous reports suggesting that the chymotryptic substrate is the most proteasome-specific of those examined[80](**Figure 21**).
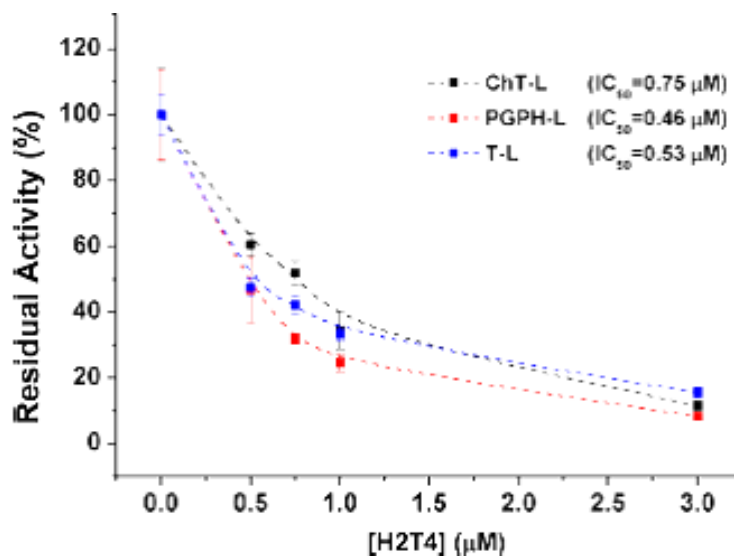
Figure 21: Concentration–response plot of H2T4 for Chymotryptic-like, Caspase-like, and Tryptic-like residual activities on 20S from cell lysates[79].

Moreover, it's known that uncontrolled heme exposure can cause acute kidney injury and endothelial cell damage[81]. Heme-triggered cell damage have been explored previously, with a focus on oxidative processes that can be catalyzed by free heme as well as on the activation of innate immunity receptors by the porphyrin.[82]

In addition to redox reactivity, heme may adversely alter cellular functions by binding to essential proteins and impairing their function.[83]

It was shown that high levels of intracellular heme disrupt cellular homeostasis by the combined activities of proteasome inhibition and oxidative damage[83]. In fact, in states of intracellular heme, excess proteasome inhibition acts in concert with the pro-oxidant activity of the iron protoporphyrin, resulting in the accumulation of damaged proteins that contribute to the triggering of cell death.[83]

These results encouraged us to continue the studies on this class of compounds.

# Chapter 3 -Experimental Session

3.1 Materials and Methods

3.1.1 Chemicals

Purified human 20S proteasome was purchased from Boston Biochem (Cambridge, MA, USA) and Enzo Life Sciences Inc. (Farmingdale, NY, USA). The fluorogenic substrates specific for the chymotriptic-like (ChT-L) proteasome activity (Suc-LLVY-AMC) and caspase-like (CP-L) proteasome activity (Z-LLE-AMC) were purchased from Boston Biochem (Cambridge, MA, USA).The T-L (Ac-RLR-AMC) substrate was purchased from Enzo Life Sciences Inc. (Farmingdale, NY, USA).

Muscovite mica in sheets was purchased from Ted Pella Inc. (Redding, CA, USA) Atomic force microscope (Multimode Nanoscope III a, Bruker; software version 5.1) equipped with a scanner suitable for nanometer/ micrometer-scale work (scanner E for Nanoscope III a) has been used. NP-ST oxide-sharpened silicon nitride probes ("tips") suitable for tapping (oscillating) mode in liquid were purchased from Bruker.
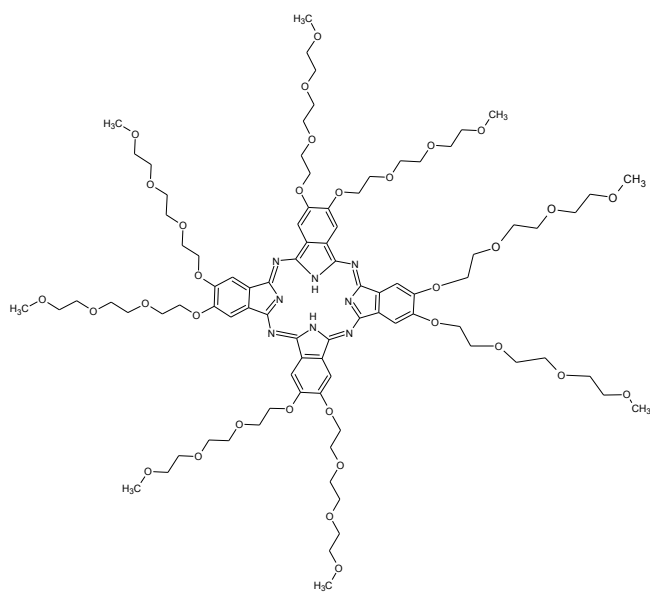
The meso-tetrakis(4-N-methylpyridyl) porphyrin (***H2T4***), mes*o*-tetra(2-N-metil-pyridyl) porphyrin (***ortho*-H2T4**), meso-tetra(3-N-metil-pyridyl) porphyrin (***meta*-H2T4**), the monophenyl-tri-(N-methyl-4-pyridyl)-porphyrin (***tris*-T4**), and the meso-tetrakis(4-sulphonatophenyl)-porphyrin (**H2TPPS**) were purchased from Midcentury. The meso-tetrakis [4-(4-N-methylpyridyl)-Phenyl]porphyrin (**pTMPyPP**) and the meso-tri(N-methylpyridyl) corrole (**TMPC**) were synthesized by Prof. Paolesse (Tor Vergata University, Rome) and coworkers. Phthalocyanine derivate (**FBPcG1**) was synthesized by Prof. T. Torres (Universidad Autónoma de Madrid). The 5-(4-carboxyphenyl)- 10,15,20-tris(Nmethylpyridinium)porphyrin- apidecin (**MTPyP-api**) was synthesized by Prof. M. Gobbo and coworkers (Padova's University). The meso (N-tetradecyl-

4-pyridyl) porphine (**TMPyP4-C14**) was obtained from Frontier Scientific Inc, Logan, UT, U.S.A (**Figure 23**).
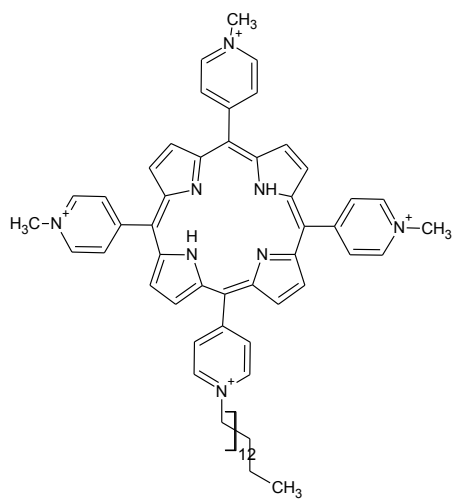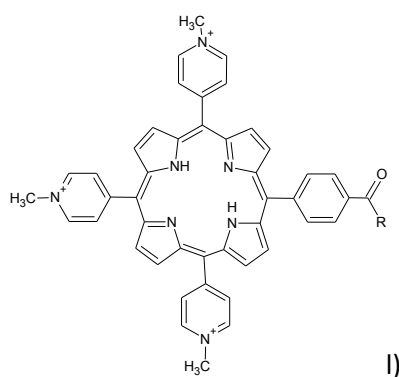

a)

b)

c)

d)

e)

f)

g)

h)

i)

31
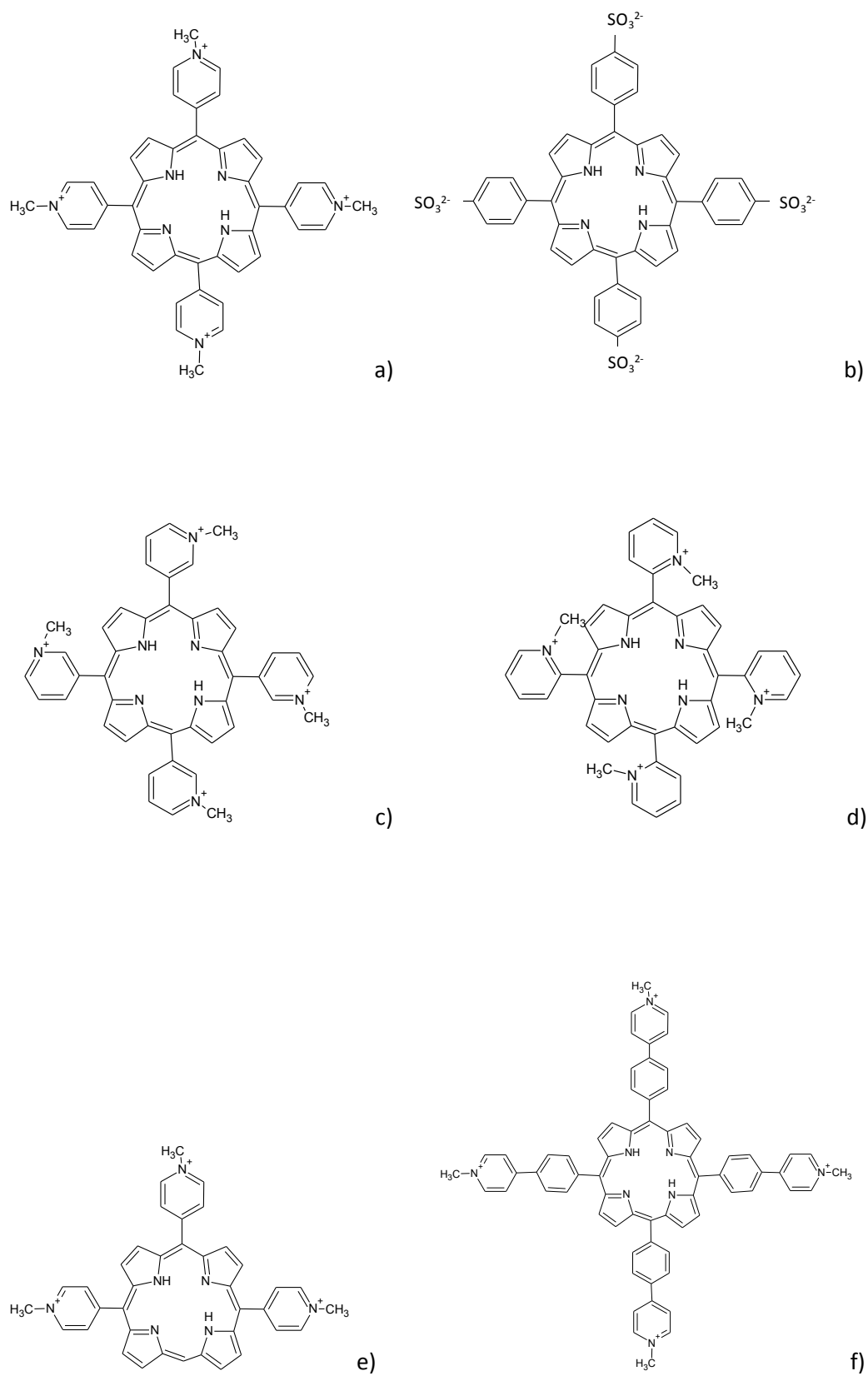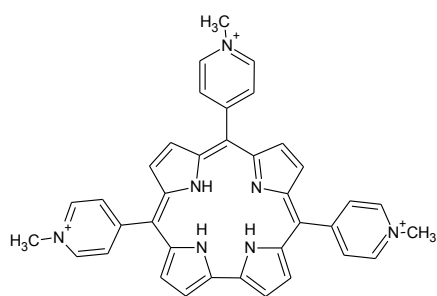
R = Gly-Asn-Asn-Arg-Pro-Val-Tyr-Ile-Pro-Gln-Pro-Arg-Pro-Pro-His(CH₃)-Pro-Arg-Leu-OH

l)

Figure 23: a) meso-tetrakis(4-N-methylpyridyl) porphyrin (**H2T4**); b) meso-tetra(2-N-metil-pyridyl) porphyrin (*ortho*-**H2T4**), c) meso-tetra(3-N-metil-pyridyl) porphyrin (*meta*-**H2T4**), d) meso-tetrakis (4-sulphonatophenyl)-porphyrin (**H2TPPS**), e) monophenyl-tri-(N-methyl-4-pyridyl)-porphyrin (**tris-T4**), f) meso-tri (N-methylpyridyl) corrole (**TMPC**); g) meso-tetrakis [4-(4-N-methylpyridyl)-Phenyl]porphyrin (**pTMPyPP**); h) Phthalocyanine derivate (**FBPcG1**); i) meso (N-tetradecyl-4-pyridyl) porphine (**TMPyP4-C14**), l) 5-(4-carboxyphenyl)- 10,15,20-tris (Nmethylpyridinium) porphyrin- apidecin (**MTPyP-api**).

Natural compounds derivatives was synthesized by Prof. Tingali and coworkers (Catania's University) (**Figure 24**).
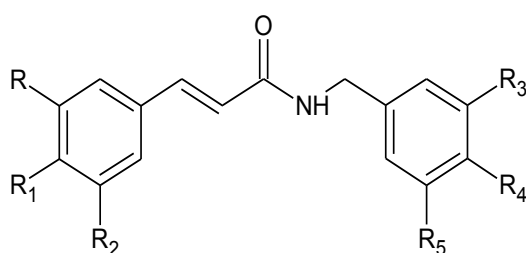
CT-E14= R: H, R1: OH, R2: OMe, R3: H, R4: Me, R5: H
CT-E15= R: H, R1: OMe, R2: OMe, R3: H, R4: Me, R5: H
CT-E12= R: H, R1: OH, R2: OH, R3: H, R4: Me, R5: H
CT-E16= R: H, R1: Me, R2: H, R3: OMe, R4: OMe, R5: OMe
CT-E21= R: OMe, R1: OH, R2: OMe, R3: OMe, R4: OMe, R5: OMe
CT-E23= R: H, R1: OH, R2: H, R3: H, R4: Me, R5: H
CT-E24= R: H, R1: OH, R2: H, R3: OMe, R4: OMe, R5: OMe

Figure 24: Structure of derivatives of natural compounds.

MCF7 cells were purchased from SIGMA. Proteasome-Glo™Cell Based Assay was purchased from PROMEGA.

3.1.2 Proteasome activity assays

The assays were performed in vitro using purified 20S proteasome, with the activity of each subunit of the proteasome (2 nM) assessed upon incubation in assay buffer (**Buffer**: HEPES 25mM, EDTA 0,5mM pH=7.6) for 30 min at 37 °C with increasing concentrations (0.5 - 10 µM for porphyrin and porphyrinoid compound and 1-10 µM for natural compounds derivates) of inhibitor and subsequently added to the AMC-labeled substrate peptide (100 µM).

The activity assays for yWT20S CP and its mutant α3ΔN were performed in buffer 100 mM Tris/HCl pH 8 and NaCl 6 mM.

Proteasome activity is monitored by measuring AMC fluorescence at 440 nm (excitation at 360 nm) for 20 min, using a fluorescence plate reader (Multiskan, Thermo) in 384 multiwell black plate. A minimum of three replicates were performed for each data point. Fluorescent substrate cleavage by the 20S proteasome was linear during this incubation time frame. The slope of the emission of AMC at 440 nm increases with time and it is correlated to proteasome activity (**Figure 25**); black line is a control (non inhibited 20S),instead other lines are 20S with increasing quantity of inhibitor (e.g. H2T4 - line red, green, blu and light-blue).

Decreasing slopes are proportional at H2T4 (inhibitor) concentration, and indicate that there is a fluorophore (AMC) decreasing.
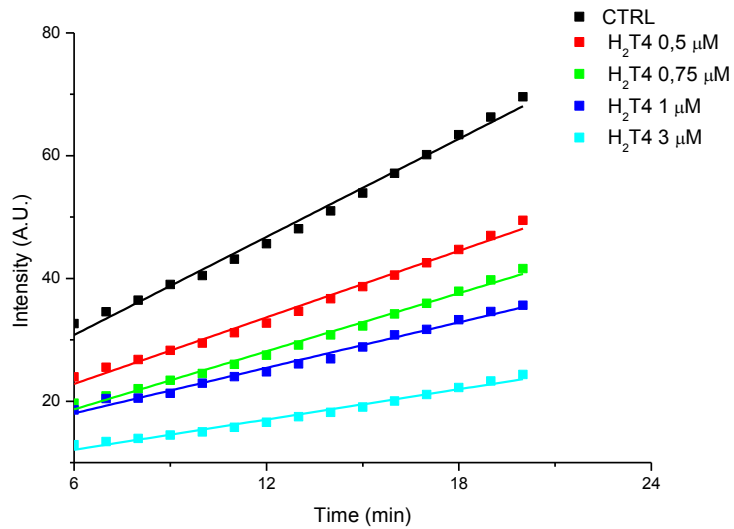
Figure 25: Fluorescense intensity at 440 nm vs time; each line indicate a specific inhibitor (i.e. H2T4) concentration, from 0 (black line) to 3 μM (light-blue line).

Data are expressed as normalized percentages of residual activity considering the slope of the control (fluorogenic peptide/proteasome in the absence of inhibitors) as 100% of proteasome activity.

Dose-response plots of the residual proteasome activity, in presence of increasing inhibitor concentration, provide a quantitative estimate of its potency.

The calculated residual activities were plotted against the logarithm of the applied inhibitor concentration and fitted to the equation

$$v(\%) = 100 \times \frac{IC_{50}}{[I] + IC_{50}} = \frac{100}{1 + 10^{(\log[I] - \log IC50)}} \; ;$$

GraphPad Prism 5 software was used.

The IC_{50} is defined as the concentration of the inhibitor, which causes 50% reduction of activity and it is thus calculated from the x-axis value of the dose−response plot occurring at a fractional activity of 50%.

3.1.3 Kinetic assays (Inhibition Mechanism)

Proteasome activity assays were performed in vitro by mixing 20S proteasome (2nM) with different concentrations of an AMC-labeled substrate peptide (*i.e.,* Suc-LLVY-AMC) in the assay buffer (**Buffer***: HEPES 25 mM, EDTA 0,5mM pH=7.6) at 37 °C, monitoring the released AMC fluorescence at 440 nm (excitation at 360nm) for 20 min, using a fluorescence plate reader (Multiskan, Thermo) in a 384 multiwell black plate. A minimum of three replicates was performed for each data point. The slope of the emission of AMC at 440 nm increases with time and it is correlated to proteasome activity (see below). Data have been analyzed by a double reciprocal Lineweaver-Burk plot and using Michelis Menten model (GraphPad Prism 5).

3.1.4 Wild Type proteasome purification from yeast

Yeast blocks of *S.cerevisiae* were dissolved in Lysis Buffer (LysB) (50mM potassium phosphate, pH 7,5,). A spatula of DNAse is added and stirred for 15 min. The yeast cells were lysed in a French press using a pressure of 2,400 psi. Cell debris was removed by centrifugation at 6X140 g for 30 min. The supernatant was transferred to a 500-ml beaker and 30% saturated Ammonium Sulphate was added. The lysate mixture was filtered to remove fatty acid and lipid[84].

Phenyl-Sepharose TM 6 Fast Flow: Flow rate for this column was maintained at 5ml /min. Column was equilibrated with two-column volumes of Buffer A (20mM potassium phosphate, pH 7,5 and 1M $(NH_4)_2SO_4$).
Lysate mixture was added to the equilibrated chromatographic column which after was washed with 1-3 column volumes of Buffer B (20mM potassium phosphate, pH 7,5). Protein elution was performed at linear gradient using 0-100% of Buffer A to Buffer B in four-column volumes[84]. The eluate was

collected in 12mL fractions. Column was washed with one-column volume of Buffer B.

Fractions collected were tested for proteasome activity through a fluorogenic assay. In fact, 29µl of each fraction was pipetted into a well of 96 well plates (Fluoro Nunc). One microliter of 10nM Y-substrate was added to each well and incubated for 30' at 37° C. Fluorescence was measured. The selected fraction were pulled and applied to the following column.

Before to start with second chromatographic process, the Ammonium Sulphate was removed by dialysis (three times)[84].

Hydroxyapatite Column: The flow rate was maintained at 4ml/min. Column was equilibrated with 20mM Potassium Phosphate pH 7,5 Buffer A. Mixture was added to the column which was washed with Buffer A. Protein elution was performed at a linear gradient of 0-50% of Buffer A to Buffer B (130mM of Potassium Phosphate, pH 7,5)[84]. The eluate was collected in 5mL fractions. Column was washed with one-column volume of 100% Buffer B. Fractions collected were tested for proteasome activity through a fluorogenic assay as above[84].

Resource Q column: The flow rate was maintained at 2ml/min. Column was equilibrtated with two-column volumes of Buffer A (20mM Tris/HCl pH 7,5). Combined fractions are added to the equilibrated column which after was washed with 1-3 column volumes of Buffer A[84]. Protein elution was performed at linear gradient of 0-50% of Buffer A to Buffer B (20mM Tris/HCl, pH 7,5 with 1M NaCl) in ten-column volumes. One milliliter fraction was collected and a fraction analysis was carried out according to previous described procedure (Fluorescence assay).

An SDS-PAGE was performed for the active fractions[17].

HiPrep^TM 26/10 Desalting Column: The flow rate was maintained at 2ml/min. Column was equilibrated with two-column volumes desalting buffer (DS: 20mM Tris/HCl pH 7,5 with 1M NaCl). Combined fraction were added to the

equilibrated column and one microliter fractions were collected. Column was washed with DS and an SDS-PAGE analysis was performed.

Proteasome will be stored at 4°C and avoid proteasome freezing[84].

3.1.5 α3ΔN (mutant proteasome) sample preparation from yeast.

The α3ΔN mutant was generated in previous experiments by the plasmid shuffle procedure[85]. Mutant yeast strains were grown in 18 I YPD (yeast extract peptone dextrose) cultures for 2 days at 30°C. Cells were harvested by centrifugation for 15 min at 5,000g and frozen at -20°C. These will be used as start sample for a new proteasome purification.

3.1.6 Atomic Force Mycroscopy (AFM) experiments

20S proteasomes (Enzo, Calbiochem) and buffer for proteasome dilution and imaging (50 mM Tris–HCl - pH 7) have been used for the AFM experiments. These experiment have been carried out using an Atomic Force Microscope with the tapping mode in liquid capability how reported in literature[27].

More in detail, proteasomes (3 µL), diluted to a concentration of about 5 nM (in such concentration an image of dispersed particles on mica should be produced), have been immobilized on a surface of mica. After about 2 min the chamber surface has been covered by a buffer droplet of 30 µL. The disk attached with the mica surface was positioned the in the microscope head, taking care not to spill the droplet. Afterwards, the chamber was positioned in the AFM head way above the sample. After the alignment of the laser with the tip, a nominal spring constant of 0.32 N/m has been used for these experiments. A field size at 1 mm × 1 mm in the Nanoscope software was choose and usually the excitation frequency was set between 9 and 10 kHz, slightly below the peak resonant frequency.

The drive voltage was set at 200–500 mV and the set point ranges from 1.4 to 1.8 V. Instead, a typical speed of scanning was set in the 2–3 Hz range[27].

After the first scan or two, it should be better verify if the quality of the image and the imaged sample is acceptable or if further adjustments or changes are needed (scan conditions, probe, protein density in the sample, or protein/buffer purity). As soon as the image is acceptable, the scanning session can proceed even for an hour with the same sample and tip.

3.1.7 Circular Dichroism (CD) - melting experiments

Far-UV CD spectra of h20S, yWT 20S CP and its mutant α3ΔN were recorded at 0.025uM of enzyme with a Jasco J-810 spectropolarimeter equipped with a Peltier thermally controlled cuvette holder (JASCO PTC-348). All measurements were performed at 25 °C unless specified. CD spectra were recorded using a 0.1-cm path length quartz cuvette, from 260 to 190 nm, at 0.1 nm data pitch, 50 nm/min, with a response time of 2s. All spectra, corresponding to an average of 10 scans, were base-line-corrected by subtracting the signal of the buffer from the CD of the sample. CD curves were recorded in 100 mM Tris/HCl pH 7.5 and NaCl 150 mM (this buffer condition stabilizes the closed conformation).

The thermally-induced unfolding of proteasome was studied by monitoring the CD signal at 222 nm upon increasing the temperature from 20 to 80 °C (heating rate = 0.5 °C/min). The melting temperatures were calculated from fitting the normalized CD 222 nm signals by a sigmoidal curve.

3.1.8 Cell Culture

Human MCF-7 breast cancer cell lines were cultured in Eagle's Minimum Essential Medium (EMEM) additioned with: 2mM Glutamine, 1% Non Essential Amino Acids and 10% Fetal Bovine Serum (FBS/FCS), 1% PenStrep. This cell line

grew attached to plastic as a monolayer in an atmosphere of 5% CO_2 and 95% air at 37 °C and 100% humidity.

3.1.9 Proteasome-GloTM Cell Based Assay

In Proteasome-Glo[TM] assay fluorogenic substrates of chymotrypsin-like active site is replaced with the luminogenic substrates Suc-LLVY-aminoluciferin (aLuc). Its cleavage by the site of the proteasome liberates aminoluciferin, which is a substrate of luciferase. Proteasome-Glo assay has allowed us to reduce the amount of cells needed to perform a single time-point measurement of all three activities by approximately 20-fold, largely because of superior sensitivity of luminescent detection over fluorescent detection.

The chymotrypsin-like proteolytic activity of the proteasome in intact MCF7 cells was determined according to manufacturer's instructions. Briefly, 800 cells/well were cultivated in 384 sterile multiwells (optical plate and white walls) in 50ul of DMEM+FBS10% + penStrep.

After cell seeding (6 h) porphyrins and porphirinoids were added in cell medium at 10μM concentration for 24h; and in positive control sample Bortezomib (1μM=IC_{50}) was added.

The substrate for the ChT-L activity (Suc-LLVY-aminoluciferin) was dissolved in Proteasome-Glo™ Cell-Based Reagent and added to intact cells (1/1 vol). After 2 min of shaking for permeabilization and further 10 min of incubation, luminescence was measured with a luminometer (Varioskan Flash ,Thermo).

3.1.10 MTT Assay

To determine cell viability the colorimetric MTT (3-(4,5-Dimethylthiazol-2-yl)-2,5-Diphenyltetrazolium Bromide)) metabolic activity assay was used; the cells were seeded in a 96-well plate at a density of 5×10^3 cells/well and exposed to varying concentrations of porphyrins in the dark for 48 h. Cells treated with only cell medium were used as control sample. After removing the supernatant

of each well and washing twice by PBS, 20 µl of MTT solution (5 mg ml^{-1} in PBS) and 100 µl of medium was introduced. After incubation for another 4 h, the resultant formazan crystals were dissolved in dimethyl sulfoxide (200 µl) and the absorbance intensity measured by a microplate reader (Varioskan Flash) at 570 nm. All experiments were performed in quadruplicate, and the relative cell viability (%) was expressed as a percentage relative to the untreated control cells.

Chapter 4 -Studies on interaction between cationic porphyrins (H2T4 and its isomeric forms) and 20S proteasome

4.1 Goal of this study

Starting from the evidences reported on paper (JACS 2012)[79] evidencing the antiproteasome potential of cationic porphyrins, the successive goal has been to elucidate the molecular mechanism on the basis of this activity, investigating the structure-function relationship.

Then a combined multidisciplinary approach (enzymatic assays, UV stopped flow, NMR experiments and computational approaches) has been adopted to inspect the proteasome inhibition by H2T4 and his two isomers, ortho-H2T4 and meta-H2T4.

4.2 Inhibition potency of H2T4 and his isomers on purified proteasome 20S

In the first step, all three proteolitic activities (ChT-L, T-L and CP-L) have been studied on purified 20S samples, instead that in lysates, in order to avoid eventual interaction with possible contaminant in the cell extracts.

The experiments confirm that H2T4 is a good and specific proteasome 20S inhibitor, both for ChT-L activity, T-L and CP-L activity (**Figure 26**).
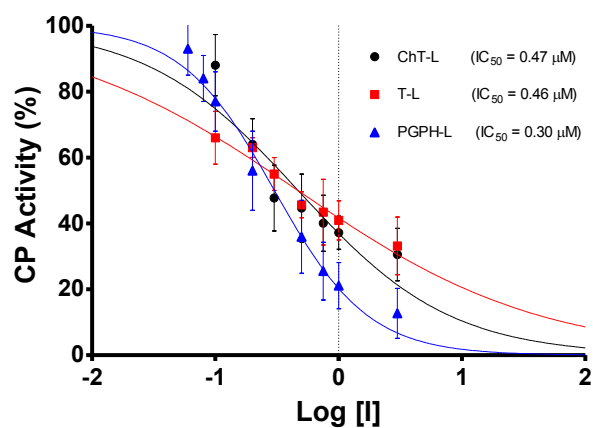
a
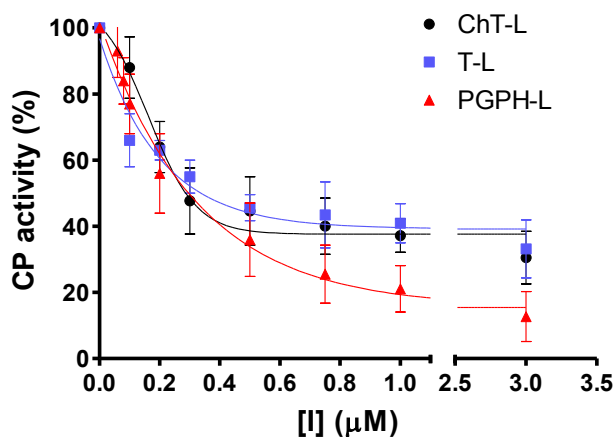
b

Figure 26: a) Semi-log plot of the residual CP activities of H2T4 as a function of inhibitor concentration. **b)** Normalized concentration-response plot for H2T4-mediated inhibition of ChT-L, T-L and PGPH-L residual activities of 20S proteasome[86].

Moreover, to better understand the effect of the positive charges's spatial distribution on the porphyrins's activity, we compared the IC50 values of H2T4 with those of the ortho-H2T4 and meta-H2T4 isomeric forms (**Figure 27**). A dose–response plots of the residual proteasome activity in presence of increasing concentration of porphyrin it's shown below.

The IC50 indicate the concentration of the inhibitor which causes 50% reduction of activity and it is thus calculated from the x-axis value of the dose–

response plot occurring at a fractional activity of 50%. The estimation of the IC50 is based on a nonlinear fit with the equation[86]

$$v(\%) = 100 \frac{IC_{50}}{[I] + IC_{50}} = \frac{100}{1 + 10^{(\log[I] - \log IC_{50})}}$$

The IC50 values and their standard errors were deduced from the fitting.

a

b
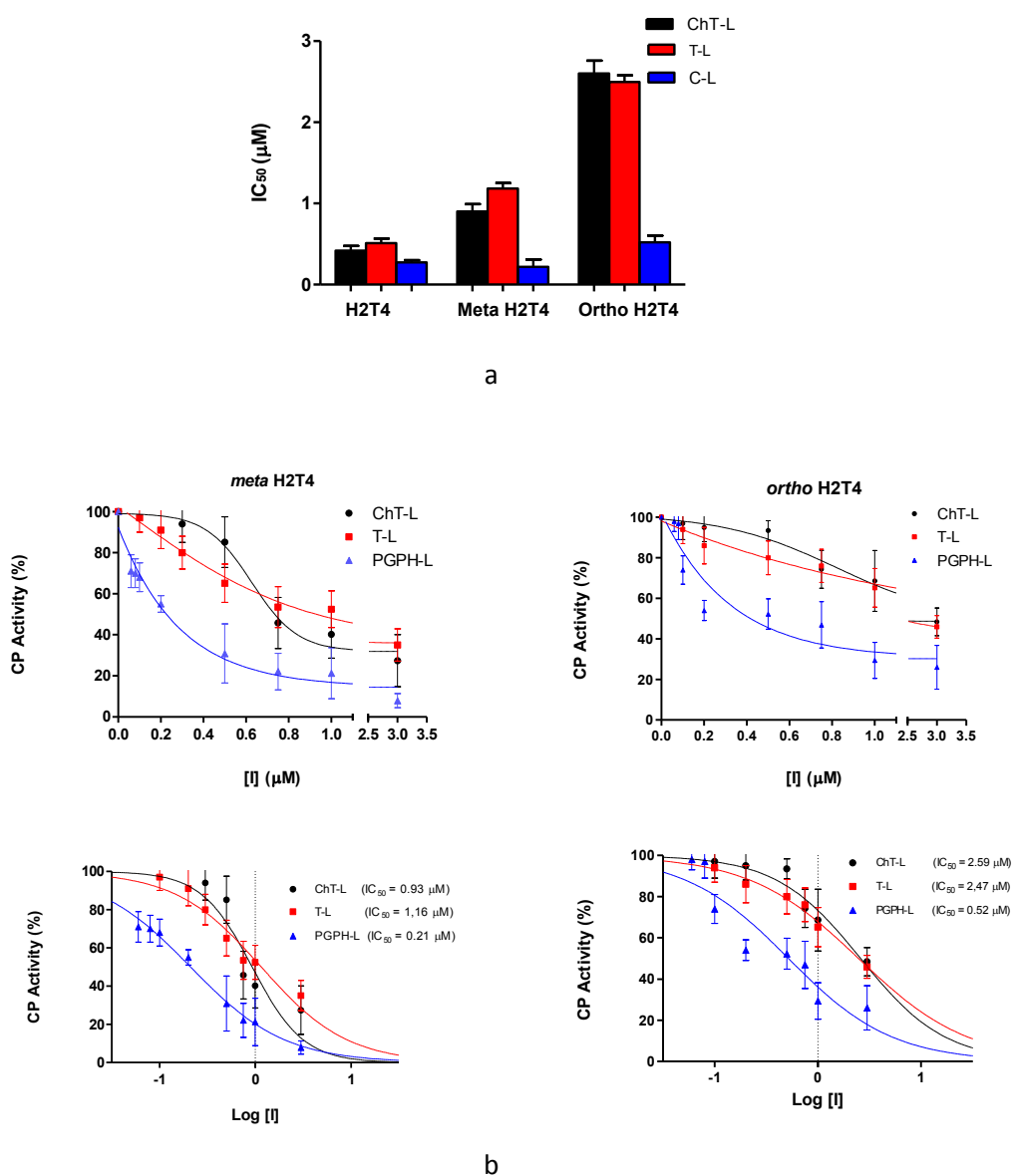
Figure 27: a) Comparison of the IC_{50} values of H2T4 – para-tetra(4-Nmethyil-pyridyl) porphyrin-, *meta*-H2T4 – meso-tetra(3-N-methyilpyridyl) porphyrin – and *ortho*-H2T4 – meso-tetra(2-N-methyil-pyridyl) porphyrin – determined for the ChT-L (black), T-L (red) and PGPH-L (blue) peptidase activities of the CP.
b) semi-log plots of residual CP activities of *meta*-H2T4 (left) and *otho*-H2T4 (right).[86]

Curve fitting parameters are reported in Table 1.

Fitting parameters	ChT-L activity	T-L activity	PGPH-L activity
	H2T4		
	Best-fit values		
IC$_{50}$	0.4692	0.4667	0.3016
	95% Confidence Intervals		
IC$_{50}$	0.2737 to 0.8043	0.3634 to 0.5993	0.249 to 0.3653
R²	0.8348	0.9583	0.9829
	Meta-**H2T4**		
	Best-fit values		
IC$_{50}$	0.9310	1.159	0.2113
	95% Confidence Intervals		
IC$_{50}$	0.4658 to 1.861	0.8074 to1.664	0.1840 to0.2427
R²	0.8187	0.9401	0.9900
	Ortho-**H2T4**		
	Best-fitvalues		
IC$_{50}$	2.592	2.476	0.5190
	95% Confidence Intervals		
IC$_{50}$	1.584 to 4.242	1.864 to 3.289	0.2905 to 0.9271
R²	0.9362	0.9813	0.8634

Table 1: Data fitting relative to the evaluation of the IC$_{50}$ values of H2T4 and its *meta-* and *ortho-* variants for all three CP peptidase activity[86].

From these experiments, it is clear that also the charge position is fundamental for obtain an optimal effect; in fact H2T4 is a better proteasome inhibitor than *orto*-H2T4 and *meta*-H2T4.

Even if the charge distance between these two different isomeric forms is only of few angstroms, this difference it is enough to influence the recognition phenomena between porphyrin and proteasome[86].

4.3 NMR analysis of H2T4/proteasome complexes

In collaboration with the research group of Prof. R. Fattorusso (Seconda Università di Napoli) and Dott.ssa D. Diana (CNR - IBB Napoli) (they and co-workers planed and performed the follows experiments), in order to identify the functional groups involved in the H2T4-CP interaction, a set of NMR experiments, such as Saturation Transfer Difference (STD), have been performed.

Initially, the structure of the ligand dissolved in the buffer (**Buffer:** 20 mM Tris–HCl, pH 7.6, 150 mM NaCl) has been analyzed by 1H NMR spectroscopy. In particular, H2T4 1H chemical shift assignment has been obtained as it follows: 9.09 (8H, s, broad, Hpyr) 9.27 (8H, d, N-methylpyridine-Hm), 8.89 (8H, d, N-methylpyridine-Ho), 3.69 (12H, s, N-methylpyridine- CH3). After, 860 nM of 20S proteasome has been added to 172 mM of H2T4 (protein : ligand ratio of 1 : 200)[85]. It was shown that the ^{1}H H2T4 chemical shifts in presence of proteasome 20S don't significantly change upon the addition of 20S proteasome, except for the pyrrole ring resonances, which display shifts downfield (from 9.10 to 9.14 ppm) (**Figures 28a** and **28b** and **Figures 28a'** and **28b'**); on the other hand, H2T4 resonances experience an overall soft line broadening[86].

Both effects, line broadening and chemical shift perturbations, confirmed the binding between H2T4 and proteasome. To structurally characterize the H2T4–20S proteasome interaction, they apply STD (Saturation Transfer Difference) NMR spectroscopy assay[87].
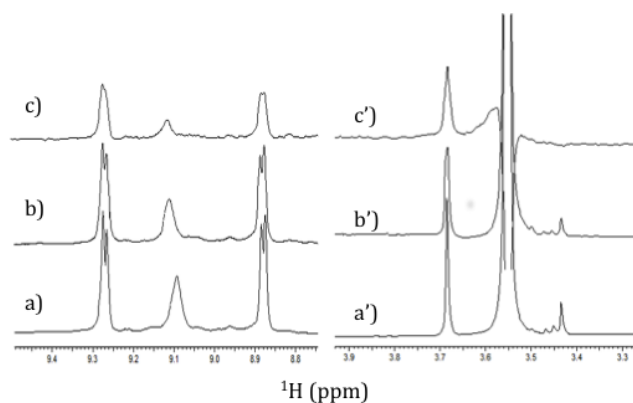
Figure 28: Low-field (left) and high-field (right) 1H NMR spectra of H2T4 (172 mM) **(a)** in Tris–HCl (20 mM) pH 7.6, NaCl (150 mM) solution, and **(b)** in the presence of 20S (860 nM); **(c)** 1H NMR STD spectrum of H2T4 in the presence of 20S (860 nM). 1H chemical shift assignment has been reported for H2T4 in presence of 20S proteasome[86].

The STD experiment confirmed the binding to the 20S proteasome. To identify the ligand moiety more closely interacting with the protein, they evaluated and compared the saturation effects of the individual H2T4 proton resonances (ISTD ¼ I_0-I_{sat})[88]. The signal showing the largest ISTD/I_0 value, the methyl group of the N-methyl pyridine, was normalized to 100% (**Figure 29**); the relative degree of saturation of the individual protons, normalized to that of the methyl group of the N-methyl pyridine, can be then used to compare the STD effect.
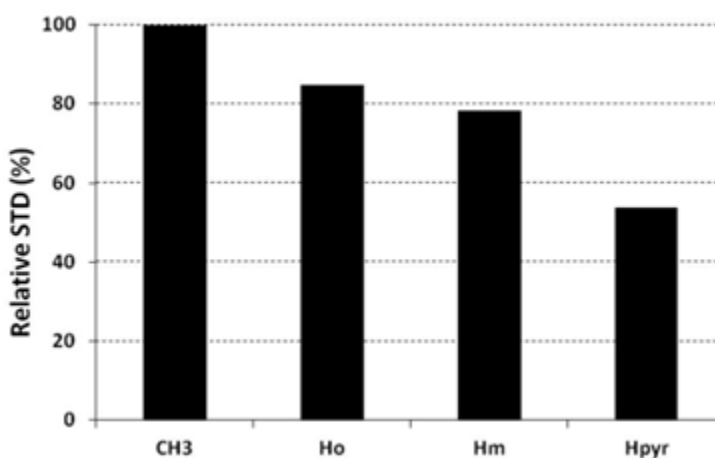
Figure 29: Diagram showing the relative STD intensities for H2T4[86].

The STD intensities show that:

- the methyl-pyridine ring plays the major role in the protein binding, mainly through its ammonium moiety.
- the pyrrole ring is likely less involved in the recognition of the 20S proteasome.

Accordingly, upon proteasome addition, the N-methyl pyridine resonances appear broadened, thus envisaging an intermediate exchange, whereas the pyrrole signals are shifted, being in a fast exchange regime[85]. As a control, a STD experiment with no added CP was also carried out; under these conditions, no signals were detected in the STD spectrum, suggesting that the saturation in the presence of 20S proteasome does not originate from non-specific interactions.

4.4 Kinetic study

Analysis of enzyme kinetics may help to identify the inhibition mechanisms. To this aim, we have addressed the inhibition mechanism of H2T4 by determining the ChT-L activity of the CP at different concentrations of substrate and inhibitor. Since H2T4 inhibits all the three proteolytic functions of the CP with a similar potency, one can assume that the inhibition mechanism is similar for all enzymatic activities.

A kinetic analysis was done following the Michaelis-Menten model. Concentration ranges from 6 to 100 µM of substrate Suc-LLVYAMC (ChT-L activity substrate) have been used.

The reaction rates were determined in presence of increasing amounts of H2T4 (range from 0 to 20µM); these results are plotted using Lineweaver-Burk (double reciprocal plot), where the values of $1/v$ as a function of $1/[S]$ and are obtain some lines with slope of K_M/V_{max}, y-intercept of $1/V_{max}$, and x-intercept of $-1/K_M$ [86](**Figure 30**).

The Lineweaver–Burk plot shown in figure 30 indicates that H2T4 inhibits the CP by a competitive mechanism.
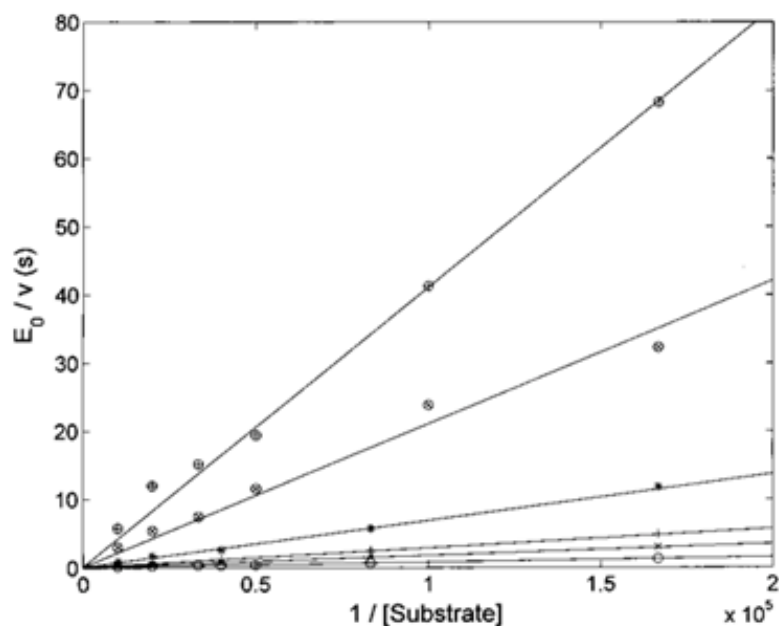
Figure 30: Double reciprocal Lineweaver–Burk plot of substrate enzymatic 20S processing in the absence of inhibitor of substrate enzymatic 20S processing in the absence of inhibitor (o) and in the presence of 0.5 µM (x), 1 µM (+), 3 µM (*), 10 µM (⊗) and 20 µM inhibitor (⊕) for various concentrations of the substrate Suc-LLVYAMC (from 6 to 100 µM)[86].

The inhibitor affinity constant K_I can be obtained by fitting data according to the follow equation:

$$\frac{[E_0]}{v} = \frac{K_m\left(1 + \dfrac{[I]}{K_I}\right)}{k_{cat}} \times \frac{1}{[S]} + \frac{1}{k_{cat}}$$

The obtained value is K_I= 3.6 (± 0.5) x10^{-7} M.

The kinetic parameters of H2T4 binding to the CP have also been determined as a function of time.

Figure 31 reports the time evolution of the fluorescent product obtained by mixing at t=0 both the substrate (100 mM final concentration) and H2T4 at different concentrations, as reported in the figure legend; the fluorescent signal was transformed into molar concentrations of fluorescent product through a calibration curve resulting from the complete processing of known concentration of substrate[86].
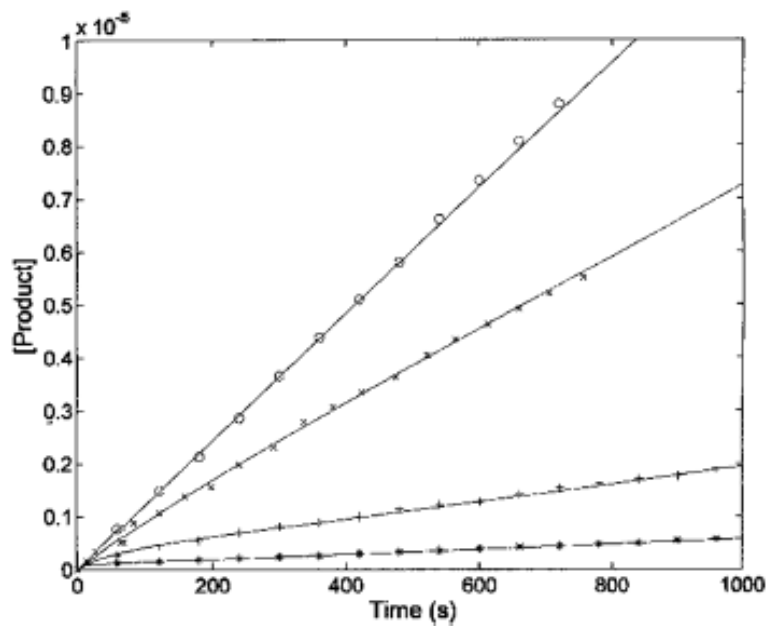
Figure 31: Kinetics of fluorescent product formation, obtained by mixing 2 nM 20S proteasome, 100 mM of substrate Suc-LLVY-AMC and different concentrations of H2T4 porphyrin: 0 (O), 0.3 μM (X) 3 μM (+) and 10 μM (*)[86].

The continuous lines correspond to the simulation curve at different concentrations of H2T4, employing K_m=7.2 x10^{-5} M, k_{cat}=10 s^{-1} (i.e., the values of K_m and k_{cat} obtained from steady-state measurements, see above), and applying values of k_{+I} and of k_{-I}, which were constrained to the obtained K_I=(k_{-I}/k_{+I}).

The kinetic parameters calculated for the H2T4 binding are $k_{+I} = 1.3 \times 10^4$ M^{-1}s^{-1} and $k_{-I} = 4.7 \times 10^{-3}$ s^{-1}; these suggest that H2T4 behaves as a fast-reacting inhibitor of the 20S proteasome, since the inhibition appears evident already few seconds after the inhibitor addition[86].

## 4.5 Molecular Modeling and stopped-flow investigation

Moreover, in collaboration with Prof. Groll from the Technische Universität München, Germany, X-ray analysis have been carried out by soaking yeast 20S proteasome crystals with H2T4. Unfortunately, the porphyrin has a high

propensity to self-aggregate in the presence of the crystallization buffer; thus, the ligand concentration in the crystallization drop was infinitesimal. After a soaking time of 24 hours, the FO-FC-electron density map did not display any striking features that could be interpreted as a porphyrin core[86].

Therefore, in order to deeper investigate the interaction between H2T4 and human 20S proteasome, in collaboration with Università Federico II di Napoli (Prof. C. Fattorusso, Dott. M. Persico and co.workers performed modeling calculations), molecular modeling studies have been performed.

Since data underlined the crucial role played on inhibitory activity by the number and relative positioning of the protonated pyridine nitrogen atoms, they generated a 3-D pharmacophore model of H2T4 by assuming the four protonated nitrogen atoms as key interaction points. Then, they evaluated the ability of the human 20S proteasome to accommodate the planar and positively charged pharmacophore of H2T4 by mapping the spatial positioning of negatively charged amino acids on the protein surface, as well as in the known functional and proteolitic binding sites. The analysis was performed considering all the experimentally determined conformational states (closed, open, and semi-closed) and the sequence homologies among the different species were calculated using the PROMALS3D[89] server (http://prodata.swmed.edu/promals3d/promals3d.ph).

Obtained results excluded that the 20S catalytic subunits are the target binding sites, and they induced to hypothesize that the proteasome gate in the a ring might be the most probable H2T4 binding site, for the competitive inhibition of 20S catalytic activities (**Figure 32B).**
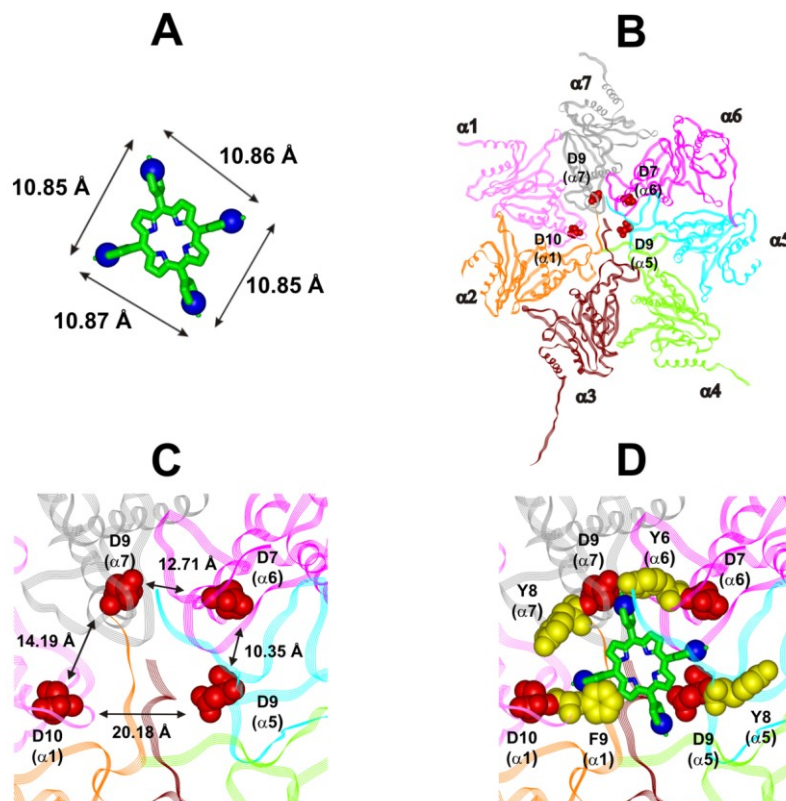
Figure 32: A) H2T4 pharmacophore and related inter-atomic distance ranges (Å). B) top view of the human 20S proteasome (PDB ID: 4R3O), only the α ring is shown for clarity of presentation. The α subunits are colored in pink (α1), orange (α2), brown (α3), light green (α4), cyan (α5), magenta (α6), and gray (α7). C) The four Asp residues are displayed as CPK and colored in red, the suitable inter-residue distances for a possible interaction with the H2T4 pharmacophore are reported. D) Positioning of H2T4 in the putative binding site; the potential interactions between H2T4 and the 20S proteasome are shown[86].

Starting from this hypothesis, they identified that the negatively charged Asp residues on the N-terminal tails of α1, α5, α6, and α7 displaying a spatial position which fit with the positively charged H2T4 nitrogens (**Figure 32**)[86]. In addition, the four adjacent aromatic residues could assist the binding by π-π interaction with the pyridine rings. Thus, H2T4 was positioned at its putative binding site on the human 20S and the obtained complex was used as starting structure for the subsequent dynamic docking calculations. Monte Carlo and a simulating annealing (SA) procedure were made, during which the ligand and

all protein atoms included in the binding domain area are left free to move(conformational search, rotation, and translation).

Indeed, in the Monte Carlo complex H2T4 binds to the gate assuming a position perpendicular to the α ring plane favorable non-bond interaction energy (it was selected as the best docked complex)[86](**Figure 33 A**).

In fact, an interactions with the negatively charged residue D9 (α5) and D7 (α6), and the aromatic residues F9 (α1), Y8 (α5) and Y6 (α6) is established[86].
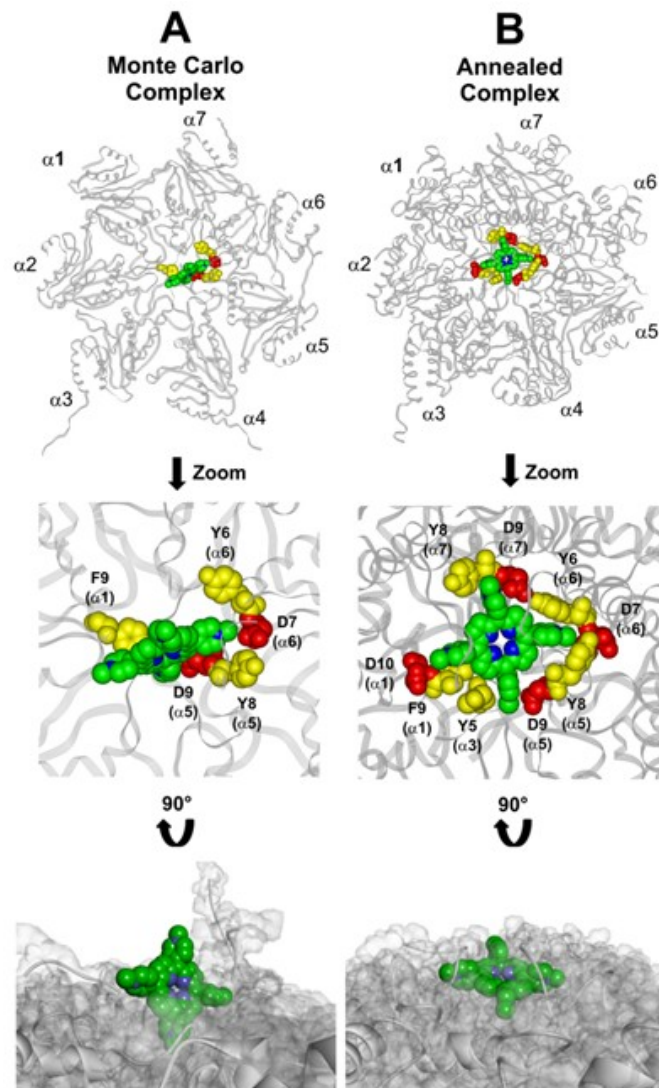

Figure 33: Results obtained by the dynamic docking procedure. H2T4-20S Monte Carlo (A) and SA (B) complexes. The α subunits are displayed as line ribbons and colored in gray. H2T4 is displayed as CPK and colored by atom type (C: green; N: blue). The amino acid residues involved in ionic and cation-π interactions are displayed as CPK and colored in red and yellow, respectively. Protein van der Waals volume is displayed as transparent surface (bottom representation)[86].

Interestingly, the H2T4 binding mode calculated by the Monte Carlo docking procedure significantly changed after it is subjected to SA calculations (**Figure 33 A vs. B**).

In fact, when this complex is subjected to the SA procedure, a much more stable ligand-protein complex is achieved, characterized by the most favorable non bond interaction energy. In this last complex, H2T4 binds parallel to the α subunits plane and interacts with the whole cluster of the identified functional residues at the N-terminal tails of α1, α3, α5, α6, and α7[86] (**Figure 33 B**).

Moreover, it was identified a cluster of negatively charged residues showing suitable inter-atomic distances for a possible interaction with the porphyrin pharmacophore at the interface between α1- β1, α2- β2, and α5-β5 subunits (**Figure 33**). These residues are involved in the modulation of enzyme conformations[90] and were already reported as the binding site of the noncompetitive inhibitor chloroquine[91].

Dynamic docking calculations, performed considering this second binding site, underlined that H2T4 is able to interact with the negatively charged residues (**Figure 34**), but with a lower affinity with respect to that showed for the gate[86].
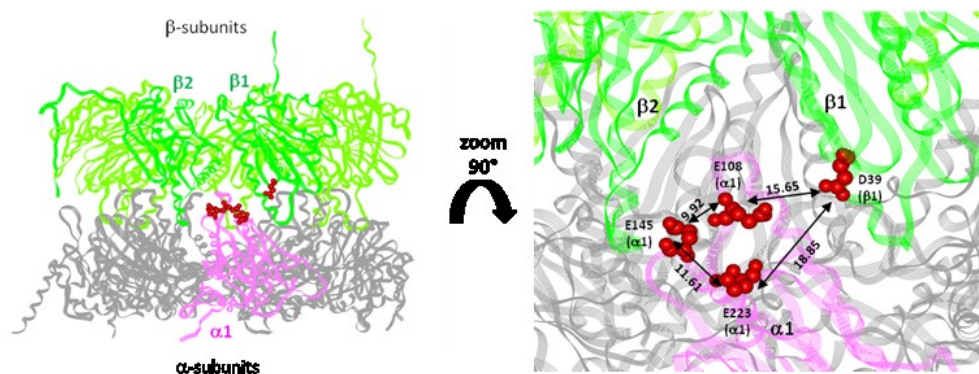
Figure 34: Transversal view of the X-ray structure of the 20S proteasome core particle (PDB ID: 3UNE). Only the α (α2- α7: gray; α1: pink) and β (green) rings are shown for clarity of presentation. The cluster of negatively charged residues at the chloroquine binding site are displayed as CPK and colored in red. Suitable inter-residue distances for a possible interaction with the H2T4 pharmacophore are reported [86].

In fact, as reported above, the 20S gate is characterized not only by a cluster of negatively charged residues but also by a cluster of aromatic residues, that contribute to the interaction with H2T4 (**Figure 35**).
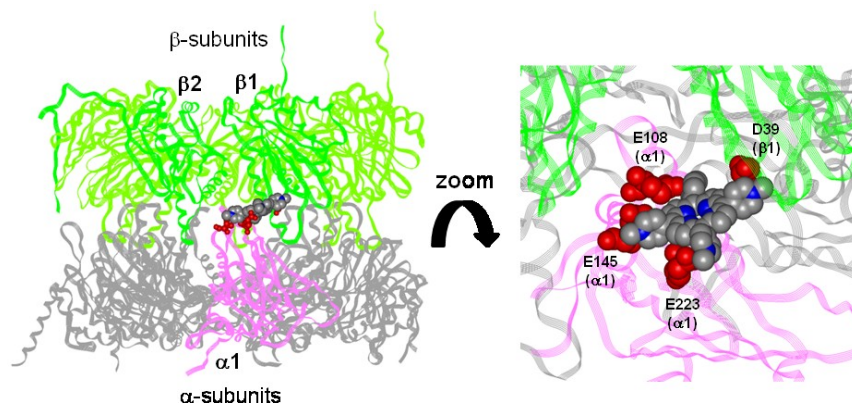
Figure 35: Overall and zoomed views of H2T4 docked in the chloroquine binding site between the α1 (pink) and β1 (green) subunits,. Only the α (α2-α7: gray; α1: pink) and β (green) rings are shown for clarity of presentation. H2T4 is displayed as CPK and colored by atom type (C: gray; N: blue). The amino acid residues involved in ionic interactions are displayed as CPK and colored in red[86].

Afterward, *meta*-H2T4 and *ortho*-H2T4 were subjected to the same dynamic docking protocol applied to H2T4.

During the docking simulation, it was evidenced that *meta*-H2T4 and *ortho*-H2T4 do not remain bound to the identified N-terminal Asp residues at the 20S gate. Moreover, in the complex characterized by the lowest non bond interaction energy, *meta*-H2T4 binds at a side of the gate, interacting only with F9 (α1) and Y8 (α5); instead *ortho*-H2T4 binds only Y6 (α6) [86] (**Figure 36**).
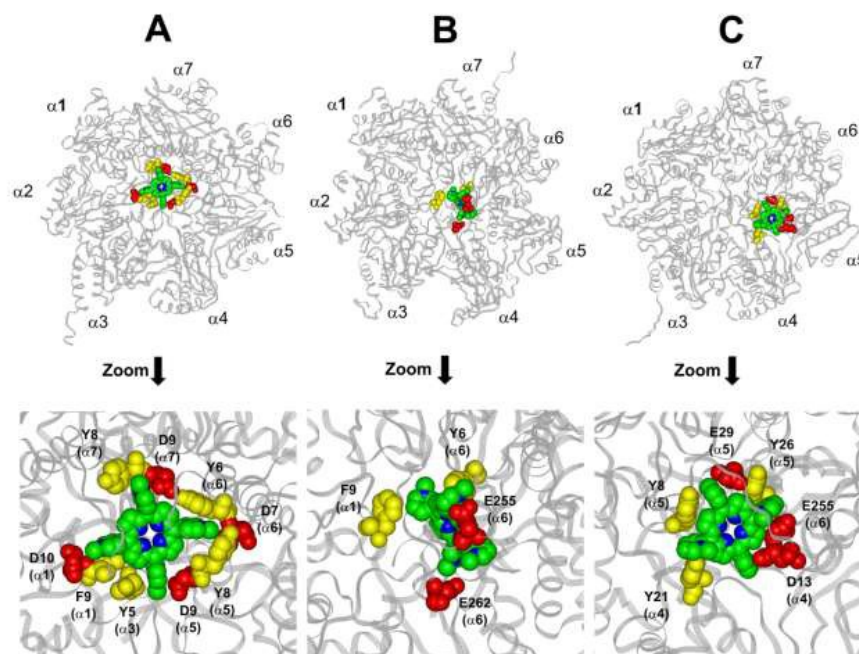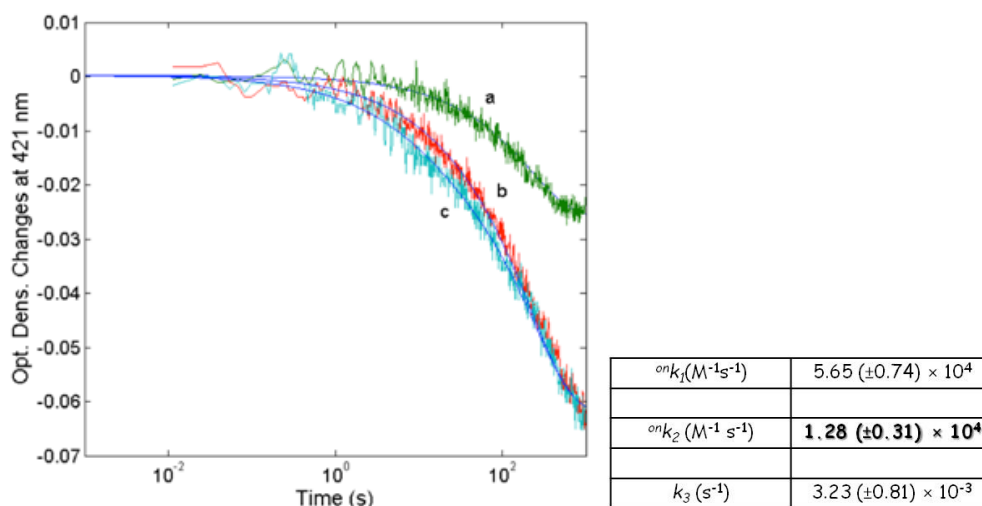
Figure 36: Comparison of the resulting complexes of H2T4 (A), *meta*-H2T4 (B) and *ortho*-H2T4 (C) bound to the human 20S CP (gray). The ligands are displayed as CPK and colored by atom type (C: green and N: blue). The amino acid residues involved in ionic and cation-π interactions are colored in red and yellow, respectively, and displayed as CPK[86].

Accordingly, meta-H2T4 and ortho-H2T4 showed a lower inhibitory potency with respect to H2T4 and inhibited the three catalytic activities to different extents (**Figure 27a**).

These molecular modeling results allow to hypothesize that H2T4 binds with an initial binding geometry on 20S proteasome α face which is then followed by a conformational change of the inhibitor-enzyme complex (i.e., induced fit mechanism)[92] resulting in the formation of a more stable complex[86].

In order to find a closer correlation between experimental observations and molecular modeling the Prof. Coletta and coworkers (from Tor Vergata University – Rome) have carried out a kinetic investigation by stopped-flow of the interaction between H2T4 and 20S proteasome.

Figure 37 is characterized by a multiphasic pattern with different patterns of concentration dependence of the rate constants.

$^{on}k_1 (M^{-1}s^{-1})$	$5.65\ (\pm 0.74) \times 10^4$
$^{on}k_2 (M^{-1}\ s^{-1})$	$\mathbf{1.28\ (\pm 0.31) \times 10^4}$
$k_3 (s^{-1})$	$3.23\ (\pm 0.81) \times 10^{-3}$

Figure 37: *Left:* Optical density changes at 421 nm for the mixing at 37°C of 1 nM 20S proteasome with different concentrations of H2T4, namely 1 μM (curve a), 2 μM (curve b) and 5μM (curve c). *Right:* Table of kinetic constants[86].

It appears evident as the process is characterized by a faster interaction step, followed by a slower event (which displays the same bimolecular rate constant observed for the competitive inhibitory process, see figure 31).

Therefore, on the basis of molecular modeling and the kinetic data we can assuming that there is a first faster interaction with the N-terminal tails of the α subunits, characterized by k_1, likely corresponding to the first encountering of the porphyrin with the α-subunits plane in a perpendicular geometry (see **Figure 33A**). This event is then followed by a tighter binding to the CP gate, characterized by k_2, which can be referred to the formation of the more stable porphyrin-protein complex characterized by a parallel geometry (see **Figure 33B**). The UV-vis stopped-flow experiment is also characterized by an additional process with $k_3 = 3.23\ (\pm 0.81) \times 10^{-3}\ s^{-1}$, whose rate is independent on porphyrin concentration, likely corresponding to a subsequent slower binding of porphyrins to the 20S proteasome at site(s) topologically distinct from that of the first two events[86].

This slower process, as suggested by molecular modeling studies, might be related to the availability of an additional binding site (cloroquine site) for H2T4 on the 20S proteasome the binding of H2T4 induces a conformational change

that may be related to the availability of another binding site for H2T4 on the 20S proteasome.

4.6 Conclusions

Our results suggest that cationic porphyrins behave as CP gatekeepers[86]. NMR studies show that the H2T4 methyl-pyridyne groups are more involved in the binding with the enzyme than the pyrrole rings and this support the hypothesis that electrostatic charges are the major driving force in porphyrin/CP interaction. Moreover, slight changes in the position of the positive charges, such as in the *ortho*- or *meta*-H2T4 analogues, generate significant effects both on the potency of the molecules and on their binding mode.

 In addition, we show that H2T4 may bind at least two sites of the CP, both characterized by the presence of a cluster of negatively charged residues, playing a key role in modulating enzyme conformations/functions. In the first, fast binding mode the porphyrin glides on and clogs up (with two temporally distinct dynamic processes) the CP gate and this generate the simultaneous inhibition of the ChT-L, T-L and PGPH-L activities. A second slower event relates to the subsequent adhesion of the porphyrin to the CP external surface and, in particular, to the grooves which separate the α from the β subunits. This slower binding mode, probably brings the conformational change of the 20S proteasome. Moreover, our data show that H2T4 "plugs" the CP gate behaving as a competitive inhibitor, even though, it is not a catalytic inhibitor, since it does not bind to the catalytic site[86]. Instead, porphyrin interferes with the physiological equilibrium of the 20S proteasome between "open" and "closed" conformations. These results coupled with porphyrin's versatile chemistry, position these molecules as a novel class of CP conformational modulators.

Chapter 5 – Focusing on 20S proteasome conformations

5.1 Goal of this study

Starting from the various evidences that identify the gate channel as the key region for the proteasome - porphyrin interaction, we focus our attention on conformational events related *to the α-face*. In particular, we tried to elucidate how the different conformations of 20S core particles, open and closed forms, influence their reactivity with porphyrins, and *viceversa* if porphyrins could be able to switch the physiological equilibrium between the open and closed conformers.

More in detail, a mutant α3ΔN 20S from yeast, with open / semi open conformation has been used for kinetic and spectroscopic investigation; moreover Atomic Force Microscopy (AFM) experiments have been carried out. In fact, AFM is very useful for the study of the proteasome's dynamic, and it distinguish different conformers (i.e open , closed) and could help us to better understand if porphyrins are able to induce an allosteric effect on the enzyme.

5.2 Kinetic Assay on WT and Mutant 20S from yeast

A Wild Type and Mutant (α3ΔN) 20S proteasome from yeast has been purify in collaboration with Prof. M. Groll and coworkers. The protein purification procedure has been described in Material and Methods.

These samples have been used also to perform experiments for a parallel project on the study of the interaction between Copper (II) ions and proteasome 20S (*Chemical Science* 2016)[93].

Here, starting from the hypothesis that porphyrin has a direct influence on the gating mechanisms of the 20S proteasome, to further validate this hypothesis,

we assayed the effect of H2T4 on the ChT-L peptidase activity on a WT yeast 20S proteasome and yeast 20S mutant proteasome (α3ΔN), where deletion of the first nine N terminal residues of the α3 subunit results in permanently open/semi-open gate conformation[94].

Our results show that H2T4 decreases both yeast WT and α3ΔN 20S proteasome ChT-L activity (**Figure 38**)
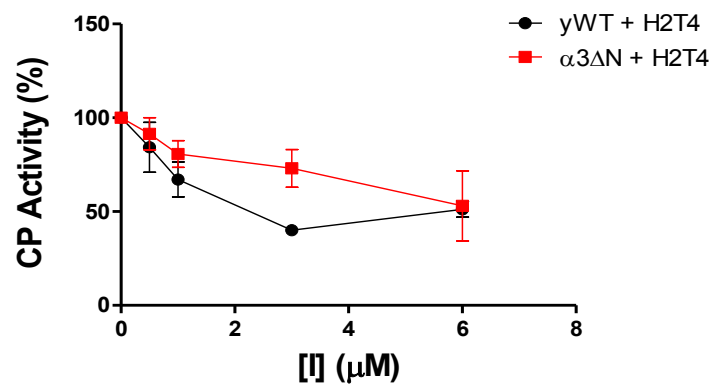
Figure 38: Concentration-response plot for H2T4-mediated inhibition of ChT-L residual activities of yWT (black) and α3ΔN (red) 20S proteasome.

5.3 AFM characterization

As we said before, this technique is useful to detect distinct conformations of the proteasome's α face. **Figure 39** presents 3D renderings of typical AFM images of particles representing the three major types of conformers (from left to right): with presumably closed gate, in intermediate conformation and with presumably open gate.
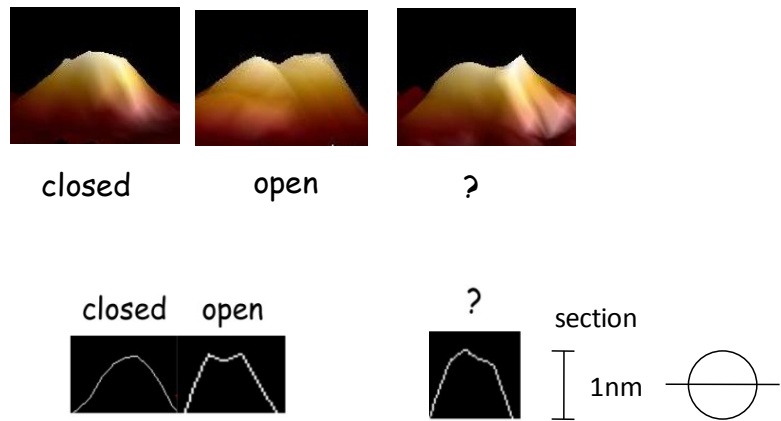
Figure 39: *Upper panel:* AFM 3D images of single 20S particles respectively in closed, open and intermediate (?) conformation. *Lower panel:* conformers sections cut in one direction.

Our goal was to investigate with AFM imaging putative conformational changes induced in the proteasome gate area by the porphyrin binding.

Atomic force microscopy (AFM) imaging of the 20S proteasomes was performed in tapping mode in liquid, as previously described.

Multiple fields were scanned for each sample to collect images of hundreds of particles. Selected fields were repeatedly scanned to monitor changes in topography of the same particles for prolonged time. Inhibitors and the SucLLVY-AMC substrate were diluted in 10/15ml of the imaging buffer and directly injected into the chamber[95].

Raw images are presented, with a standard plain-fit and flattening [NanoScope software version 5.12; Scanning Probe Image Processor (SPIP) version 6.02; Image Metrology, Hørsholm, Denmark] used as the only processing tools. The dimensions of particles were approximated, and α shape of the α face in top-view proteasomes was judged with the help of a section tool in the NanoScope version 5.12 or SPIP software (Image Metrology)[94].

As previously reported, approximately 25% of wild-type 20S proteasomes (*S. cerevisiae* and human) imaged without addition of a ligand were in open state, and 75% in closed state (1:3 ratio). Instead, a ratio 3:1 of open-to-closed conformers has been observed when a substrate specific for one of the three active centers is added.[33]

A typical AFM image of a field (1µmx1µm) of 20S proteasome particles on a mica surface is presented below (**Figure 40**).
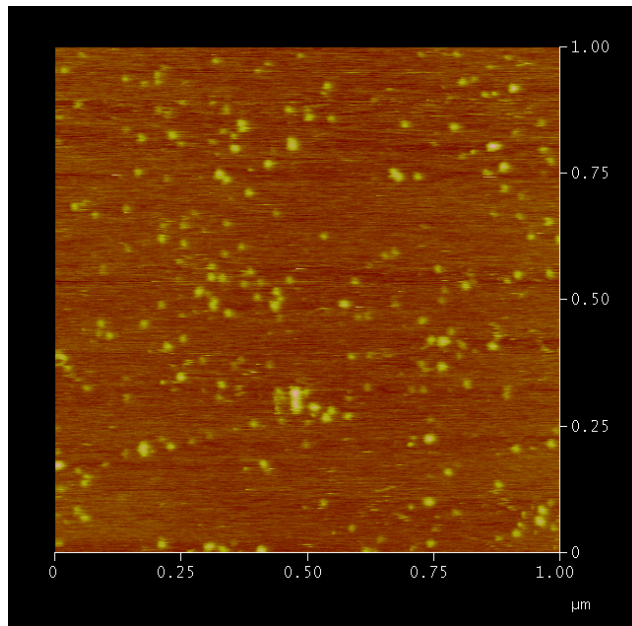
**Figure 40:** AFM image of a 1µmx1µm fragment of mica with attached 20S proteasome particles.

In the experiment with inhibitors, they are injected directly in to the chamber; when H2T4 have been injected its concentration couldn't be higher than 1µM for a probably tip coating phenomena (**Figure 41**).
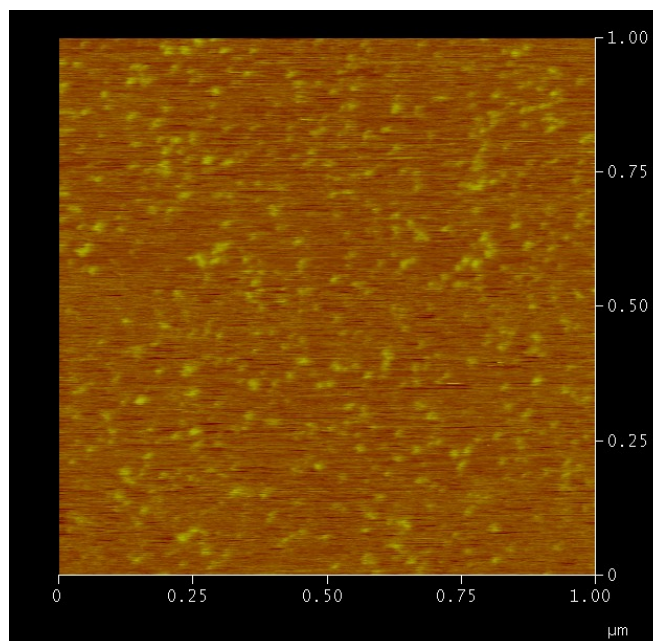
Figure 41: Poor quality ("blurred") image due to probably tip coating phenomena by H2T4.

The addition of H2T4 at 0,2µM to 20S proteasome allows to detect a different partition of conformers; more in detail: the percentage of closed forms decreased; in fact they are shifted from 69% in the control to 49% in the sample treated with H2T4 (**Figure 42**).

Next, the substrate for ChT-L activity was added to the 20S proteasomes already pretreated with H2T4. Remarkably, the partition of conformers did not change significantly: only a small increase of open and decrease of intermediate conformers have been observed, instead of the expected strong shift toward the majority of open conformers (3:1; open:closed) upon the addition of substrate.
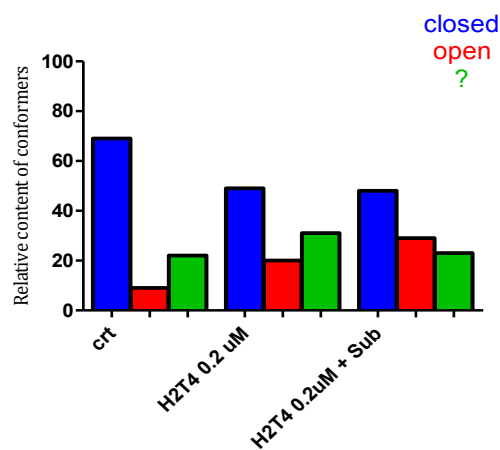
	% closed	% open	% intermediate (?)
Control	69	9	22
20S + H2T4	49	20	31
20S + H2T4 + Suc LLVY- MCA	48	29	23

Figure 42: *Upper panel: AFM Experiment* - The top histogram represents the % of closed (blue) open (red) and intermediate (green) conformers in : control (h20S), h20S treated with H2T4 [0,2] µM and h20S treated with H2T4 [0,2] µM and then with the model substrate for the ChT-L peptidase (SucLLVY-MCA;[100] mM). *Lower panel*: table showing the % of closed - open and intermediate (?) conformers respectively for the control (h20S), h20S + H2T4 [0,2]µM, h20S + H2T4 [0,2]µM and Substrate Suc LLVY-MCA [100] µM.

Moreover, when the proteasomes were scanned for a prolonged time a consistent increase in abundance of open conformers was showed immediately after addition of the porphyrin, whereas an increase in abundance of intermediate conformers was slightly slower to manifest.

Interestingly, addition of the substrate quickly shifted the equilibrium toward more of the open particles, but the distribution of conformers soon returned to pattern H2T4-treated proteasomes (**Figure 43**).
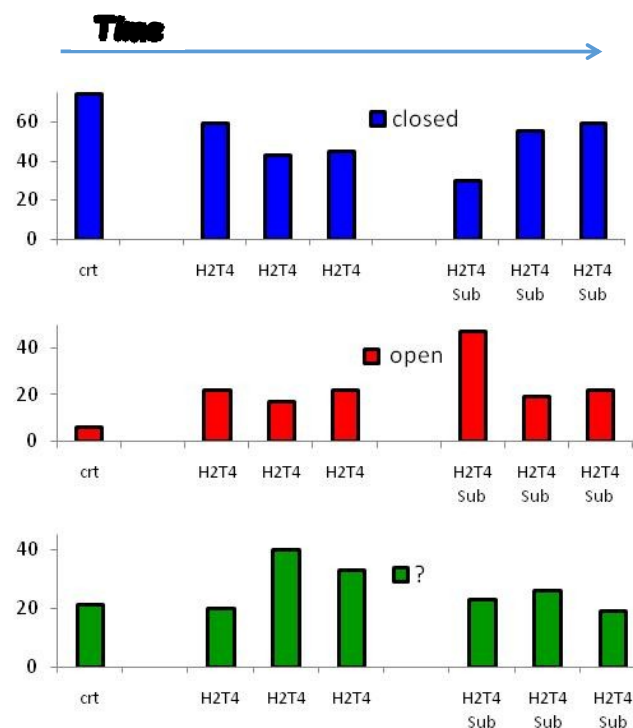
Figure 43: *Time-course of conformational changes studied by AFM.* Proteasome particles were scanned and imagined continuously under control conditions, after addition of H2T4 and after addition of the peptide substrate on the top of H2T4 (about 3 min per scan). Blue histograms are the % of closed conformers; red histograms are the % of open conformers and green histograms are the % of intermediate (?) conformers.

Afterwards, experiments at different scan rates have been performed. In fact, to modify the scan rate could be useful to evaluate different temporal events.

AFM imaging was performed with a typical scan rate of 2,24 Hz. Under these conditions an increase in both open and intermediate conformers have been detected (**Figure 42 - Figure 44**). Scanning with a lower rate did not result in changes in the partition of conformers; in contrast an increase of open particles have been detected at higher scan rates (3.05 Hz and 4.07 Hz) (**Figure 44**).
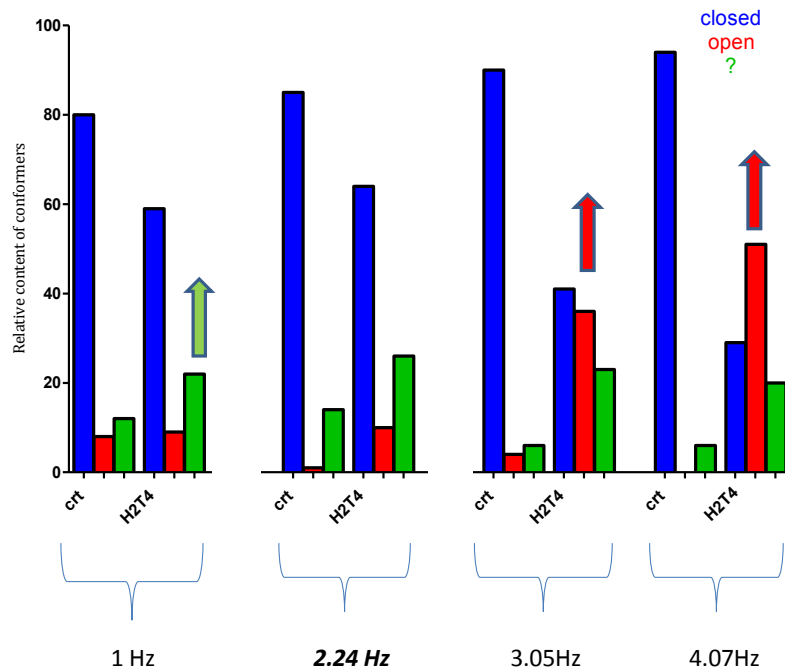

Figure 44: *AFM imaging at different scan rates* - Each column represents the % of closed (blue) open (red) and intermediate (green) conformations. Treatment with H2T4 promotes changes in conformational dynamics of proteasome particles. The changes, especially the increase in abundance of open conformers, are more pronounced at higher scan rates, when chances of detecting fast conformational transitions are elevated.

5.4 Circular Dichroism (CD) and Melting investigation

Circular dichroism (CD) is a valuable spectroscopic technique to prove that a chiral compounds has indeed been synthesized or resolved into pure enantiomer and to probe also the structure of biological macromolecules in solution. CD signals only arise where the optically active compound absorbs the radiation, therefore are easily assigned to distinct structural features of a molecule. As a results, using the CD induced into the backbone amide transition from ~190 nm to ~240 nm, the distinctive CD spectra have been described for pure protein conformations, such as the α-helix, β-sheets (with different ones sometimes being given for parallel and anti parallel sheets), β-turns, and also the "random coil". For this reason the CD of biological macromolecules such as proteins, oligonucleotides and so on, is most commonly used to probe changes in the conformation of the macromolecules itself. However, CD spectroscopy can be employed also to probe the interaction of biological macromolecules with small ligands, especially achiral ones. Induced CD signals can arise from ligands which have no intrinsic chirality but acquire chirality when bound in an asymmetric environment such as provided by a protein.

Proteasome is a very complex protein, and to distinguish between different conformations adopted by Wild Type and Mutant α3ΔN 20S, using CD, it was unexpected. Surprisingly, we obtained two different spectra for each 20S structure (**Figure 45**)
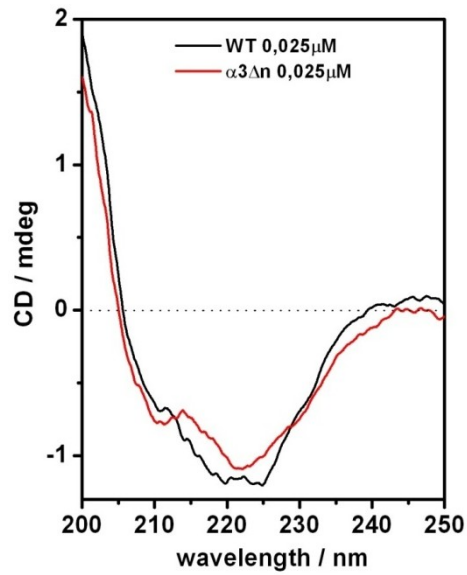
Figure 45: Circular Dichroism (CD) spectra of WT 20S (0,025μM) (black) and α3ΔN 20S (0,025μM) (red).

These spectra show a significant difference in the ratio between the bands at 208 and 222 nm, suggesting a clear indication of a conformational change. Moreover, performing the addition of cationic porphyrin to a solution of proteasome, an interesting features was displayed in the 20S CD spectrum.

Indeed, when 10 μM of H2T4 are add to yWT proteasome, changes in the CD spectrum of proteasome have been detected. The obtained spectrum of the yWT with H2T4 moves toward the Mutant α3ΔN features (in agreement with the AFM data).

On the contrary, on α3ΔN 20S H2T4 does not induce any spectral change (**Figure 46**) (Table 2).
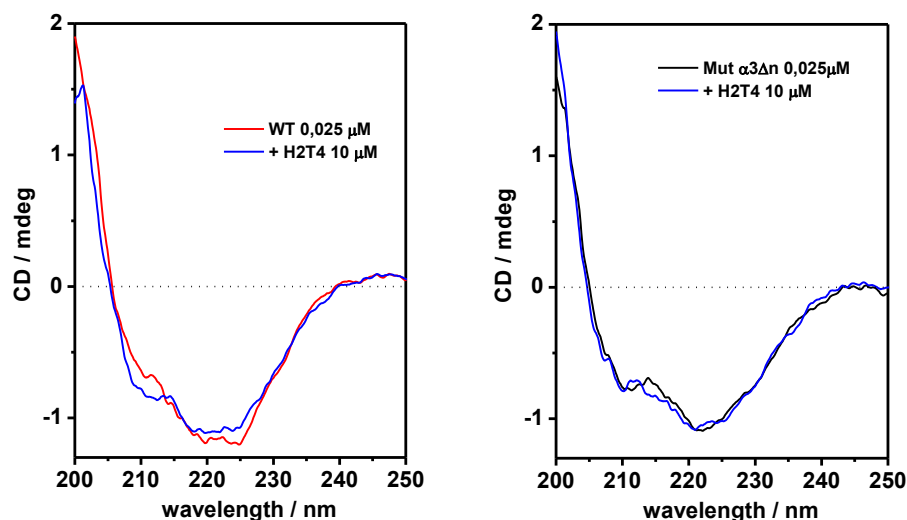
Figure 46: *Right*: Circular Dichroism (CD) spectra of WT 20S (0,025μM) (red) and WT 20S (0,025μM) in presence of H2T4 10 μM (blue). *Left:* Circular Dichroism (CD) spectra of α3ΔN 20S (0,025μM) (black) and α3ΔN 20S (0,025μM) in presence of H2T4 10 μM (blue).
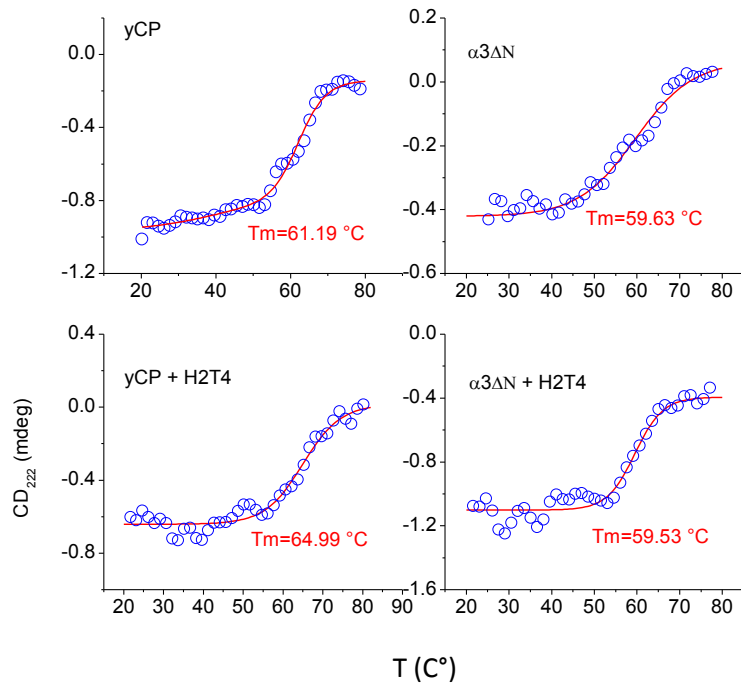
Ratio 208/222 nm			
WT 20S	WT 20S + H2T4	α3ΔN 20S	α3ΔN 20S + H2T4
0,38	0,55	0,48	0,51

Table 2: CD band ratio 208/222 nm in presence of WT 20S, WT 20S + H2T4, α3ΔN 20S and α3ΔN 20S + H2T4.

Afterwards, melting experiments have been performed in order to evaluate the effect of the cationic porphyrin on the complex stability.

How showed in **Figure 47** in the presence of H2T4 the α3ΔN 20S melting temperature doesn't change respect to the unbounded form alone in solution. On the contrary, difference of ≈ 4 C° is observed comparing the melting temperature of yWT with that one obtained for yWT/H2T4 complex.

**Figure 47**: Variable temperature CD spectra (λ:222nm) of γWT CP (0,025μM) (*in the upper left*), γWT CP (0,025μM) in presence of H2T4 10 μM (*bottom left*), α3ΔN CP (0,025μM) (*in the upper right*) and α3ΔN CP (0,025μM) in presence of H2T4 10 μM (*bottom right*) performed from 20°C to 80° C.

At this point, our hypothesis was that a possible stabilization of the proteasome in open conformation could be the result of the interaction between H2T4-20S.

In order to validate the circular dichroism technique as new method useful to detect different proteasome conformations, CD and melting experiments have been performed also with human 20S proteasome and compared to the 20S-Bortezomib complex as reference model.

Noteworthy, Bortezomib is a proteasome inhibitor and its boronic acid group is able to switch the physiological equilibrium from closed to open proteasome conformation (see Cap. 2)

Starting from these evidences, CD spectra of two complexes formed by human 20S/Bortezomib and human 20S/H2T4 have been performed and compared with the CD spectrum of human 20S alone (**Figure 48**).
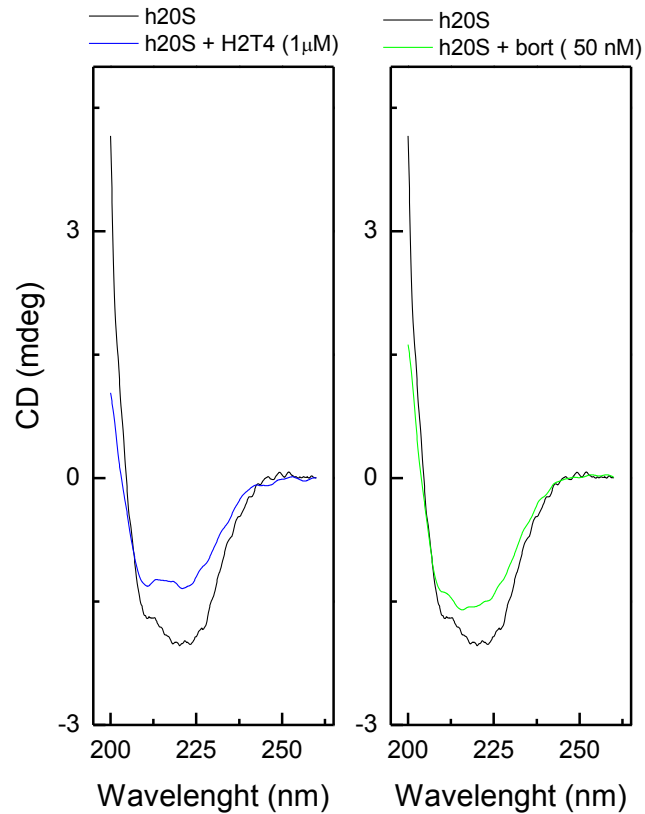
Figure 48: *Right*: Circular Dichroism (CD) spectra of h20S (0,025µM) (black) and h20S in presence of H2T4 [1 µM] (blue). *Left:* Circular Dichroism (CD) spectra of h20S (0,025µM) (black) and h20S in presence of bortezomib [50 nM] (green).

How it's possible to see, in both case there is a difference between the ratios 208/222 nm detected for h20S and h20S/Bortezomib - h20S/H2T4 (table 3).

Ratio 208/222 nm		
Human 20S	Human 20S + Bortezomib	Human 20S + H2T4
0,66	0,80	0,79

Table 3: CD band ratio 208/222 nm in presence of h20S, h20S + Bortezomib, and h20S + H2T4.

Moreover, melting experiments have been carried out (table 4).

T_m		
Human 20S	Human 20S + Bortezomib	Human 20S + H2T4
56.85°C	68.60°C	68.37°C

Table 4: Melting temperatures from variable temperature CD spectra (λ:222nm) in presence of h20S, h20S + Bortezomib and h20S+H2T4, performed from 20°C to 80° C.

The T_m extrapolate from melting experiments shown an increase of temperature for both samples (20S + Bortezomib - 20S + H2T4).

Hypothesis was that a possible stabilization of the proteasome in open conformation could be the result of the interaction between H2T4-20S.

5.5 Conclusion

These new results allowed us to conclude that H2T4 behaves as an allosteric modulators of proteasome. Both AFM and CD experiments, confirms its capability to switch the equilibrium of open-closed conformers. Moreover, we demonstrate that Circular Dichroism is a interesting technique useful to detect conformational changing on 20S proteasome structure.

Chapter 6 - Porphyrin and Porphyrinoid compounds: inhibition potency on purified proteasome 20S

6.1 Goal of this study

The goal of this work is to verify how the modification either of substituents groups in the *meso*-positions either the porphyrin ring could modulate the proteasome inhibition potency and mechanism.

Also in this case, we started from the parental molecule H2T4, and diversified strategies have been employed in order to obtain derivatives with combined biological activities.

Therefore, we initially analyzed the proteasome inhibitory effect of p-TMPPyP**,** where porphyrin has been conjugated to phenylpyridins groups, resulting then a porphyrin with the positive charges distanced respect the parental molecule H2T4.

Second, we verify how the conjugation with an active peptide could influence the inhibitory activity of porphyring ring; in fact, a porphyrin conjugate with a membrane-active peptide, was done. This derivative(MTPyP-APi), synthesized by Prof. M. Gobbo and co-workers,[96] is a porphyrin attached with apidaecin, an antimicrobial peptide (AMPs) proline rich.[97] AMPs are small peptides produced by most eukaryotic organisms as part of their non-specific innate immune system and have been receiving a lot of attention as promising tools to combat the worldwide spread of antibiotic resistance[98]. They are active against a wide range of pathogenic microorganisms including Gram-positive and -negative bacteria, fungi, parasites and some viruses. Many of them are amphipathic because of the presence of properly spaced cationic and hydrophobic residues that favor interactions with the plasma membrane, perturbing its structure and allowing cell entrance of the peptide that eventually causes the death of the microorganism.[99] In the last years, an increasing number of studies have reported that some types of AMPs are active also toward cancer cells[100] with a certain degree of selectivity. It is well established that the primary interaction of these peptides with the plasma membrane relies on electrostatic attractions

between the positive charges of the peptide and the negative charges of the cell surface[101]. Bacterial and tumor cells share the property of presenting more abundant negative charges on their surface with respect to normal eukaryotic cells and this peculiarity can reasonably explain the higher cytotoxic activity of several AMPs toward bacterial and tumor cells with respect to normal cells[102]. It was shown that the conjugation to the N-terminus of the peptides definitely increased the spectrum of photoactivity of the hydrophobic porphyrin (MTPyP-api), used as a model photosensitizers. Moreover, a similar compound displays the increase capability to bind and enter tumour cells[103]. Therefore, the behavior on 20S of MTPyP-api derivative to the relative naked tricationic porphyrin (Tris T4), have been compared. Then, tri-cationic corrin (TMPC), has been included in this study; in this last case the positive charge number is unchanged but the size ring is reduced.

An attempt to compare the inhibitory ability of negative molecule, such as phthalocyanine FBPcG1, has been done and finally, the introduction of alkylic chain (14 carbon length) in the porphyrinic ring has been evaluated (C14) [104].

6.2 Porphyrin and Porphyrinoid compounds: fluorescence activity assay on purified proteasome 20S and kinetic mechanism studies

In the first step, inhibitory abilities on all proteolitic activities (ChT-L, T-L and CP-L) have been studied, determined the IC_{50} values on purified human 20S samples, and these data are reported in **Figure 49**. As we can observe Tris-T4, MTPyP-api, C14 and p-TMPPyP show low IC_{50} values, instead, corrin (TMPC), phtalocyanin (FBPcG1) as well as apidecin chain have high IC_{50} values and then scarce potency (see table 5).
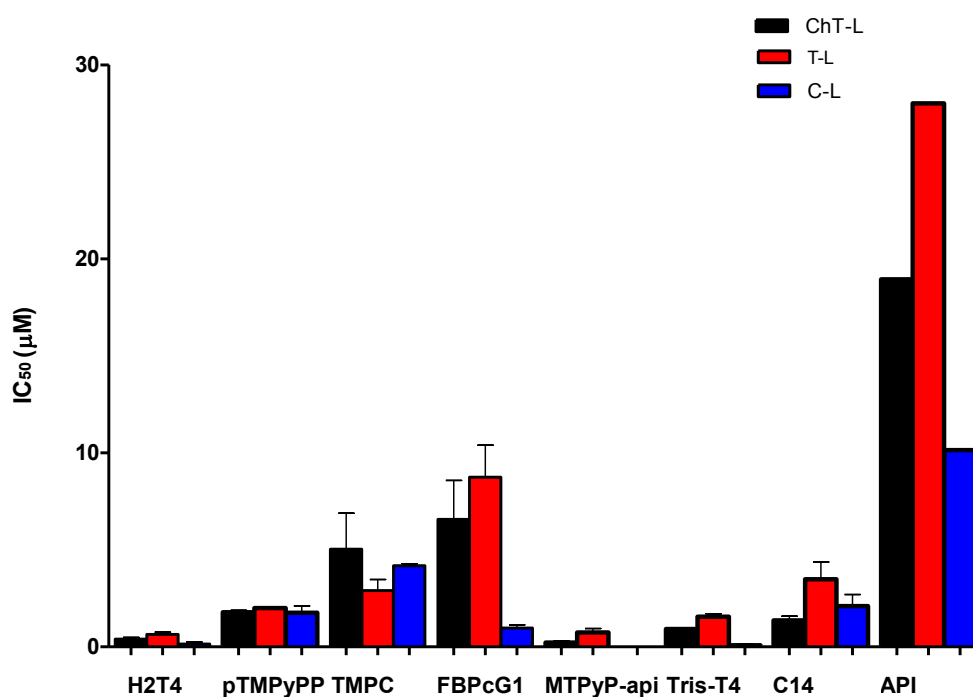
Figure 49: Comparison of the IC_{50} values of H2T4, p-TMPyPP, TMPC, FBPcG1, MTPyP-api, Tris-T4, C14 and API determined for the ChT-L (black), T-L (red) and C-L (blue) peptidase activities of the CP.

	H2T4	Tris-T4	MTPyP-api	p-TMPyPP	TMPC	FBPcG1	C14
ChT-L IC$_{50}$	0,39±0,12	0,92±0,06	0,22±0,1	1,8±0,15	5,04±2,6	6,57±2,8	1,37± 0,29
T-L IC$_{50}$	0,64 ±0,2	1,56±0,2	0,56±0,2	2,00±0,09	2,90 ±0,8	8,74 ±2,3	3,49± 1,26
C-L IC$_{50}$	0,14±0,15	0,08±0,1	0,01±0,003	1,75±0,5	4,18 ±0,1	0,97±0,23	1,37± 0,29

Table 5: IC$_{50}$ values for each tested compound

In order to investigate the inhibition mechanism of porphyrins and porphyrinoids, a kinetic analysis was done by means of the Michaelis-Menten model and precisely by graphical Lineweaver-Burk representation. The concentration of substrate Suc-LLVYAMC (ChT-L activity substrate) ranges from 6 to 100 µM. The reaction rates were determined in presence of increasing amounts of inhibitor (range of µM); these results are plotted using Lineweaver-Burk (double reciprocal plot), where the values of $1/v$ as a function of $1/[S]$ and are obtain some lines with slope of K_M/V_{max}, y-intercept of $1/V_{max}$, and x-intercept of $-1/K_M$ (**Figure 50**).
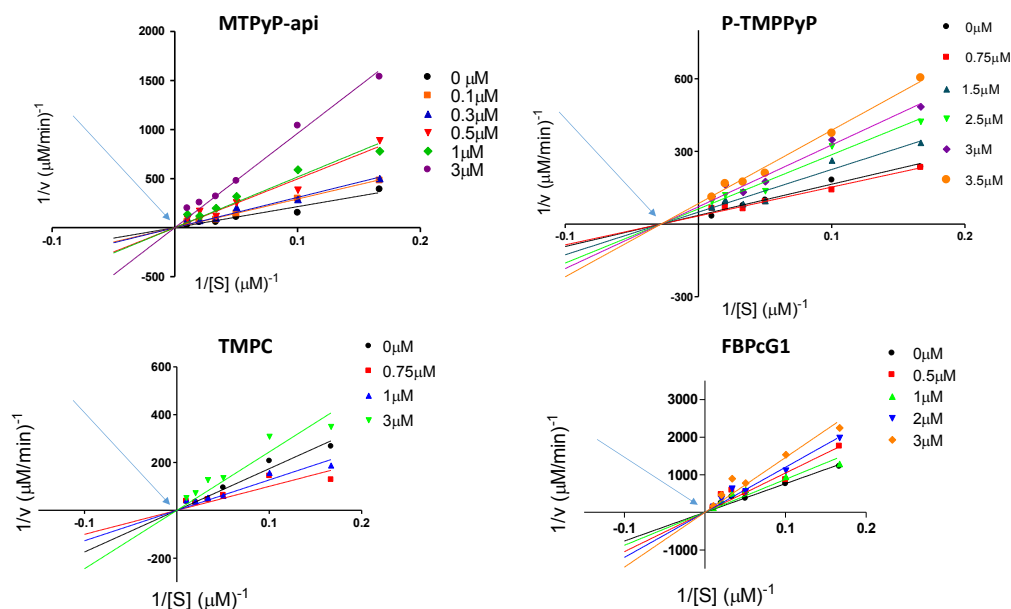
Figure 50: Double reciprocal Lineweaver-Burk plot of substrate enzymatic 20S processing in the absence of inhibitor (black) and in the presence of increase amount of inhibitor (MTPyP-api, p-TMPPyP, TMPC, FBPcG1) for various concentrations of the substrate Suc-LLVY-AMC.

Analyzing the Lineweaver-Burk plots, all compounds seem to have a behavior as competitive inhibitors; only the derivate p-TMPyPP has characterized by a different inhibition mechanism (non-competitive or mixed mechanism).

These data represent the interesting evidence that it is possible modify the inhibition mechanism introducing elongated arms in periphery of porphyrin molecule.

For this reason a deeper investigation of this molecule has turned on using molecular modeling calculation and AFM experiments.

The p-TMPyPP is the derivative displaying the most interesting behavior as non-competitive proteasome inhibitor. Then we decide to perform a detailed analysis based on molecular modeling calculation and AFM imaging.

(Also in this case the computational analysis has been performed by Prof. C. Fattorusso and co-workers in Naples University).

First of all, they generated a 3-D pharmacophore model of this molecule (how previously for H2T4) (**Figure 51**).
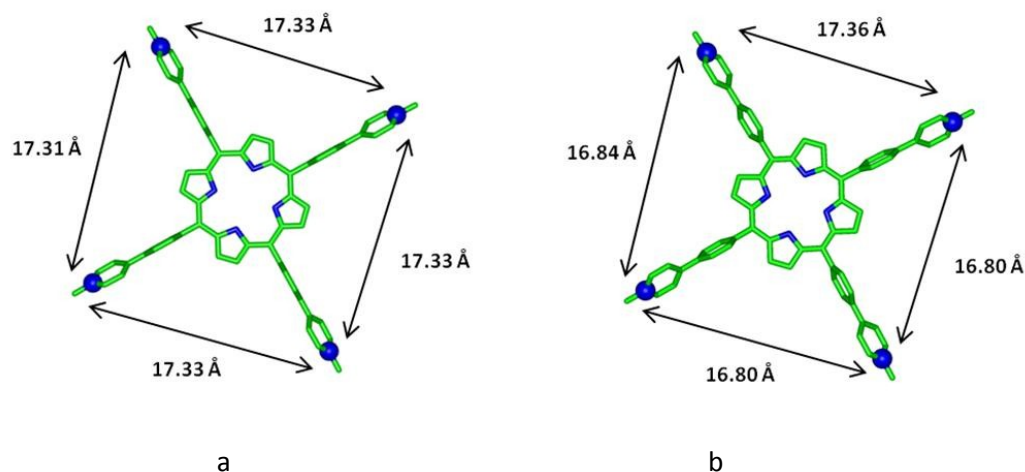
Figure 51: pTMPyPP pharmacophore and related inter-atomic distance ranges (Å). a) MM calculation. b) PM7 calculations.

How it possible to observe the four positive charged nitrogens on the same plane of porphyrin ring have a distance longer than H2T4 (which was about 11 Å).

Afterwards, they selected two starting points for the docking studies of pTMPyPP:

1) α4-α5 groove which are connected to the catalytic subunit β5 (experimental evidence not shown here)

2) 20S gate (previous starting point[86])
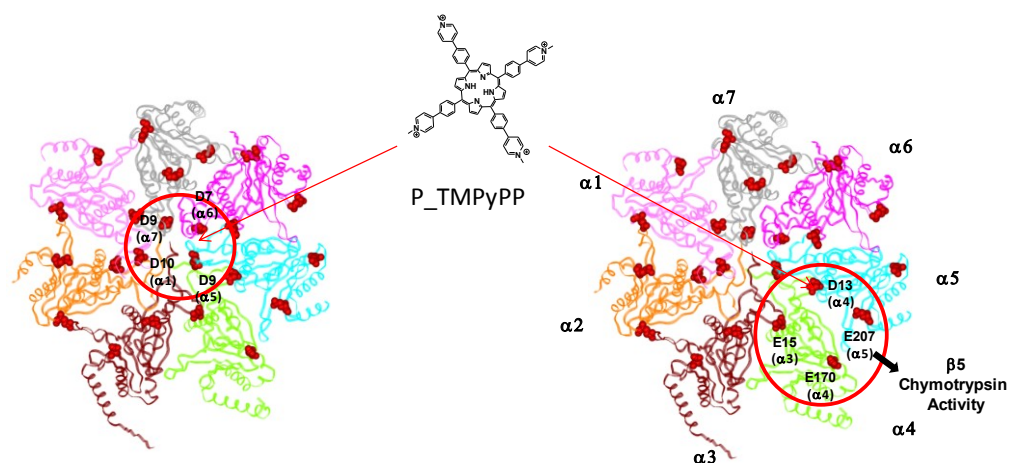

Figure 52: TMPyPP - starting point for docking calculations

Docking calculation showed that the negatively charged residues in the groove α4-α5 display suitable spatial positioning for a possible interaction with the positively charged pTMPyPP nitrogens, only in this solution pTMPyPP is involved in electrostatic interactions with all positively charged nitrogens. Instead, when pTMPyPP bounds at the gate, is not involved in electrostatic interactions with all positively charged nitrogens.

Interestingly, the residue E170 (α4) is involved in the interaction with PA200 while the residues E24 (α4) and E207 (α5) are involved in the interaction with 19S; by that means pTMPyPP binds the same sites of regulator proteins.

Here is reported the complex resulting from docking studies (starting point groove α4/α5) which shown the best compromise between complex energy and non-bond interactions (**Figure 53**).
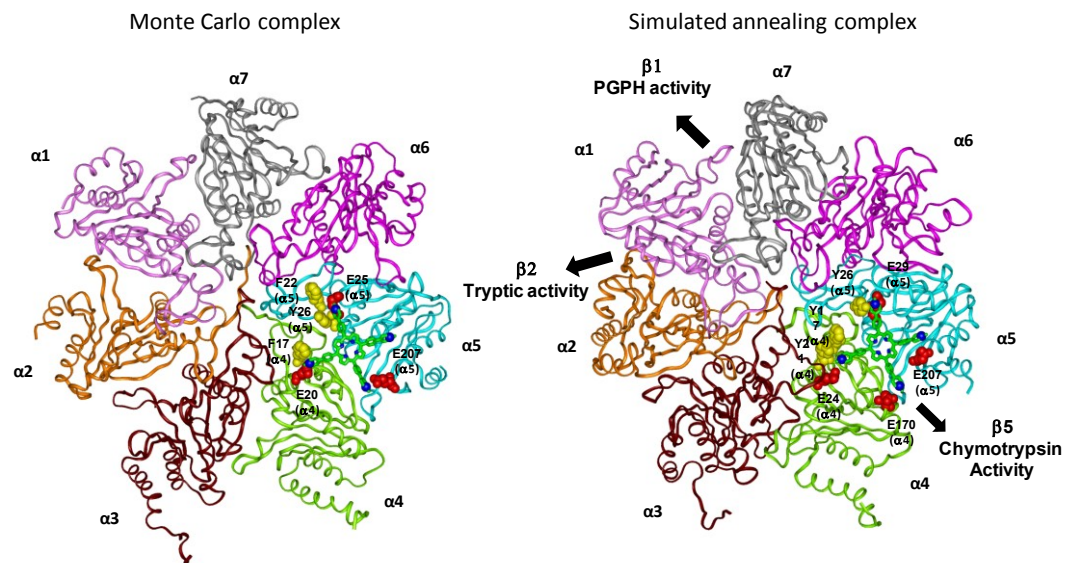
Figure 53: Complex resulting from docking studies (starting point groove α4/α5)

Moreover, considering that pTMPyPP inhibits all three catalytic activities with similar potency and a non competitive mechanism (how previously shown), this means that the presence of negatively charged residues similarly oriented at the grooves between α1-α2, α2-α3 (data not show here) could be binding sites for pTMPyPP.

Afterwards, preliminary AFM experiments have been performed. From this investigation a very unusual behavior has been observed.

In fact, how previously said, a canonical control shown a percentage of closed 20S ≈ 75%. The addition of pTMPyPP at 1,5 μM to 20S proteasome allows to detect ,in this condition, an increase of open conformers (**Figure 54**).
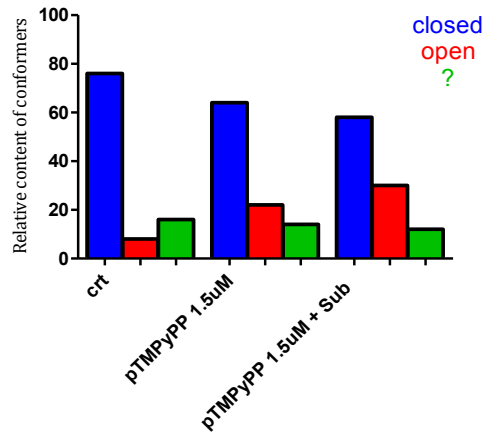
Figure 54: *AFM Experiment* - The histograms represent the % of closed (blue) open (red) and intermediate (green) conformers in : control (h20S), h20S treated with pTMPyPP 1,5µM and h20S treated with pTMPyPP 1,5µM and then with the model substrate for the ChT-L peptidase (SucLLVY-MCA; 100µM).

Sometime, spontaneous opening process can occur, for example, after few days from the samples preparation. In this case, AFM is very useful technique to check the "status" of the sample. Starting from this knowledge, we performed an experiment in this "unusual" condition. In fact, a control with ≈ 40% of open conformers was detected and when 1,5µM of pTMPyPP was added, surprisingly, an increase of closed particles have been observed (**Figure 55**).
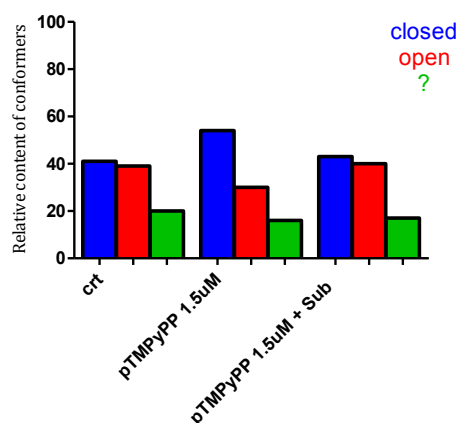
Figure 55: *AFM Experiment* - The histograms represent the % of closed (blue) open (red) and intermediate (green) conformers in : control (h20S), h20S treated with pTMPyPP [1,5] µM and h20S treated with pTMPyPP [1,5] µM and then with the model substrate for the ChT-L peptidase (SucLLVY-MCA; 100 µM).

These data confirm that this porphyrin is able to shift the open-closed equilibrium.

In **Figure 56** are reported conformational changing of 20S structure when it's treaty with pTMPyPP.

a   b   c

d   e   f
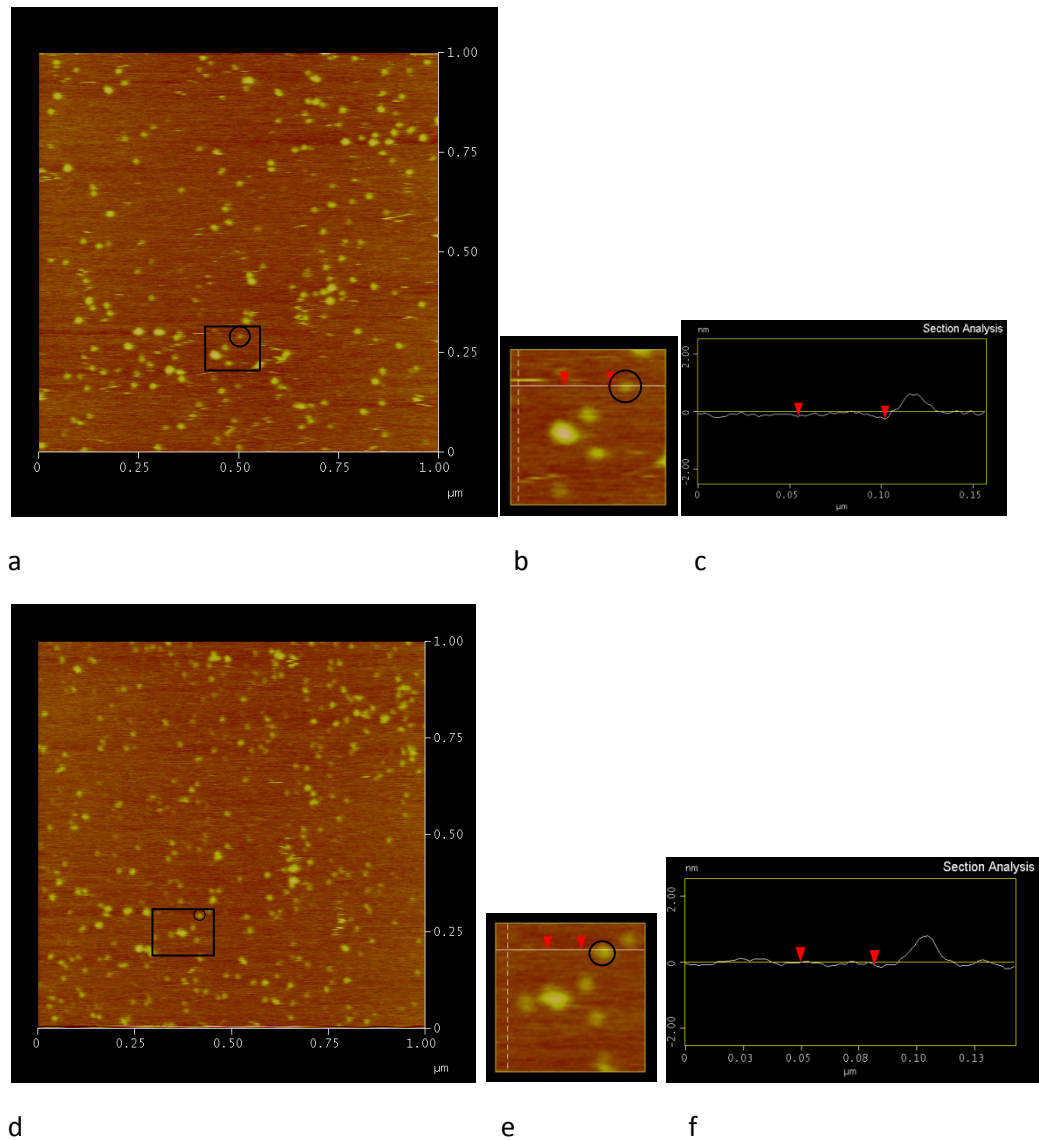
Figure 56: AFM topographs of 1μm × 1μm fields of h20S proteasomes electrostatically immobilized on mica and imaged in tapping mode in liquid. *Upper panel*: AFM image in presence of 20S. a) proteasome particles loosely and randomly dispersed b) zoom on the selected open particle c) frontal sections through the middle of the molecule, parallel to its long axis. *Lower panel*: AFM image in presence of 20S and pTMPyPP. d) proteasome particles loosely and randomly dispersed e) zoom on the selected closed particle f) frontal sections through the middle of the molecule, parallel to its long axis.

How it's possible to observe, the same 20S particle detected in control image with open conformation, in presence of porphyrin is switched in closed conformation.

So far, this interesting phenomenon remains unexplained.

However, molecular modeling results and AFM experiments are just a preliminary investigation on this interesting compound which have to be better characterized in the next future.

6.3 Porphyrins and porphyrinoids effectiveness on intact cells: in cell proteasome activity and vitality evaluation

In parallel of in vitro and in silico investigations a cellular effectiveness of these compounds have been begun.

Relative chymotrypsin-like activity was determined also in intact cells, by means a luminometric assay. MCF7 cells (800 cells/well) were treated with 10 µM of porphyrin/porphyrinoid compounds and 1µM of Bortezomib as positive control. Moreover, we decided to test (how negative control) the tetra anionic porphyrin H2TPPS already used during the preliminary investigation on this class of compounds.

Data are means ± SEM, n=2 per treatment, and quadruplicate analyses of each sample were performed (**Figure 57**).
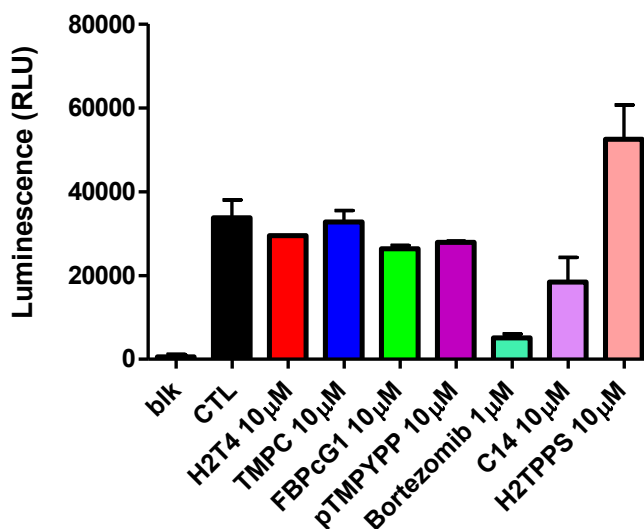
Figure 57: Proteasome inhibition on intact cells (MCF7) by Proteasome-Glo[TM] assay of different porphyrins and porphyrinoids.

The obtained results show that , surprisingly, H2TPPS is able to activate the 20S proteasome in cell; all the others compounds assayed, both porphyrins and porphyrinoids, at 10 μM, induce only a mild proteasomal inhibition, probably related to their insufficient ability to arrive at the target. This is proved by the C14 behavior; in fact, when this porphyrin derivative, it is assayed on 20S purified assay, its potency is comparable to H2T4, but on intact cells it's the most potent proteasome inhibitor. This behavior is surely ascribable to his increased cellular uptake due to the hydrophobic chain[104].

Also the evaluation of cell viability, performed by MTT method, highlight the cellular uptake is determinant in the cytotoxicity of these examined molecules. The majority of porphyrins and porphyrinoids examined scarcely influence the tumor cell growth, by also in this assay the unique efficient derivative is C14: at 10 μM it is able to reduce significantly the cell proliferation (≈55%) (**Figure 58**).
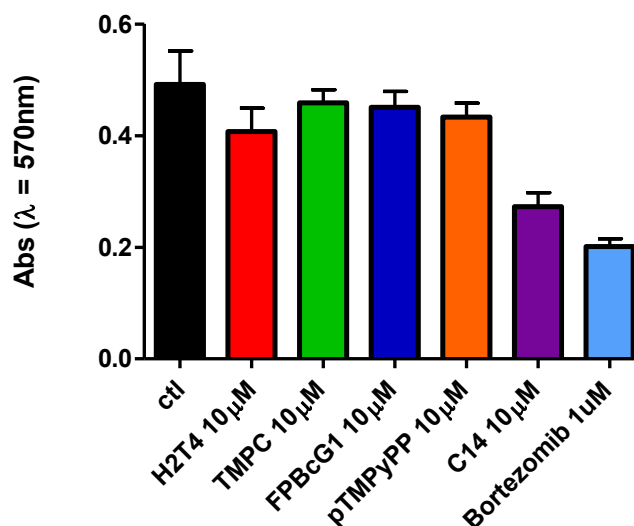
Figure 58: MTT assay on MCF7 cells with several porphyrinoids and porphyrins. All experiments were made in quadruplicate for each compound.

6.4 Conclusions

The investigation on new porphyrins/porphyrinoids compounds have shown that at the moment neither corroles neither phtalocyanines seem promising proteasome inhibitors. Moreover, the introduction of a peptide chain in to the porphyrin ring does not influence their potency and the mechanism, but could enrich the molecule of new functional properties. Instead, the presence of alkyl chain could be a promising tool to improve the cellular uptake for clinical application.

Lastly, very promising is how the different dislocation of crucial positive charges which can introduce an allosteric effect in the inhibition mechanism. In fact the compound pTMPyPP is result not only a non- competitive inhibitor, but, from preliminary molecular modeling calculations, it seems to interact in different regions of the 20S proteasome respect to H2T4. Moreover, AFM experiments were able to detect conformational change on CP when it's treaty with pTMPyPP.

Chapter 7 - Anionic porphyrin H2TPPS actives 20S proteasome

7.1 Goal of this study

Inhibition on 20S proteasome by cationic porphyrin is now an ascertained and well characterized phenomenon. Quite interestingly and surprisingly investigations on the effect exerted by H2TPPS on proteasome activity shown that the tetra anionic porphyrin activates 20S proteasome in cell. These preliminary evidences strongly indicate that a deeper study of the behavior of this molecule is needed.

7.2 Anionic porphyrin H2TPPS: fluorescence activity assay on purified human 20S and yeast wild-type/mutant 20S proteasome

As usual, we firstly verified the ChT-L activity of H2TPPS on isolated proteolytic system. How reported in **Figure 59** H2TPPS activates the human 20S proteasome in a dose-dependent way.
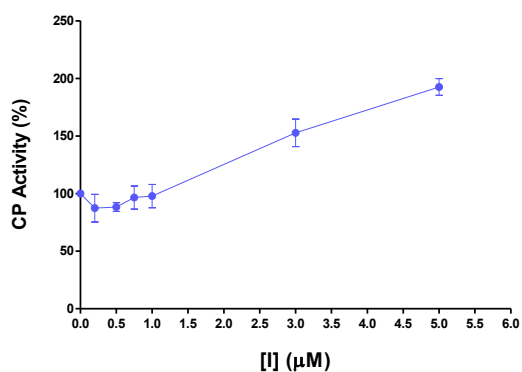
Figure 59: Concentration–response plot of H2TPPS for Chymotryptic-like residual activities on purify h20S proteasome

Starting from these data, we decided to test H2T4 activity on two yeast conformers: closed (Wild Type) and open (mutant α3ΔN 20S CP) (**Figure 60**).
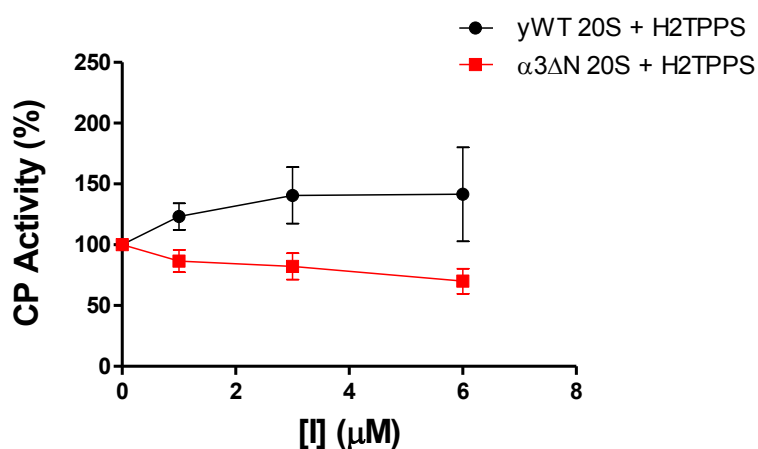
**Figure 60:** Concentration–response plot of H2TPPS for Chymotryptic-like residual activities on yWT and α3ΔN 20S proteasome

Opposite effects were observed; on yWT H2TPPS is a proteasome activator, in agreement with the results obtained with h20S; instead, on the α3ΔN 20S, H2TPPS behaves as an inhibitor. It is rational to hypothesize that this porphyrin stabilizes an intermediate "semi-open" form. So when it interacts with WT, the closed particles will switched in semi-open, and then the effect is an increase of activity, when H2TPPS interact with α3ΔN, the open particles will switched in semi-open and in this case an inactivation is observed.

These results suggested us to carry out a deeper investigation on this molecule using spectroscopic and microscopic approaches.

7.3 Spectroscopic investigation: Circular Dichroism experiments

The use of CD spectroscopy to monitor the conformational (open/close) state and possible conformational changes in the 20S proteasome structure upon interactions with H2TPPS was very useful in this case. In particular, the ratio of the 208/222 bands in the UV region shows that the yWT 20S was in a

conformational state different from that monitored in chapter 4, being the ratio indicative of a more open conformation. Interestingly, proteasome shows an activity different to that observed before how reported in **Figure 61** in which the two different control's sets are compared.
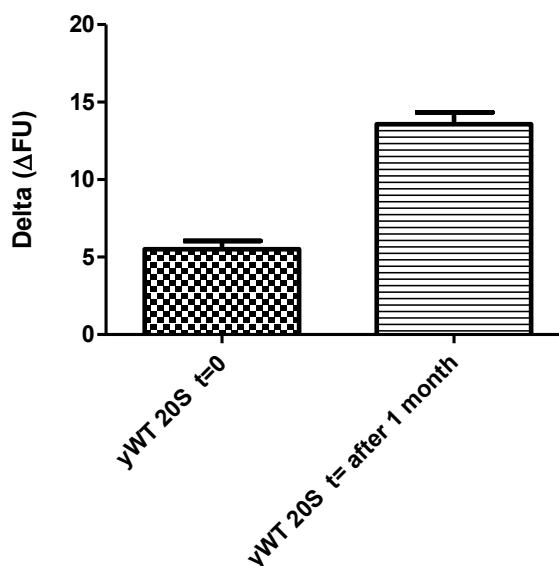
Figure 61: Histograms showing the different yWT 20S delta values obtained during the first set of experiments (see cap.5) and after one month from the fluorescence kinetic assay.

Nevertheless, we decided to treated yWT 20S with H2TPPS (10uM) and acquire the CD spectrum. In this condition, how shown in **Figure 62**, no spectral change has been detected.

The same CD experiments were performed for the α3ΔN and α3ΔN treated with H2TPPS: in presence of porphyrin an unchanged α3ΔN CD spectrum was obtained.
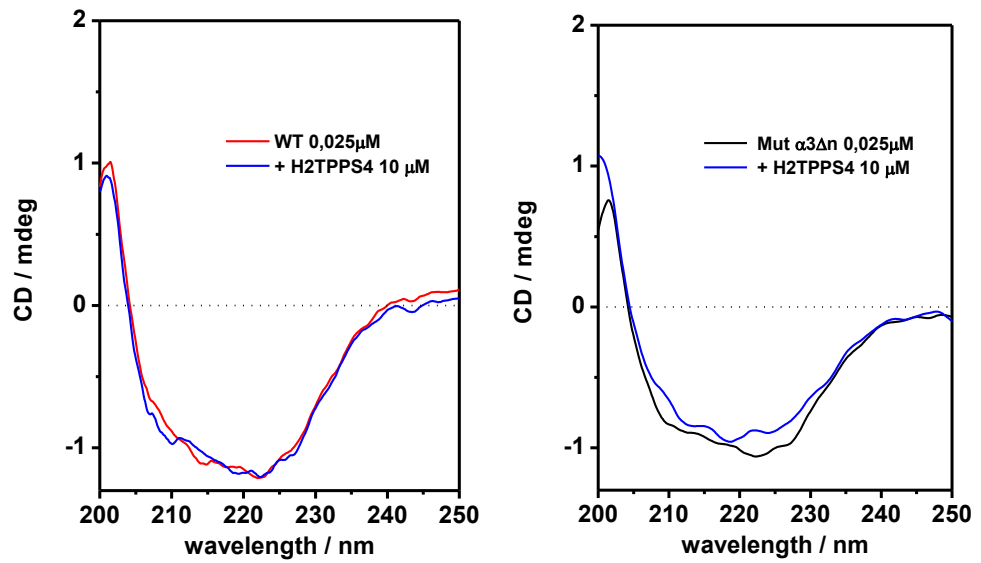
Figure 62: *Right*: Circular Dichroism (CD) spectra of WT 20S (0,025μM) (red) and WT 20S (0,025μM) in presence of H2TPPS 10 μM (blue). *Left:* Circular Dichroism (CD) spectra of α3ΔN 20S (0,025μM) (black) and α3ΔN 20S (0,025μM) in presence of H2TPPS 10 μM (blue).

Afterward, we registered the CD spectra of the above solutions in the visible region (H2TPPS absorption region); different induced CD signals were observed (**Figure 63**).
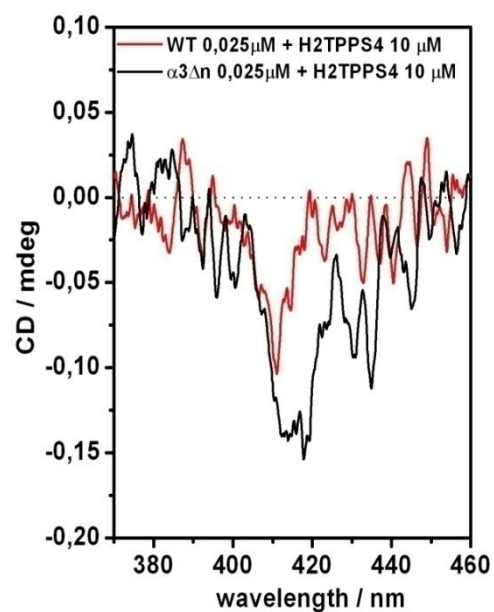
Figure 63: Induced CD spectra, in the visible region, of H2TPPS (10μM) in presence of WT 20S (red line) and α3ΔN 20S(black line).

Furthermore, experiments on human 20S were performed (See cap. 5) with H2TPPS at 1 uM (**Figure 64**): the spectrum acquires a similar feature of that observed when 20S interacts with bortezomib.
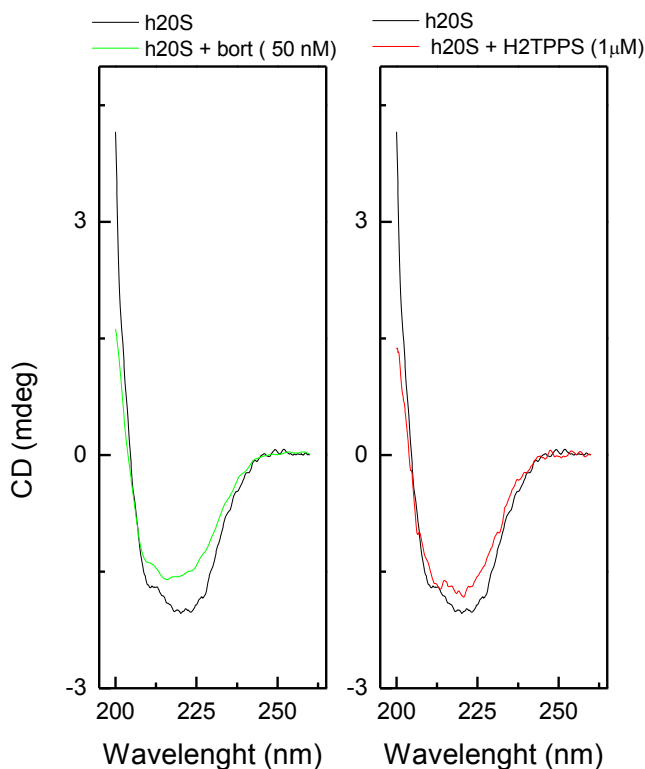
Figure 64: *Right*: Circular Dichroism (CD) spectra of h20S (0,025μM) (black) and in presence of bortezomib 50 nM (green). *Left:* Circular Dichroism (CD) spectra of h20S (0,025μM) (black) and in presence of H2TPPS 1 μM (red).

Ratio 208/222 nm		
Human 20S	Human 20S + Bortezomib	Human 20S + H2TPPS
0,66	0,80	0,67

Table 6 : CD band ratio 208/222 nm in presence of h20S, h20S + Bortezomib, and h20S + H2TPPS.

Finally, melting experiments have been carried out and the T_m are shown in table 7.

T_m		
Human 20S	Human 20S + Bortezomib	Human 20S + H2TPPS
56.85°C	68.60°C	66,91°C

Table 7: Melting temperatures from variable temperature CD spectra (λ:222nm) in presence of h20S, h20S + Bortezomib and h20S+H2TPPS, performed from 20°C to 90° C.

The T_m extrapolate from melting experiments shown for the sample h20S + H2TPPS an increase of temperature if compare to control.

7.4 AFM characterization

AFM experiments with H2T4 I have been performed as previously described (see Cap. 5).

Treatment of the h20S CP with the anionic porphyrin (1µM) lead an increase in the number of stiffer, less dynamic particles with an alpha ring in an unusual shallow-dip conformation ("intermediate", not fully open - Figure 38). Instead after addition of 2µM of H2TPPS, the partition of conformers is similar to control (**Figure 65**).
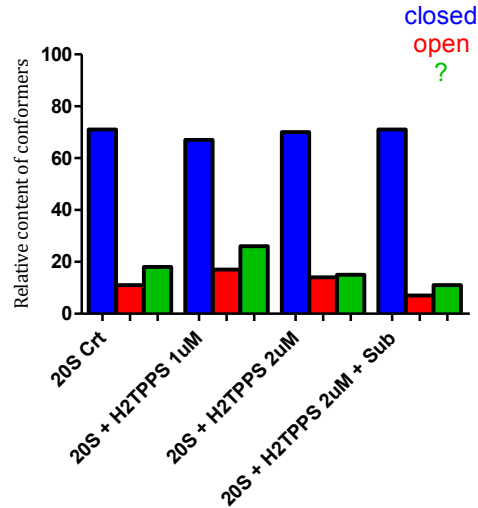
	% closed	% open	% intermediate (?)
control	71	11	18
20S + H2TPPS 1μM	67	17	26
20S + H2TPPS 2μM	70	14	15
20S + H2TPPS 2μM + Suc LLVY- MCA	71	7	11

Figure 65: *Upper panel: AFM Experiment* - The histograms represent the % of closed (blue) open (red) and intermediate (green) conformers in : control (h20S), h20S treated with H2TPPS 1μM,), h20S treated with H2TPPS 2μM and h20S treated with pTMPyPP 2μM and then with the model substrate for the ChT-L peptidase (SucLLVY-MCA; 100 mM).
Lower panel: table showing the % of closed - open and intermediate (?) conformers respectively for the control (h20S), h20S + H2TPPS 1 μM, h20S + H2TPPS 2 μM, h20S + H2TPPS 2μM and Substrate Suc LLVY-MCA 100 μM.

Interestingly, addition of the substrate to porphyrin-treated CP does not result in a shift toward the typical open-gate molecules, suggesting "stiffening" of the proteasome structure upon binding the porphyrin.

7.5 Conclusion

Activity assays on purify h20S proteasome confirm that H2TPPS behaves as a proteasome activator. Interesting, its capability to activate the enzyme is kept in presence of yWT 20S but it's lost with α3ΔN 20S.

AFM experiments demonstrated that a treatment with porphyrins is able to switch the equilibrium of open-closed conformers. More in detail: treatment of the 20S CP with the anionic porphyrin induce an increase in the number of stiffer, less dynamic particles with an alpha ring in an unusual shallow-dip conformation ("intermediate", not fully open) and the substrate addition to porphyrin-treated CP does not result in a shift toward the typical open-gate molecules, suggesting "stiffening" of the proteasome structure upon binding the porphyrin.

Circular Dichroism investigation allowed us to confirm that H2TPPS generate a spectral changing in the h20S signal.

Until now we are not able to explain the H2TPPS interaction mechanism on 20S proteasome.

For this reason, molecular modeling calculation and new spectroscopic - AFM experiments will be performed in a near future.

Chapter 8- Derivatives of natural compounds: inhibition potency on purified proteasome 20S

8.1 Natural compounds and their capability to inhibit proteasome

Resveratrol, pterostilbene, morin hydrate and quercetin are commonly found in nature (**Figure 66**), and have antioxidant, free radical scavenging, anti-inflammatory, and hypolipidemic properties.[105]

Resveratrol, pterostilbene and quercetin are active components in grapes, blueberries and red wine, contributing to the lower incidence of cardiovascular disease in the French population[106], and morin hydrate (isoflavonoid found in tea leaves) has been shown to be an effective hypocholesterolemic agent[107].

It was show that trans-resveratrol, trans-pterostilbene, morin hydrate, and quercetin are proteasome inhibitor.
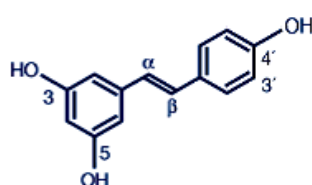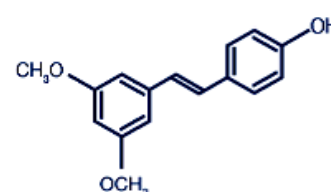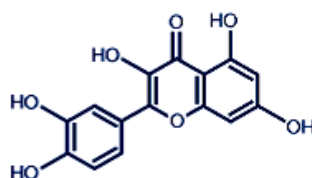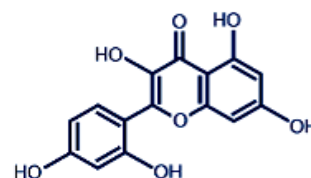

Figure 66: Chemical structures of various compounds used in this study.

Furthermore, recently much attention has focused on the role and mechanism of several flavonoids as inhibitors of oxidative processes[108].

Derivatives of benzoic and cinnamic acids are ubiquitous in plant food (i.e., fruits, vegetables, coffee)[109], and therefore a certain quantity of them is consumed in our daily diet.

Cinnamic acid derivatives (**Figure 67**), especially those combining the cinnamoyl moiety with hydroxyl groups, present strong free radical scavenging properties.
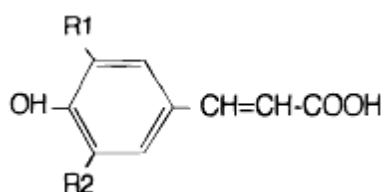
Figure 67 : Cinnamic Acid derivatives

Acids, esters, amides, hydrazides and related derivatives of cinnamic acid with such activities are reported in the literature for their health benefits.[110,111]

Recently, antitumor activities of various cinnamic acid derivatives were explored by many research groups[112,113] and it was found that some compounds presented a promising anti-cancer activity[114].

Other interesting forms of polyphenol derivatives are avenanthramides (Avns). Several forms of Avns have been identified, Avn-a, -b, and -c of which are the major forms.[115]

cAvin is the most abundant with an amount two times greater than that of Avn-a or Avn-b[116]. In vitro experiments indicate that Avn-c (**Figure 68**) has more antioxidant activity than Avn-a or Avn-b[117], and its activity is comparable to the synthetic antioxidant, butylated hydroxytoluene (BHT).[118]
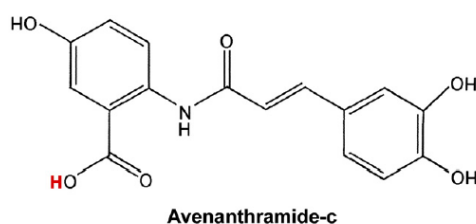
Avenanthramide-c
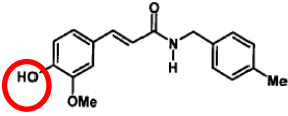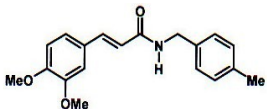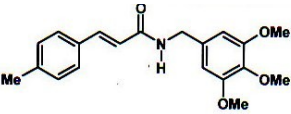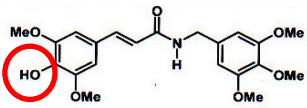
Figure 68: Structure anenanthramide-c

Natural and synthetic Avns exhibit potent antioxidant activity in vitro and in vivo[119]. Moreover, Avns extracted from oats combined with vitamin C synergistically inhibited LDL oxidation[120]. It was demonstrate that Avns possess potential anti-inflammatory properties, which may lend to their potential beneficial effect in the prevention of atherosclerosis through inhibition of NF-κB activation[121].

8.2 Goal of this study

Starting from these already published evidences, we decided to test bio-inspired molecules how new potential proteasome inhibitors.

8.3 Screening of bio-inspired molecules

Preliminary screening on bio-inspired compounds, synthesized by Prof. Tringali and coworker (Catania's University) was done. The table 8 below shows the studied molecules:
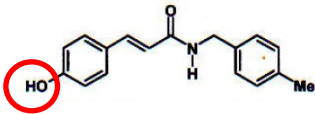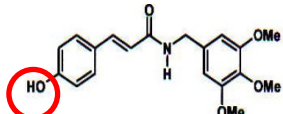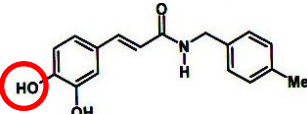
Table 8: bio-inspired compounds, synthesized by Prof. Tringali and coworker (Catania's University) used in the preliminary screening.

Preliminary canonical fluorescence activity assays on 20S proteasome have been performed for all these compounds. The results showed us that the molecules with oxydril group in *para* position are the most active, except for CT-E12 that showed a lower inhibition capability (Table 9).

In order to confirm these results, new experiments were performed only on the selected compounds (CT-E 14, CT-E21, CT-E23, CT-E24) both on purify 20S and in cell.

These first results were encouraging, but unfortunately but not always reproducible. In fact, we noticed that after few weeks from the samples dissolving in DMSO, the inhibition potency of these compounds significantly decreased. In the follow graph is reported an explicative example of the inhibition assay on purified 20S proteasome in presence of 3µM of inhibitor performed at time zero and after few days from the samples dissolution (**Figure 69)**.
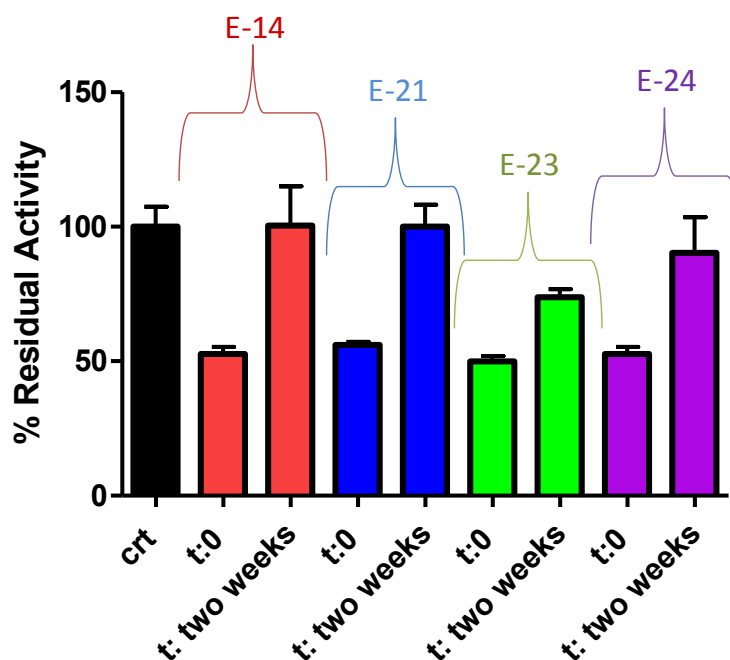
Figure 69: The graph show the comparison of the ChT-L residual activities(percentage) of CT-E14 (red), CT-E 21 (blu), CT-E23 (green) and CT-E24 (violet) at 3uM.The graph shows the values obtained at t:0 and after two weeks from the sample dissolution. Control was normalized to 100%.

In parallel of assay on purified 20S proteasomes, the derivatives of natural compounds were tested as proteasome inhibitors also on intact cells (MCF7) by Proteasome-Glo^{TM} luminometric cell based assay. The first results were promising; in fact, all compounds have shown inhibition activity, mainly for the molecule CT-E14.

A second experiment, performed some few weeks after samples dissolution, showed a poor inhibition potency that could be ascibable to the instabiliy of these molecules previously evidenced. Moreover, an MTT assay performed in parallel with the second Poteasome Glo^{TM} assay experiment, also gives indication that these derivatives are poor active: they scarcely influence the cell vitality of tumor cells at 10µM concentration (**Figure 70**).
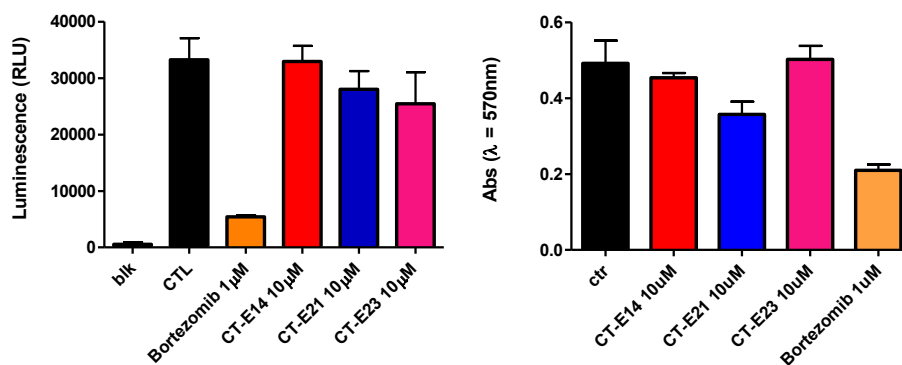
Figure 70: *Right:* Proteasome-Glo^{TM} assay on MCF7 cells obtained with 10µM of inhibitor concentration for each derivatives. *Left:* MTT assay on MCF7 cells with several derivatives of natural compounds tested at a concentration of 10µM; a positive control (Bortezomib 1µM) was also tested. All experiment was made in quadruplicate for each compound.

The observation that the inhibition potency decreases induced us to examine in depth the reason for this unusual behavior. In particular, we collected both UV-visible and mass spectrometry spectra (data not shown) that excluded any structural modification of the investigated molecules. The decreased potency with time of these soluble but solvophobic molecules can found an explanation in their expected tendency to aggregate in aqueous solutions. In fact, aggregated species might be less active than monomers owing to their increased steric hindrance. Also, it is known that: i) aggregation phenomena can be very slow and, ii) the absorption spectra of small aggregates (from dimers to tetramers) might be similar to that of the monomer. Then, in order to investigate the variation of the aggregated state with time, DLS (Dynamic Light Scattering) experiments will be performed in the near future. After these, a new screening on these compound will be carried out.

Conclusion

Our research collocate porphyrins as how new family of proteasome modulators.

We have demonstrated that the number and the type of charges in the *meso* positions are fundamental to obtain opposite effect i.e.: activation and inhibition respectively.

In fact, different approaches confirm that electrostatic charges provide the major driving force in porphyrin/CP interaction and that H2T4 displays a competitive inhibition mechanism which occurs through a "plugging" of CP gate by preventing the substrate access into the catalytic chamber, behaving as a CP gatekeeper.

Furthermore, it interferes with the physiological quaternary equilibrium of the 20S proteasome between "open" and "closed" conformations. In particular, we shown that it can affects the dynamic mechanism of 20S CP gating shifting the equilibrium on open conformers how shown in AFM experiments and CD spectra.

Extending the study on other decorated porphyrin/porphyrinoid derivatives for new proteasome inhibitors results that:

the different dislocation of crucial positive charges introduces an allosteric effect in the inhibition mechanism, without altering significantly the potency. In fact, the compound pTMPyPP is result not only a non- competitive inhibitor, but, from preliminary docking calculations and AFM experiments, it seems to interact in different regions of the 20S respect to H2T4 and it is able to generate conformational change on CP.

Furthermore, either the introduction of peptide chain either the presence of alkyl chain could enrich the molecule of the new functional properties (they could be a promising tool to improve the cellular uptake for clinical application).

Finally, examining the tetra anionic pophyrin H2TTPS, surprisingly, we demonstrate that this compound is a CP activator which is able to "stiffen" the enzyme.

In conclusion, our results suggest that porphyrins's behavior on 20S proteasome, coupled with their versatile chemistry, propose these compounds as "lead" pharmacophores which, if properly decorate or changing the type of charges, can modulate the proteasome behavior acting either as inhibitors with different type of mechanism and interaction sites or as activators.

References

[1] Schmidt M., Finley D.; *BBA-Mol. Cell. Res.,* **2014**, 1843 , 13-25.

[2] Ciechanover A., Orian A., Schwartz A.L., *J Cell Biochem* Suppl., **2000**; 34: 40-51.

[3] Gaczynska M., Osmulski P.A., Ward W.F., *Mech Ageing Dev*; **2001**; 122: 235-54.

[4] Chondrogianni N., Georgila K., Kourtis N., Tavernarakis N., and Gonos E. S.; *The FASEB Journal*, **2015**, 29, 611-622

[5] Ruschak M., Slassi M., Kay L. E. and Schimmer A. D.; *J. Natl. Cancer Inst*, **2011**, 103**,** 1007–1017.

[6] a) Olausse K.A., Dubrana K., Domot J., Spano J-P., Sabatier L., Soria J-C.; *Crit. rev. Oncol. Hematol.,***2006**, 57(3):191-214.
 b) Blasco M. A*., Nature reviews Genetics,***2005**, 6(8):611-622.
 c) Neidle S., Parkinson G., *Nat. rev. Drug Discovery,* **2002**, 1(5):383-393.

[7] Dougherty T. J., Gomer C. J., Henderson B. W., Jori G., Kessel D., Korbelik M., Moan J., Peng Q., *J. Nati. Cancer Intitute*, **1998**, 90 (12),889-901.

[8] a) Miura M., Micca P.L., Fisher C.D., Gordon C.R. Heinrichs J.C., SlatkinD.N.,*The British J. Radiol.,***1998**, 71, 773-781.
 b) Fairchild R.G., Kahl S.B., Laster B.H., Kalef-Ezra J., Popenoe E.P., *Canc. Res.,* **1990**, 50, 4860-4865.

[9] Maiti, N. C.; Mazumdar, S.; Periasamy, N. *J.Phys. Chem*. B; **1998**,102, 1528–1538.

[10] Lauceri R; Raudino A.; Monsù Scolaro L; Micali N; Purrello R.; *J.Am. Chem. Soc*.; **2002**, 124, 894–895.

[11] Segawa H; Takehara C; Honda K; Shimidzu T; Asahi T; Mataga N. *J.Phys. Chem*.; **1992**, 2, 503–506.

[12] Pasternack R. F.; Francesconi L.; Raff D.; Spiro E.; *Inorg. Chem*.; **1973**, 11, 2606–2611.

[13] Di C., Kenyon G. D.; Marina S. C.; Deborah J. K.; Landis-Piwowar K. R; Dou Q. P.; *Biochem. Pharmacol.;* **2005**, 69, 1421–1432

[14] Qureshi A. A, Guan X. Q., Reis J. C, Papasian C. J., Jabre S., Morrison D.C., Qureshi N., *Lipids in Health and Disease;* **2012**, 11-76

[15] Smith D. M.; Wang Z.; Kazi A.; Li L.; Chan T. H.; Dou Q. P. *Mol. Med*.; **2002**, 8, 382–392.

[16] Pontiki E.,Hadjipavlou-Litina D., Litinas K., Geromichalos G, *Molecules;* **2014**, 19, 9655-9674.

[17] Gallastegui N; Groll M.; *Trends Biochem. Sci.;* **2010**, 35, 634–642.

[18] Hershko A.; Ciechanover A.; *Annu. Rev. Biochem.;* **1998**, 67,425–479.

[19] Pickart C. M.; Cohen R. E.; *Nat. Rev. Mol. Cell Biol.;* **2004**, 5, 177–87.

[20] a) Murata S., Yashiroda H., Tanaka K.; *Nat. Rev. Mol. Cell Biol.*, **2009**, 10, 104.
b) N. Gallastegui, M. Groll, *Trends Biochem. Sci.*; **2010**, 35, 634.

[21] a) Unno M., Mizushima T., Morimoto Y., Tomisugi Y., Tanaka K., Yasuoka N., and Tsukihara, T.; *J. Biochem.,* **2002***, 131, 171–173.
b) Groll M., Ditzel L., Lowe J., Stock D., Bochtler M., Bartunik H. D., and Huber R., *Nature,* **1997**, 386, 463–471.

[22] Coux O., Tanaka K., Goldberg A.L; *Annu. Rev. Biochem*., **1996**, 65, 801-847.

[23] Baumeister W., Walz J., Zühl F., Seemüller E.*, Cell,* **1998**, 92, 367-380.

[24] Arendt C. S., Hochstrasser M., *Proc. Natl. Acad. Sci*. USA, **1997**, 94, 7156.

[25] Heinemeyer W., Fischer M., Krimmer T., Stachon U., Wolf D. H, *J. Biol. Chem*. **1997**, 272, 25200.

[26] Kisselev A. F., Callard A., Goldberg A. L., *J. Biol. Chem*. **2006**, 281, 8582.

[27] Gaczynska M., Osmulski P., Methods in Molecular Biology, **2011**, 736, 117-132

[28] a) Groll M., Ditzel L., Lowe J., Stock D., Bochtler M., Bartunik H. D., and Huber R., *Nature.* 1997, 386, 463–471.
b) Unno M., Mizushima T., Morimoto Y., Tomisugi Y., Tanaka K., Yasuoka N., and Tsukihara T., *J. Biochem.* **2002**, 131, 171–173.
c) Groll M., Berkers C. R., Ploegh H. L., and Ovaa H., *Structure,* **2006**, 14, 451–456.
d) Groll M., Kim K. B., Kairies N., Huber R., and Crews C. M.; *J. Am. Chem. Soc.* **2000**, 122, 1237–1238.

[29] Groll M.; Bajorek M.; Kohler A.; Moroder L.; Rubin D.M.; Huber R.; Glickman M.H.; Finley D. *Nat. Struct. Biol.*, **2000**, *7*, 1062–1067.

[30] Finley D., Chen X. and Walters K. J.; *Trends in Biochemical Sciences*, **2016**, Vol. 41, No. 1, 77-93

[31] a)Forster A.; Whitby F.G.; Hill C.P. *EMBO J.*, **2003**, *22*, 4356–4364.
b) Forster A.; Masters E.I.; Whitby F.G.; Robinson H.; Hill C.P. *Mol. Cell*, **2005**, *18*, 589–599.
c) Groll M.; Bajorek M.; Kohler A.; Moroder L.; Rubin D.M.; Huber R.; Glickman M.H.; Finley D. A .; *Nat. Struct. Biol.*, **2000**, *7*, 1062–1067.
d) Liu C.W.; Corboy M.J.; DeMartino G.N.; Thomas P.J.; *Science*, **2003**, *299*, 408–411.

[32] Gaczynska M.; Osmulski P.A., *Antioxid. Redox Signal.*, **2014**, *21*, 2286–2301.

[33] Osmulski P.A.; Hochstrasser M.; Gaczynska M.; *Structure*, **2009**, *17*, 1137–1147.

[34] Osmulski P.A.; Gaczynska M.; *J. Biol. Chem.*, **2000**, *275*, 13171–13174.

[35] Groll M., Bochtler M., Brandstetter H., Clausen T. and Huber R. Ch*em. Biochem,* **2005**, 6, 222–256.

[36] Groll M.; Ditzel L.; Lowe J.; Stock D.; Bochtler M.; Bartunik H.D.; Huber R.; *Nature.*, **1997**, *386*, 463–471.

[37] Lander G.C.; Martin A.; Nogales E.; *Curr. Opin. Struct. Biol.*, **2013**, *23*, 243–251.

[38] a) Lander G.C.; Estrin E.; Matyskiela M.E.; Bashore C.; Nogales E.; Martin A.; *Nature*, **2012**, *482*, 186–191.

b) Da Fonseca P.; He J.; Morris E.P.; *Mol. Cell*, **2012**, *46*, 54–66.

c) Lasker K.; Förster F.; Bohn S.; Walzthoeni T.; Villa E.; Unverdorben P.; Beck F.; Aebersold R.; Sali A.; Baumeister W. ; *Proc. Natl. Acad. Sci. U.S.A.*, **2012**, *109*, 1380–1387.

[39] McConkey D.J., Zhu K., *Drug Resist. Updates*, **2008**, 11, 164.

[40] McNaught K. St P., Olanow C. W., Halliwell B, Isacson O. and Jenner P.; *Nature Reviews Neuroscience*, **2001**, 2, 589-594

[41] a) Chu-Ping M., Vu J H., Proske R.J., Slaughter C. A. and DeMartino G.N.*, J. Biol. Chem*., **1994,** 269, 3539-3547.

b) Coux O., Tanaka K., Goldberg A.L., *Annual review of biochemistry*, **1996,** 65, 810-847.

c) DeMartino G.N., Slaughter C.A., *Journal of Biological Chemistry,* **1999**, 274, 22123-22126.

d) Glickman M.H., Rubin D.M., Coux O., Wefes I., Pfeifer G., Cjeka Z., BaumeisterW., Fried V.A, Finley D., *Cell*, **1998**, 94, 615-623.

e) Rubin D.M, Glickman M.H., Larsen C.N., Dhruvakumar S., Finley D., J EMBO, **1998**, 17, 4909-4919.

[42] Groll M, Bajorek M, Köhler A., Moroder L., Rubin D.M., Huber R.,. Glickman M.H., Finley D., *Nature Structural Biology*, **2000**, 7, 1062 – 1067.

[43] Groll M., Huber R.; *The International Journal of Biochemistry & Cell Biology,* **2003**, 35, 606–616

[44] Gaczynska M, Osmulski PA, Ward WF., *Mech Ageing Dev,* **2001**; 122 : 235-54.

[45] Chondrogianni N, Stratford FL, Trougakos IP, Friguet B, Rivett AJ, Gonos ES.; *J. Biol. Chem.,* **2003**; 278: 28026-37.

[46] Chondrogianni N, Trougakos IP, Kletsas D, Chen QM, Gonos ES., *Aging Cell,* **2008**; 7: 717-32.

[47] Chondrogianni N., Stratford F.L., Trougakos I.P., Friguet B., Rivett A.J., Gonos E.S. ; *J. Biol. Chem.,* **2003**; 278: 28026-37.

[48] Dennissen F.J., Kholod N., van Leeuwen F.W.; *Prog. Neurobiol.,* **2012**; 96: 190-207.

[49] Tseng B.P., Green K.N., Chan J.L., Blurton-Jones M., La Ferla F.M..; *Neurobiol. Aging*, **2008**; 29: 1607-18.

[50] Dehvari N, Mahmud T, Persson J, Bengtsson T, Graff C, Winblad B, Rönnbäck A, Behbahani H.; *Neurochem Int* , **2012**; 60: 533-42

[51] Chadwick L., Gentle L., Strachan J., Layfield R.; *Neuropathol. Appl. Neurobiol.*, **2012**; 38: 118-31.

[52] Bendotti C., Marino M., Cheroni C., Fontana E., Crippa V., Poletti A., De Biasi S.; *Prog. Neurobiol.* , **2012**; 97: 101-26.

[53] Crippa V., Sau D., Rusmini P., Boncoraglio A., Onesto E., Bolzoni E., Galbiati M., Fontana E., Marino M., Carra S., Bendotti C., De Biasi S., Poletti A.; *Hum. Mol. Genet*.; **2010**; 19: 3440-56.

[54] Onesto E., Rusmini P., Crippa V., Ferri N., Zito A., Galbiati M., Poletti A., *J Neurochem*, **2011**; 118: 266-80.

[55] Trippier P.C., Zhao K.T.,. Fox S.G.,. Schiefer I.T., Benmohamed R., Moran J., Kirsch D.R., Morimoto R.I. and Silverman R.B., *ACS Chem. Neurosci.*, **2014**, 5 (9), pp 823–829

[56] Lee B. H., Lee M. J., Park S., Oh D. C., Elsasser S., Chen P.C., Gartner C., Dimova N., Hanna J., Gygi S. P., Wilson S. M., King R. W., and Finley D.; *Nature*; **2010**, 467, 179–184.

[57] Adams J., *Cancer Cell.,* **2004, 5**, 417-421.

[58] McConkey D. J., Zhu K., *Drug Resist. Updates;* **2008**, 11, 164 –179;

[59] Obeng E. A., Carlson L. M., Gutman D. M, Harrington W. J. Jr., Lee K. P., Boise L. H., *Blood,* **2006**, 107, 4907 – 4916;

[60] S. T. Nawrocki, J. S. Carew, K. Dunner, Jr., L. H. Boise, P. J. Chiao, P. Huang, J. L. Abbruzzese, D. J. McConkey, *Cancer Res*. **2005**, 65, 11510 – 11519;

[61] Bianchi G., Oliva L., Cascio P., Pengo N., Fontana F., Cerruti F., Orsi A., Pasqualetto E., Mezghrani A., Calbi V., Palladini G., Giuliani N., Anderson K. C., Sitia R., Cenci S., *Blood,* **2009**, 113, 3040 – 3049;

[62] L. R. Dick, P. E. Fleming, *Drug Discovery Today,* **2010**, 15, 243 – 249;

[63] Bazzaro M., Lee M. K., Zoso A., Stirling W. L., Santillan A., Shih Ie M., Roden R. B., *Cancer Res*., **2006**, 66, 3754 – 3763

[64] a) Crawford L. J.; Walker B.; Ovaa H.; Chauhan D.; Anderson K. C.; Morris T. C.; Irvine A. E. *Cancer Res.* **2006**, 66, 6379–86.
   b) Milardi D.; Arnesano F.; Grasso G.; Magrì A.; Tabbì G.; Scintilla S.; Natile G.; Rizzarelli E. *Angew. ChemInt. Ed.,* **2007**, 46, 7993–7995.
   c) Arena G.; Fattorusso R.; Grasso G.; Grasso G. I.; Isernia C.; Malgieri G.; Milardi D.; Rizzarelli E.; *Chem. Eur. J.,* **2011**, 17, 11596–11603.

[65] Demo S. D.; Kirk C. J.; Aujay M. A.; Buchholz T. J.; Dajee M.; Ho M. N.; Jiang J.; Laidig G. J.; Lewis E. R.; Parlati F.; Shenk K. D.; Smyth M. S.; Sun C. M.; Vallone M. K.; Woo T. M.; Molineaux C. J.; Bennett M. K*.; Cancer Res.,* **2007**, 67, 6383–6391.

[66] Sprangers R., Li X, Mao X, Rubinstein JL, Schimmer AD, Kay LE., *Biochemistry*, **2008**, 47, 6727-6734.

[67] Li et al*., J. Natl. CancerInst*. **2010**, 102: 1069-1082.

[68] Li et al, *Nat. Med*. **2000**, 6,: 49-55.

[69] Gaczynska M., Osmulski P.A, Gao Y., Post M. J, and Simons M.; *Biochemistry, ***2003***, 42, 8663-8670.*

[70] Robert A. Copeland, *Evaluation of Enzyme Inhibitors in Drug Discovery*, Wiley-Interscience, **2005**.

[71] a) Gunasekaran K., Ma B. and Nussinov R., *Proteins*, **2004**, 57, 433–443.
   b) Henzler-Wildman K. A., Thai V., Lei M., Ott M., Wolf-Watz M., Fenn T., Pozharski E., Wilson M. A., Petsko G. A., Karplus M., Hubner C. G., and Kern D.; N*ature,* **2007,** 450, 838–844.

[72] Osmulski, P. A., and Gaczynska, M.; *Biochemistry*, **2002***, 41, 7047–7053.

[73] a) Tinazli, A., Piehler, J., Beuttler, M., Guckenberger, R., and Tampe, R., *Nature Nanotech.* **2007**, 2, 220–225.
   b) Osmulski, P. A., and Gaczynska, M.; *Biochemistry*, **2002***, 41, 7047–7053.

[74] Groll, M., Ditzel, L., Lowe, J., Stock, D., Bochtler, M., Bartunik, H.D., and Huber, R.; *Nature*, 1997, 386, 463–471.

[75] da Fonseca, P.C.A., and Morris, E.P.;. J. Biol. Chem., **2008**, 283, 23305–23314.

[76] Gaczynska M., and Osmulski P.A.; *Curr. Opin. Colloid Interface Sci.,* **2008**, 13, 351–367.

[77] Osmulski, P.A., and Gaczynska, M.; *J. Biol. Chem.,* **2000**, 275, 13171–13174.

[78] Szokalska A., Makowski M., Nowis D., Wilczy G. M., Kujawa M., Wójcik C., Salwa I.P., Bil J., Janowska S., Agostinis P., Verfaillie T., Bugajski M., Gietka J., Issat T., Mrówka P., Stoklosa T., Hamblin M. R., Mróz P., Jakóbisiak M., Golab J., *Cancer Res.;* **2009**, 69, 4235-4243.

[79] Santoro A. M., Lo Giudice M. C., D'Urso A., Lauceri R., Purrello R. and Milardi D., *J. Am. Chem. Soc.,***2012**, 134, 10451.

[80] Rodgers K. J.; Dean R. T. ; *Int. J. Biochem. Cell. Biol.,* **2003**, 35, 716–727.

[81] Balla G., Vercellotti G., Eaton J.W., Jacob H.S. *Trans Assoc Am Physicians*, **1990;** 103: 174–179.

[82] a) Schaer D.J., Buehler P.W., Alayash A.I., Belcher J.D., Vercellotti G.M.; *Blood,* **2013**; 121: 1276–1284.
 b) Higdon AN, Benavides GA, Chacko BK, Ouyang X, Johnson MS, Landar A., Zhang J., Darley-Usmar V.M.; *Am J Physiol Heart Circ Physiol*.; **2012**; 302: H1394–H1409.
c) Lin S, Yin Q, Zhong Q, Lv FL, Zhou Y, Li JQ et al. ; *J Neuroinflammation,* **2012**; 9: 46.
d) Fortes G.B., Alves L.S., de Oliveira R., Dutra F.F., Rodrigues D., Fernandez P.L., Souto-Padron T., De Rosa M.J., Kelliher M., Golenbock D., Chan F.K., Bozza M.T., *Blood* **2012**; 119: 2368–2375.
e) Schaer C.A., Deuel J.W., Bittermann A.G., Rubio I.G., Schoedon G., Spahn D.R., Wepf R.A., Vallelian F., Schaer D.J., *Cell Death Differ* , **2013**; 20: 1569–1579.
f) Pimenova T., Pereira C.P., Gehrig P., Buehler P.W., Schaer D.J., Zenobi R., *J Proteome Res* **2010**; 9: 4061–4070.
g) Vallelian F., Schaer C.A., Kaempfer T., Gehrig P., Duerst E., Schoedon G. et al. *Blood,* **2010**; 116: 5347–5356.

[83] Vallelian F., Deuel J.W., Opitz L., Schaer C.A., Puglia M., Lönn M., Engelsberger W., Schauer S., Karnaukhova E., Spahn D.R., Stocker R., Buehler P.W. and Schaer D.J., *Cell Death and Differentiation,* **2015,** 22, 597–611

[84] Gallastegui N; Groll M.; *Methods in Molecular Biology.;* **2012**, 832, 373–390.

[85] Sikorski R.S., and Boeke J.D., *Methods Enzymol.*, **1991**, 194, 302–318.

[86] Santoro A. M., Cunsolo A., D'Urso A., Sbardella D., Tundo G. R., Ciaccio C., Coletta M., Diana D., Fattorusso R., Persico M., Di Dato A., Fattorusso C., Milardi D. and Purrello R.; *Chem. Sci.*, **2016**, 7, 1286–1297

[87] a) Klages J., Coles M. and Kessler H., *ed. P. A. Bartlett and M. Entzeroth, RSC Publishing, Cambridge,* **2006**, ch. 12, pp. 263–290 and *Mol. BioSyst*., **2006**, vol. 2, pp. 318–332.
 b) Meyer B. and Peters T., *Angew. Chem*., **2003,** 42(8), 864.
 c) Klein J., Meinecke R., Mayer M. and Meyer B., *J. Am. Chem. Soc*., **1999,** 121(22), 5336.
d) ACD/Percepta, version 14.0.0, Advanced Chemistry Development, Inc., Toronto, ON, Canada, 2013, http:// www.acdlabs.com.
e) Dewar M. J. S. and Thiel W*., J. Am. Chem. Soc.,* **1977,** 99, 4899.
f) Davis I. W., Leaver-Fay A.,. Chen V. B, Block J. N., Kapral G. J., Wang X., Murray L. W., Arendall W. B., Snoeyink J., Richardson J. S. and Richardson D. C., *Nucleic Acids Res.,* **2007,** 35, W375.
g) Mayer M. and Meyer B*., J. Am. Chem. Soc.,* **2001**, 123, 6108.

[88] Pons J., Evrad-Todeschi N., Bertho G., GharbiBenarous J., Tanchou V., Benarous R. and Girault J. P., *Biochemistry,* **2008**, 47, 14.

[89] Pei J.; Kim B. H.; Grishin N. V.; *Nucleic Acids Res*., **2008**, *36*, 2295–2300.

[90] Ruschak A. M. and Kay L. E., *Proc. Natl. Acad. Sci. U. S. A.,***2012**, 109(50), E3454.

[91] Sprangers R., Li X., Mao X., Rubinstein J. L., Schimmer A. D. and Kay L. E., *Biochemistry,* **2008**, 47(26), 6727.

[92] Hammes G.G., Chang Y.C., Oas T.G. *Proc Natl Acad Sci U S A*., **2009**, *106* (33),13737-13741.

[93] Santoro A.M., Monaco I., Attanasio F., Lanza V., Pappalardo G., Tomasello M. F., Cunsolo A., Rizzarelli E., De Luigi A., Salmona M. and Milardi D.; *Scientific Reports*, **2016**, 6, 33444

[94] Köhler A., Bajorek M., Groll M., Moroder L., Rubin D. M., Huber R., Glickman M. H., Finley D.; *Biochimie,* **2001**, 83 325–332

[95] Pawel A. Osmulski and Maria Gaczynska; *Mol Pharmacol,* **2013**, 84:104–113

[96] Dosselli R., Tampieri C., Ruiz-González R., De Munari S., Ragàs X., Sánchez-García D., Agut M., Nonell S., Reddi E., and Gobbo M.; *J. Med. Chem*. **2013**, 56, 1052−1063

[97] Gobbo M.; Benincasa M.; Bertoloni G.; Biondi B.; Dosselli R.; Papini E.; Reddi E.; Rocchi R.; Tavano R.; Gennaro R., *J. Med. Chem*., **2009**, 52, 5197−5206.

[98] a) Hamblin M. R.; Hasan T.; *Photochem. Photobiol. Sci*. **2004,** 3, 436−450.
   b) Foote, C. S.; *Photochem. Photobiol*. **1991**, 54, 659−659.
   c) Redmond, R.; Gamlin, J. *; Photochem. Photobiol.* **1999**, 70, 391−475.

[99] Stark G. *; J. Membr. Biol.,* **2005,** 205, 1−16.

[100] Gaspar D., Veiga A. S. and Castanho M. A. R. B., *Front. Microbiol*., **2013**, 4, 294–310.

[101] Mader J. S. and Hoskin D. W., *Expert Opin. Invest. Drugs,* **2006**, 15, 933–946.

[102] Reddi E.; Ceccon M.; Valduga G.; Jori G.; Bommer J.; Elisei F.; Latterini L.; Mazzucato U. *Photochem. Photobiol.,* **2002,** 75, 462–470.

[103] Moret F., Gobbo M. and Reddi E.; *Photochem. Photobiol. Sci*., **2015**, 14, 1238–1250

[104] Rapozzi V., Zorzet S., Zacchigna M., Della Pietra E., Cogoi S. and Xodo L. E; *Molecular Cancer,* **2014**, 13:75

[105] a) Bradamante S., Barenghi L., Piccinini F., Bertelli A.A.E., de Jonge R., Beemster P., de Jong J.W.,*Eur J Phamacology*, **2003**, 465,115–123.

b)Remsberg C.M., Yanez J.A., Ohgami Y., Vega-Villa K.R., Rimando A.M., Davies N.M.,*Phytother Res*, **2008**, 22,169–179.

c) Middleton E. Jr, Kandaswami C., Theoharides T.C.,*Pharmacol Rev,* **2000**, 52(4),673–751.

[106] Law M., Wald N., *British Medical Journal,* **1999**, 318,1471–1480.

[107] Yugarani T., Tan B.K.H., Reh M., Das NP,*Lipids,* **1992**, 27,181–186.

[108] Van Acker S. A.B.E., Van Den Berg D., Tromp M.N.J.L., Griffioen D. H., Van Bennekom W. P., Van Der Vijgh W. J.F., Bast A., *Free Radical Biology & Medicine*, **1996**, 20, 3, 331-342.

[109] Herrmann K., *Crit. Rev. Food Sci. Nutr.* **1989**, *28*, 315-347.

[110] Bernini R.; Mincione E.; Barontini M.; Provenzano G.; Setti L. *Tetrahedron,* **2007**, *63*, 9663–9667.

[111] Sova M., *Mini Rev. Med. Chem.,* **2012**, *12*, 749–767.

[112] Bandgar B.P.; Gawande S.S.; Bodade R.G.; Totre J.V.; Khobragade C.N., *Bioorg. Med. Chem.* **2010**, *18*, 1364–1370.

[113] a) Cheng J.H.; Huang A.M.; Hour T.C.; Yang S.C.; Pu Y.S.; Lin C.N., *Eur. J. Med. Chem.* **2011**, *46*, 1222–1231.

b) Kanagalakshmi K.; Premanathan M.; Priyanka R.; Hemalatha B.; Vanangamudi A., *Eur.J. Med. Chem.* **2010**, *45*, 2447–2452.

[114] Pontiki E., Hadjipavlou-Litina D., Litinas K. and Geromichalos G., *Molecules,* **2014**, *19*, 9655-9674.

[115] Peterson D. M*., J. Cereal Sci*.,**2001**,33:115–229.

[116] Matsukawa T.; Isobe T.; Ishihara A.; Iwamura H. *Naturforsch. [C]***, 2000**, 55:30–36;.

[117] Ji L. L.; Lay D.; Chung E.; Fu Y.; Peterson D. M., *Nutr. Res.* ; **2003**,23:1579–1590.

[118] Peterson D. M.; Hahn M. J.; Emmons C. L*., Food Chem.***; 2002**, 79:473–478.

[119] Dimberg L. H.; Theander O.; Lingnert H., *Cereal Chem.***1993**, 70:637–641.

[120] Chen C. Y.; Milbury P. E.; Kwak H. K.; Collins F. W.; Samuel P.; Blumberg J. B*., J. Nutr.* ; **2004,** 134:1459–1466.

[121] Guo W., Wise M., F., Collins W., Meydani M., *Free Radical Biology & Medicine,* **2008***,* 44, 415–429

Acknowledgements